FACULDADE DE ENGENHARIA DA UNIVERSIDADE DO PORTO

Development of a Drop Weight Machine for Adhesive Joints Testing

Diogo do Paço Casal Antunes

Integrated Master in Mechanical Engineering
Specialization in Automation

Supervisor: Prof. António Mendes Lopes
Co-Supervisors: Inv. Carlos Moreira da Silva
Prof. Lucas FM da Silva

February, 2019

Development of a Drop Weight Machine for Adhesive Joints Testing

Diogo do Paço Casal Antunes

Integrated Master in Mechanical Engineering

Specialization in Automation

February, 2019

Resumo

Os materiais adesivos estão a ser considerados, cada vez mais, como um dos melhores métodos para unir peças de diferentes características, estando, por isso, a ser muito procurados na indústria automóvel e aeroespacial. Assim, é importante acompanhar este crescente interesse neste tipo de ligações com estudos que as caraterizem devidamente.

Os membros do Grupo de Investigação de Adesivos da FEUP preocupam-se em contribuir para este novo campo de investigação, estudando as propriedades destes materiais e as suas técnicas de adesão. Logo, é importante o grupo possuir o equipamento adequado para o poder fazer. Contudo, apesar de usufruir de vários equipamentos de teste, ainda necessita de um para realizar testes de impacto a baixa velocidade.

Como tal, o principal objetivo desta dissertação é continuar o trabalho feito por quatro ex-alunos de mestrado da FEUP no desenvolvimento de uma máquina de impacto, nomeadamente uma máquina de queda de massas. Esta dissertação inclui o processo de implementação de um sub-sistema anti ressalto e de um novo conjunto bigorna-impactor, dotado de um acelerómetro e de uma célula de carga piezoelétricos. Para além destas novas implementações, houve também a necessidade de ajustes e adições nos circuitos elétrico, pneumático e de comando, assim como o desenvolvimento de uma interface para operar a máquina. Após a máquina estar toda equipada, foram realizados testes que validaram o seu funcionamento.

Abstract

Adhesive materials are increasingly being considered as one of the best methods for joining parts with different characteristics and, therefore, are highly sought out in the automotive and aerospace industries. Thus, it´s important that the growing interest in this type of bonding is supported by studies that correctly characterizes them.

The members of the Adhesives Investigation Group of FEUP are interested in contributing to this field of research by studying these materials´ properties and techniques. So, it´s important they are provided with the adequate equipment to be able to do it. However, despite having several testing machines, they still require one that performs impact tests at low velocities.

As such, the main objective of this dissertation is to continue the work done by four previous master´s students of FEUP in the development of an impact machine, namely a drop weight machine. This dissertation includes the implementation of an anti-rebound sub-system and a new anvil-impactor assembly, equipped with a piezoelectric accelerometer and a piezoelectric load cell. In addition to these new implementations, there was also the need for some adjustments and new components in the electrical, pneumatic and control circuits, as well as the development of an interface to operate the machine. After the machine is completely equipped, impact tests were made to validate it.

Acknowledgements

Firstly, I would like to thank to all my family and friends for the support, caring and happiness they constantly give me, which makes me want to continue to construct my character and be the best person I can be.

To my supervisors, Prof. António Mendes Lopes, Inv. Carlos Moreira da Silva and Prof. Lucas da Silva, for all the advices, knowledge and support they gave during this dissertation.

To all ADFEUP´s members for the positive and motivational environment they provided me. In addition, I would like to give special thanks to Eng. Eduardo Marques, Eng. José Machado and Eng. Ricardo Carbas for their great accessibility, help and knowledge.

And finally, to Mr. André Alves, Mr. Domingues Carvalho, Mr. Joaquim Silva, Mr. Pedro Falcão and Mr. António Ramalho for all their time and patience, without whom the work of this dissertation wouldn´t be possible.

Diogo Antunes

Contents

Resumo i

Abstract iii

Acknowledgements v

Acronyms xv

1. Introduction 1

1.1. Context and Motivation 1

1.2. Objectives 1

1.3. Methodology 2

1.4. Thesis Outline 3

2. Literature Review 5

2.1. Adhesives 5

2.2. Impact tests for adhesive joints 6

2.2.1. Block Impact Test 7

2.2.2. SHPB Test 8

2.2.3. Drop Weight Test 10

2.3. Commercial Drop Weight Machines 11

2.3.1. Zwick Roell – HIT and DWT Series 11

2.3.2. Instron – CEAST 9000 series 12

2.3.3. Imatek – IM10 and DWTT series 13

2.3.4. ADFEUP´s Drop Weight Machine 13

3. Developed sub-systems 17

3.1. Anti-rebound sub-system (ARS) 17

3.1.1. Rotating Structure 18

3.1.1.1. Main Body 19

3.1.1.2. Needle Bearings 19

3.1.1.3. Impact and Actuation Axles 20

3.1.1.4. Actuation Axle Connector 28

3.1.1.5. Shock-Absorbers Pads 28

3.1.2. Fixed Structure 29
3.2. Anvil-impactor sub-system 31

4. Actuation and Control Logic **37**
4.1. Pneumatic circuit 37
4.1.1. Cylinders 38
4.1.2. Directional valves 39
4.1.3. Air treatment unit 41
4.1.4. Pneumatic accessories 41
4.2. Electronics 42
4.2.1. Lifting sub-system 42
4.2.2. Velocity acquisition sub-system 43
4.2.3. Sensors 44
4.2.3.1. Optical detector 45
4.2.3.2. Microswitches 46
4.2.3.3. Inductive detector 46
4.2.3.4. Photoelectric detector 47
4.2.3.5. Proximity sensor 48
4.2.3.6. Accelerometer 49
4.2.3.7. Press force sensor 51
4.2.4. Boards 53
4.2.4.1. DAQ board 53
4.2.4.2. Encoder board 54
4.2.4.3. PCB 56
4.2.5. Power circuit´s hardware 57
4.2.6. Emergency circuit´s hardware 59
4.3. Command Sequence and Interface 60
4.3.1. Highest-level routine 61
4.3.2. MAIN sub-routine 61
4.3.3. INIT sub-routine 63
4.3.4. FIND_VELAQ sub-routine 63
4.3.5. CHECK_ANVIL sub-routine 64
4.3.6. TEST sub-routine 64
4.3.7. GRAB_ANVIL sub-routine 70
4.3.8. MANUAL sub-routine 70
4.3.9. SOS sub-routine 72
5. Adhesive Joints Tests **75**

5.1. Test parameters 75
5.1.1. Specimen of the type 1 75
5.1.2. Specimen of the type 2 76
5.2. Results and discussion 76

6. Conclusions and Future Developments **81**
6.1. Conclusions 81
6.2. Future developments 83

Bibliography **85**

Appendix A **89**

Appendix B **115**

Appendix C **127**

Appendix D **133**

Appendix E **147**

List of Figures

2.1 - Stress distribution comparison between bonded surfaces using standard fasteners and adhesive materials [2]. 5

2.2 - Block impact test apparatus [2]. 7

2.3 - Possible impact cases between the hammer and the upper block of the specimen [2]. 8

2.4 - Basic setup and Lagrangian diagram for compressive tests on a SHPB machine [8]. 8

2.5 - Solution for the SHPB tensile test, as proposed by Chen [2, 10]. 9

2.6 - Basic setup and Lagrangian diagram for tensile tests on a SHPB machine [8]. 10

2.7 - a) Butt joint example; b) Single lap joint example. 10

2.8 - HIT series commercialized by Zwick Roell [11]. 12

2.9 - FEUP´s Rosand IFW5 drop weight machine. 14

2.10 - ADFEUP´s drop weight machine initial state. 15

3.1 - Final model of the ARS, made in *SolidWorks 2018*. 17

3.2 - The two positions of the ARS. 18

3.4 - SKF® NKI 35/20 TN needle bearing [17]. 19

3.5 - Free body diagram for the dynamic study of the interaction between anvil and ARS. 20

3.6 - ACE MC3350EUM-0 [19]. 25

3.7 - Stopping force along industrial shock-absorber´s stroke [20]. 25

3.8 - Parameters´ values inserted in the developed Matlab Simulink model, considering the maximum drop weight. 26

3.9 - Angular acceleration obtained in the developed Matlab Simulink model, considering the maximum drop weight. 27

3.10 - Factor of safety obtained when a $5063\ N$ is applied to the ARS´ rotating structure, recurring to *SolidWorks 2018*. 27

3.11 - New design of the actuation axle connector, made in *SolidWorks 2018*. 28

3.12 - Designed shock absorber pad, made in *SolidWorks 2018*. 28

3.13 - Final design of the ARS´ fixed structure, made in *SolidWorks 2018*. 29

3.14 - Currently implemented ARS´s arrangement. 30

3.15 - Initial anvil-impactor assembly. 31

3.16 - New specimen fixing structure. 32

3.17 - New anvil-impactor assembly design, made in SolidWorks 2018. 32

3.18 - Graph of the displacements-load of carbon fibre reinforced polymer (CFRP) substrates tested under impact at different temperatures: room temperature (RT), low temperature (LT) and high temperature (HT) [22]. 33

3.19 - Results for the angular acceleration obtained in the developed Matlab Simulink model, considering the minimum drop weight. 34
3.20 - Final arrangement of the anvil-impactor assembly. 35

4.1 - Diagram of the implemented pneumatic circuit. 37
4.2 - Stages of the clamp of the carriage´s cylinder functioning [5]. 38
4.3 - FESTO DSNU-32-100-PPV-A [24]. 39
4.4 - a) PARKER B3R5BXXXXH; b) PARKER B3R5BXXXXH symbol [25]. 39
4.5 - a) FESTO MHE2-MS1H-5/2-M7-K; b) FESTO MHE2-MS1H-5/2-M7-K symbol [27]. 40
4.6 - FESTO MSB4-AGA:C4:H3:N3-WP [28]. 41
4.7 - Lifting sub-system. 42
4.8 - Transtecno ECM-100/040 [29]. 43
4.9 - Electromen EM-115 [30]. 43
4.10 - Velocity acquisition sub-system. 43
4.11 - OMRON EE-SX670-WR [33]. 45
4.12 - OMRON EE-SX670-WR´s lead connections [33]. 45
4.13 - OMRON EE-SX670-WR´s Dark-ON mode [33]. 46
4.14 - Cherry D459-V3RD [34]. 46
4.15 - RS Pro 701-8253 [35]. 47
4.16 - OMRON E3FA-DN23 [36]. 47
4.17 - OMRON E3FA-DN23´s lead connections [36]. 48
4.18 - OMRON E3FA-DN23´s Dark-ON mode [36]. 48
4.19 - FESTO SME-8M-DS-24V-K-0,3-M8D [37]. 48
4.20 - Different types of accelerometer per application [21]. 49
4.21 - KISTLER 8704B5000 [38]. 50
4.22 - LabAmp of the type KISTLER 5165A [39]. 50
4.23 - Accelerometer configuration in the provided Kistler´s software. 51
4.24 - KISTLER 9333A [40]. 52
4.25 - Press force sensor configuration in the provided Kistler´s software. 52
4.26 - Measurement Computing´s PCIM-DDA06/16 [41]. 53
4.27 - Intecno ME22-300-6.000-2-LS1´s signals throughout time. 55
4.28 - Measurement Computing´s PCI-QUAD04 [43]. 55
4.29 - PS2502-4. 56
4.30 - Computer output conversion for a single line. 56
4.31 - Computer input conversion for a single line. 56
4.32 - Designed printed circuit board, in *gerber* format [6]. 57
4.33 - a) RS Pro 240W DRP240 Series [44]; b) RS Pro 96W MDR-100 Series [45]; c) RS Pro 10W MDR-10 Series [46]. 58

4.34 - a) SIEMENS 5SM3312-0 [47]; b) Schneider Electric´s Tesys GB2DB21 [48]; c) Schneider Electric´s Tesys GB2CB09 [49]; d) ABB SH201T-C10 [50]; 58

4.35 - Schneider Electronics´s XALK178E emergency button [51]. 59

4.36 - How transitions are processed in Simulink Stateflow®. 60

4.37 - Highest-level routine. 61

4.38 - Initial interface window. 61

4.39 - MAIN sub-routine. 62

4.40 - Select operating mode interface window. 62

4.41 - INIT sub-routine. 63

4.42 - FIND_VELAQ sub-routine. 63

4.43 - CHECK_ANVIL sub-routine. 64

4.44 - Set parameters interface window. 65

4.45 - Confirmation of the chosen parameters interface window. 65

4.46 - Set weights interface window. 66

4.47 - Manual control (TEST sub-routine) interface window. 67

4.48 - Lift anvil-impactor assembly interface window. 67

4.49 - Release anvil interface window. 68

4.50 - Results interface window. 68

4.51 - TEST sub-routine. 69

4.52 - GRAB_ANVIL sub-routine. 70

4.53 - Manual interface window. 71

4.54 - MANUAL sub-routine. 71

4.55 - SOS sub-routine. 72

4.56 - Emergency interface window. 72

4.57 - Command sequence´s flowchart. 73

5.1 - Single lap joint of type 1. 76

5.2 - Impact force versus time for the specimen of type 1 obtained in the ADFEUP´s drop weight machine (orange), Rosand´s machine (gray) and numerical data from *Abaqus* (blue). 77

5.3 - Impact force versus time for the specimen of type 2 obtained in the ADFEUP´s drop weight machine (orange), Rosand´s machine (gray) and numerical data from *Abaqus* (blue). 77

5.4 - Rosand machine´s specimen fixing structure. 78

5.5 - Three different experimental tests for specimens of type 1. 79

6.1 - Final state of the ADFEUP´s drop weight machine. 82

List of Tables

2.1 - Studied properties of adhesive joints and associated types of test [7]. 6
2.2 - Different impact tests categorized by velocity [7]. 7
2.3 - CEAST 9300 series´ machines specifications [13]. 12

3.1 - NKI 35/20 TN needle bearing properties [17]. 19
3.2 - Fasteners used to assemble the ARS. 30
3.3 - Fasteners used to assemble the new anvil-impactor assembly. 35

4.1 - Selected FESTO DSNU-32-100-PPV-A´s accessories [24]. 39
4.2 - Pneumatic circuit accessories. 41
4.3 - L298N board connections to the electrical circuit lines. 44
4.4 - Bit channels and the respective electrical circuit line association. 54

Acronyms

ADFEUP	Adhesives Investigation Group of FEUP
ARS	Anti-rebound sub-system
TAST	Thick Adherent Shear Test
DCB	Double Cantilever Beam
SENB	Single-Edge Notched Beam
CT	Compact Tension
ENF	End-Notched Flexure
SHPB	Split Hopkinson pressure bar
FEA	Finite element analysis
PZT	Lead zirconate titanate
CAI	Compression after impact
CFRP	Carbon fibre reinforced polymer
IEPE	Integrated Electronic PiezoElectric
DAQ	Data acquisition
PCB	Printed circuit board

Chapter 1

Introduction

1.1. Context and Motivation

An adhesive is a natural or synthetic substance capable of bonding two dissimilar surfaces, due to some physical or physicochemical phenomena, and can be the result of single or multi-component preparations. The use of adhesives has been a recurrent practice to mankind, dating back to ancient times, however only just about one century ago came to be a more serious contender for structural bonding [1, 2].

Adhesive joints have different properties when compared with other types of connections and, because of that, are sometimes preferred instead of screws, rivets or welds. Take for instance applications where lightweight is needed, such as in the automotive, the aeronautical and the aerospace areas [2]. Since there is an arising interest on this type of bonding and because it´s a relatively new field, it´s of great importance that further studies are made.

It was for the purpose of studying adhesives properties and contributing to this field of research that the Adhesives Investigation Group of FEUP (ADFEUP) was created. This group is responsible for multiple research projects and, therefore, needs the adequate equipment to correctly characterize adhesives under specific load conditions. Impact loading is one of the tests used to characterize them and is one of the concerns of ADFEUP, thus, an impact test machine is needed to provide means to carry out those experiments.

1.2. Objectives

This dissertation focus is to continue the work of four previous master's dissertations students, Castro [3], Barbosa [4], Ramos [5] and Sousa [6], into further development of a drop weight machine for adhesive joints impact testing.

The original specifications for the drop weight machine were defined by the first two authors, Castro [3] and Barbosa [4], and are as follows:

- Maximum energy on impact of 700 J;
- Minimum energy on impact of 50 J (at maximum velocity);
- Maximum velocity of 5 m/s;
- Anvil positioning resolution of 1mm;

In addition to these specifications, the machine should also have a variety of sub-systems that help in the execution of the machine´s actions.

This dissertation will revolve around the construction and improvement of some of these sub-systems, like the anti-rebound sub-system (ARS) and the new anvil-impactor assembly, which will have a piezoelectric accelerometer and a piezoelectric press force sensor implemented. It will also be needed to improve and finalize the pneumatic and electrical circuits, as well as to develop the command software and interface that controls them.

1.3. Methodology

Initially, an evaluation of the drop weight machine´s state of development was made. For that purpose, all the previous masters dissertation´s reports were analysed and the requirements to start the project identified.

Although the design for the ARS had already been initiated by Sousa [6], most of the parts still needed adjustments as well as the drawings for their manufacture. Also, as it was said in the previous section, a new anvil-impactor assembly was to be implemented and it was needed to design some parts that would allow the mounting of a load cell and an accelerometer. Since the ordering of all material and fabrication of the mechanical parts would take a significant amount of time to be completely ready, the first task of this project was to finish all the drawings of the mechanical parts and order the materials for their manufacture.

After that starting stage, a careful revision of the pneumatic and electrical circuit was done. It was concluded that those circuits would have to be changed to implement the new sub-systems and hardware, as well as making some corrections. The missing components were identified and ordered.

Having both pneumatic and electrical circuits assembled, the next step was to program the command software, to define how the drop weight machine should operate, and an user-friendly interface, for an easy interaction.

Lastly, some impact tests on adhesive joints were performed to validate the machine functioning and to eliminate some malfunctions that could have been found.

1.4. Thesis Outline

This thesis is organized into six chapters, each one covering a different topic that is considered relevant to better understand the work done.

In the present chapter, a brief introduction to the project is presented.

In chapter 2, a literature review about adhesives, impact testing and commercial drop weight machines is made.

Chapter 3 describes the development of the ARS and the anvil-impactor assembly. It will include their final design and the simulations made to ensure the functionality of the machine under the specified working conditions.

Chapter 4 focuses on the hardware used for the actuation mechanisms and on the command logic that controls them.

In chapter 5, some results of impact tests, performed in adhesive joints, are shown and posteriorly compared with results obtained with a different machine, namely a Rosand IFW5, and with numerical data for the same working conditions.

Finally, in chapter 6 this dissertation will be concluded and present some proposals for the future work on ADFEUP´s drop weight machine.

Chapter 2

Literature Review

In this chapter, a literature review on adhesives, different types of impact tests on adhesive joints and commercial drop weight machines is presented.

2.1. Adhesives

As it was said in section 1.1, adhesives are substances capable of joining two bodies with different surface characteristics, called the substrates, and can be the result of a single-component or a multi-component preparation. The use of this type of technology dates to ancient times, in which most of the adhesives were from natural products such as bones, milk, skins, fish or plants. Since 1990, adhesives made from synthetic polymers were introduced and 40 years later they became a more serious contender for structural bonding because of the progressive development of the polymer's properties [2].

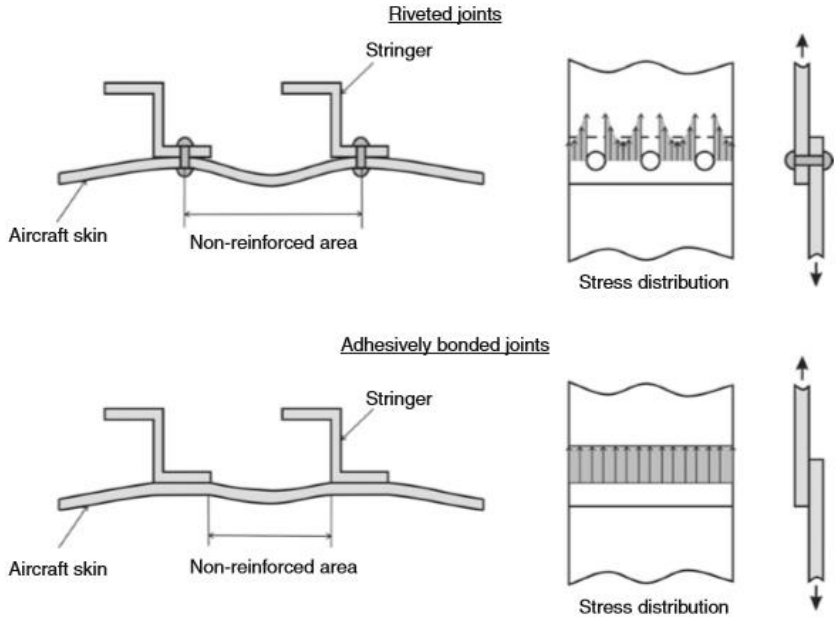

Figure 2.1 - Stress distribution comparison between bonded surfaces using standard fasteners and adhesive materials [2].

There are many advantages that can be pointed out when comparing adhesive joints with other methods of joining bodies. One of those advantages, and perhaps the most important, is that they allow a more uniform stress distribution along the bonded area, enabling a higher stiffness. This is due to adhesives being spread over a large area and because they don't require holes in the surfaces, as what happens with screws and rivets. This behaviour is shown in Figure 2.1. Among the other advantages that adhesives offer, it is known that they provide better damping across the bond, contribute for weight reduction and allow a flexible joint designs [2].

Although all these advantages can be enumerated, adhesive joints also have some disadvantages, such as low resistance to perpendicular forces to the joint´s plane, low stability in extreme temperature or humidity, require surface preparation and long curing times [2].

2.2. Impact tests for adhesive joints

When a high load is applied in an, almost, instantaneous period of time on a material, it can be considered as an impact load. When this type of loading is used to test adhesives, they are subjected to high strain rates and, consequently, properties like stiffness, yield stress and elongation are affected [7]. These properties can be studied by means of specific tests, that can be seen in Table 2.1.

Table 2.1 - Studied properties of adhesive joints and associated types of test [7].

Measured properties	**Tests**
Tensile stiffness and strength	Tensile test
Shear stiffness and strength	Thick Adherent Shear Test (TAST), Torsion test, Arcan test
Fracture toughness (Mode I)	Double Cantilever Beam (DCB) test, Single-Edge Notched Beam (SENB) test, Compact Tension (CT) test
Fracture toughness (Mode II)	End-Notched Flexure (ENF) test
Fracture toughness (Mixed mode)	Custom specimen designs

However, different types of tests are made to assess the impact behaviour of adhesive joints. These tests give important information about the adhesive joint tested, like the adherent properties, surface preparation or joint geometry [7]. When studying the structural integrity of adhesive joints under impact conditions, three questions should be kept in mind:

- Is the bonded joint´s strength reduced by high load rates?
- Can the bonded structure withstand large amounts of energy under impact?
- Can the impact behaviour of the bonded joint be understood and predicted?

To answer these questions, it´s important to have simple, yet accurate, tests that can be made in a reliable and repeatable way [8]. There are some tests that can be performed on adhesive joints and they are usually divided in terms of velocity, as it is shown in Table 2.2 [7].

Table 2.2 - Different impact tests categorized by velocity [7].

Test classification	Crosshead speed	Suitable test equipment
Low velocity	Up to 5 m/s	Pendulum impact tester
Medium Velocity	Between 5 and 10 m/s	Drop weight impact tester
High velocity	Between 10 and 100 m/s	Split Hopkins pressure bar (SHPB) tester

In the next sections, a description of the block impact test, SHPB test and drop weight impact test is presented.

2.2.1. Block Impact Test

The block impact test is a form of pendulum impact test, similar to the Izod impact test and to the Charpy impact test, that are used to measure resilience. This test´s set-up consists on an upper block that is adhesively bonded with a larger block, which, in turn, is attached to the base of the test equipment. The test is carried out by striking the upper block with the hammer (the pendulum) in a parallel direction to the bond surface, as Figure 2.2 demonstrates. The energy required to fracture the specimen is then obtained by the energy lost by the hammer [2].

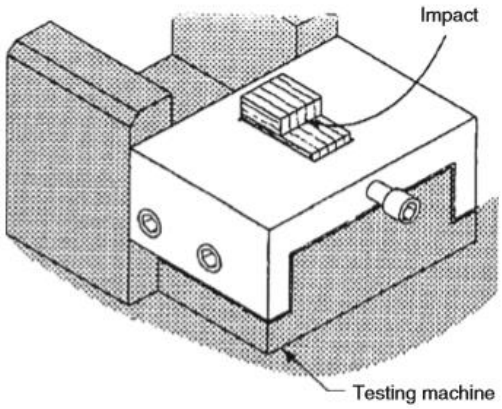

Figure 2.2 - Block impact test apparatus [2].

Adams and Harris [9] made a finite element analysis (FEA) of the standard specimen for this test with the aim of determining the stress concentration in the specimen. First, the authors identified three different possible cases of contact between the hammer and the specimen, in the moment of impact, which are represented in Figure 2.3. In the cases where misalignment occurs (case 2 and 3), some peeling is identified, meaning that the results obtained wouldn’t be for a pure shear load. And even when the hammer hits the

upper block in a perfectly aligned way (case 1), the results show the stresses along the bond are not constant. Due to these analysis´ results Adams and Harris [9] concluded that block impact test results could not be taken as absolute information about energy absorption of the bond, even though it can still be useful for comparing the behaviour of different types of adhesives [2, 8].

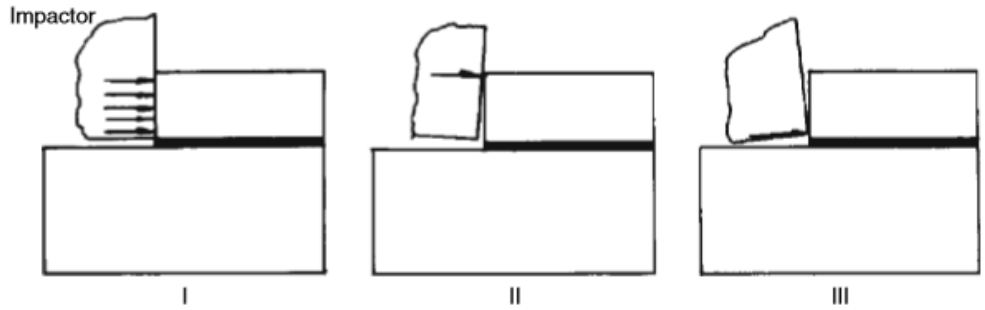

Figure 2.3 - Possible impact cases between the hammer and the upper block of the specimen [2].

2.2.2. SHPB Test

The split Hopkinson pressure bar test is the main test used to study the dynamic behaviour of a great variety of different materials at medium to high strain rates ($0.5 – 5 \times 10^3$ s^{-1}). Originally, its name came from the apparatus that B. Hopkinson used when testing the pressure wave propagation, generated by a projectile, through metals. His experiment was to strike one of the ends of a long and thin bar, which was placed horizontally, with a projectile, creating a pressure pulse that would propagate to the other end. In that second end, there would be a partially attached cylinder that would later be projected by the generated pulse against a ballistic pendulum capable of measuring the momentum contained [2].

Later, Kolsky introduced a new variant of the technic used by Hopkinson, that is the most commonly used nowadays, in which he added a second bar after the cylinder, originating the name "Split Hopkinson Pressure Bar". In this case, the projectile, fired from a pneumatic gun, strikes the first bar (given the name of incident bar or input bar), generating a pressure pulse that will be transmitted to a specimen. At this point, part of the impact energy will be reflected and the other part will propagate through the specimen and eventually be transmitted to a second bar (called the transmitter bar or output bar) [2]. The basic setup for the described experiment can be seen below, as well as a Lagrangian diagram that shows the propagation of the pulse throughout time, in Figure 2.4.

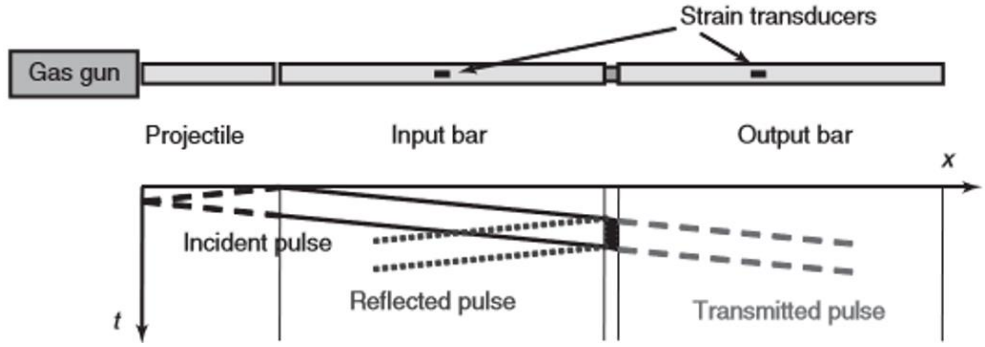

Figure 2.4 - Basic setup and Lagrangian diagram for compressive tests on a SHPB machine [8].

By measuring the reflected and the transmitted pulses in their respective bars, with help of strain gauges, it is possible to obtain the stress, σ, the strain, ε, and the strain rate, ε̇, by using the Expressions (2.1) - (2.3):

$$\sigma(t) = E_0 \frac{A_0}{A} \varepsilon_{trans}(t) \tag{2.1}$$

$$\varepsilon(t) = -2 \frac{c_0}{L} \int \varepsilon_{refl}(t)\, dt \tag{2.2}$$

$$\dot{\varepsilon}(t) = -2 \frac{c_0}{L} \varepsilon_{refl}(t) \tag{2.3}$$

Where E_0, A_0 and c_0 are the Young´s modulus, the cross section and the pressure wave velocity of the bar; A and L are the cross section and the length of the specimen; ε_{trans} and ε_{refl} are the transmitted and reflected strain pulses, respectively, directly measured by resistance or piezoresistive strain gauges. These equations consider that the specimen achieves an equilibrium state, which requires that the pulse´s length is smaller than the specimen´s length. With the calculated results it is possible to reconstruct a dynamic strain-stress diagram of the specimen [2, 8].

Although the described method is used to test compressive loads, there´s also one to test tensile loads, introduced by Chen [10], that just requires a small modification, which is to insert a split ring around the specimen, Figure 2.5. This mechanical part is longer then the specimen and is responsible to transmit the full strain pulse generated in the first bar to the second, without the contribution of the material to be tested. When the transmitted pulse reaches the free end of the second bar it will be reflected as a tensile pulse. The split ring can only constraint compressive loads and not tensile loads, therefore it will allow the material to be tested in tension. In this case, since the second bar is the one that transmits the tensile load to the specimen, this will be the input bar, and the first bar will be the output bar. The setup for this experiment and for its corresponding Lagrangian diagram is shown in the Figure 2.6 [8].

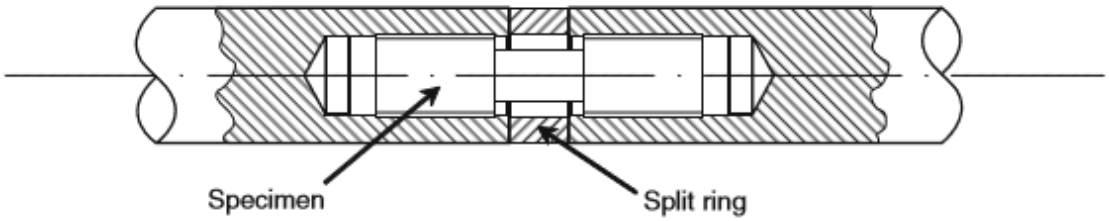

Figure 2.5 - Solution for the SHPB tensile test, as proposed by Chen [2, 10].

As it was previously stated, the SHPB impact test can be performed in many materials but regarding to adhesives this method is mostly used on adhesive materials themselves

or in the form of a butt joint or lap joint [2]. Figure 2.7 shows a representation of the mentioned joints.

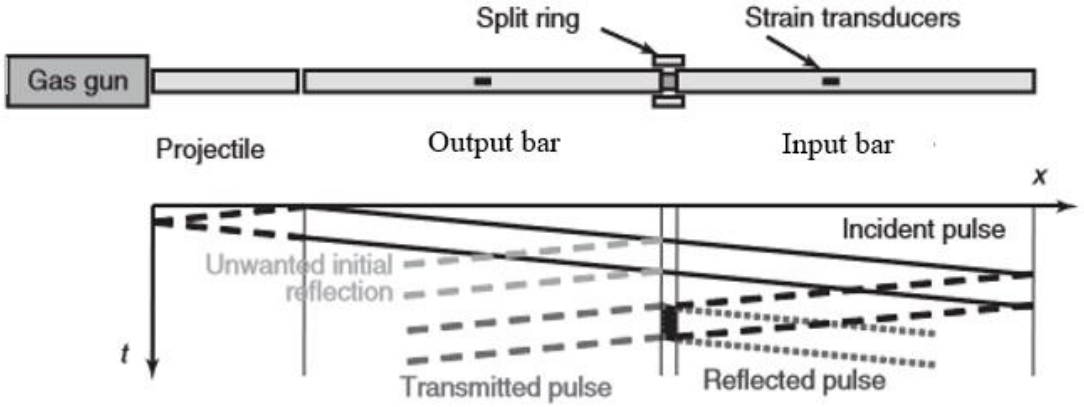

Figure 2.6 - Basic setup and Lagrangian diagram for tensile tests on a SHPB machine [8].

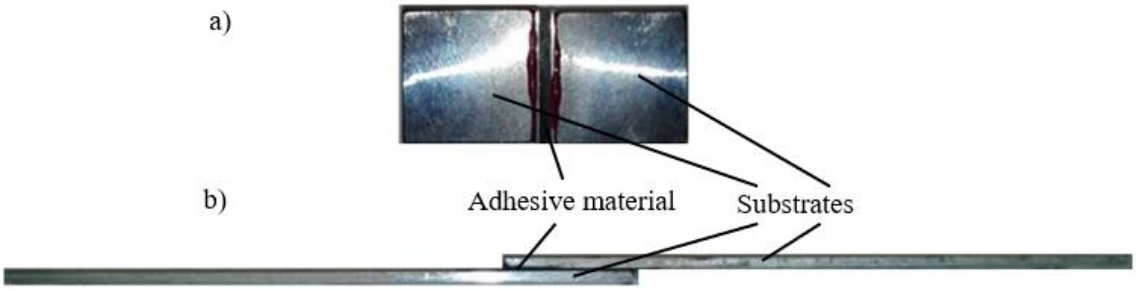

Figure 2.7 - a) Butt joint example; b) Single lap joint example.

2.2.3. Drop Weight Test

Another type of impact test and the most important for this dissertation is the drop weight test, performed in a drop weight machine (sometimes also referred as drop tower). This test is performed by simply releasing a drop mass from a defined height on an adhesive material or adhesive joint. The specimen can be tested under compressive or tensile loads depending on how it´s fixed on the structure that holds it.

The specimen will be hit by an impactor that carries a kinetic energy equal to the potential energy that the same impactor has before being released. However, it´s not always like this, since drop weight machines can have an acceleration unit sub-system that increases the impact energy by means of an elastic mechanism. In addition to this sub-system, there are also others that can be equipped like an environmental chamber, that changes the specimen´s surrounding conditions and, consequently, its properties, or an anti-rebound mechanism, that holds the machine´s impactor after the first impact (preventing posterior impacts).

The most used hardware to measure the impact load in these types of tests are piezoelectrical sensors, usually an accelerometer or a load cell. This type of sensors creates an electric charge (piezoelectricity) that is directly proportional to the mechanical load applied to a piezoelectric material, like a crystal quartz, or a ceramic, such as the lead zirconate titanate (PZT). They are built in a very robust and compact structure, since

they don´t have moving parts, and provide great reliability in their measurements, which are good properties for impact applications.

In order to understand the specification ranges and special features that the current commercialized drop weight machines have, a description of some of these machines´ series is presented in the next section.

2.3. Commercial Drop Weight Machines

There are many models of drop weight machines available in the market and although they are not specially designed to test adhesive joints, they can still be used for that purpose. The main differences between the machines are their specifications, like the maximum drop weight and the maximum drop height (or maximum velocity on impact, since all potential energy is going to be converted in kinetic energy), which will, consequently, influence their energy range. Most of the companies that sell this type of impact equipment provide a complete series of machines with different ranges in their specifications, so they can satisfy the needs of various costumers. In this sub-chapter some commercial drop weight machines are presented, as well as their specifications and functionalities.

2.3.1. Zwick Roell – HIT and DWT Series

The HIT and DWT series, commercialized by the company Zwick Roell, provide a great variety of drop weight machines that allow different testing conditions on the material to be tested.

The HIT series, shown in Figure 2.8 was especially designed to perform impact tests on plastics and some of them can also do compression after impact (CAI) on composite materials. It is composed by machines whose maximum energy on impact ranges from 100 to 670 J, maximum drop height ranges from 1000 to 1500 mm and maximum dropping mass´s weight that ranges from 10.2 to 40 kg. However, if the machine is equipped with an acceleration unit its maximum energy on impact greatly increases. Take for instance the Amsler HIT 2000F, in which the initial potential energy is 440 J and maximum drop weight is 29.4 kg (therefore, its maximum height is 1500 mm, achieving a maximum velocity of 5.4 m/s), if an acceleration unit is installed in this machine, it can reach an energy of 2000 J at 19.4 m/s. Some of these machines are also prepared to prevent multiple impacts using an ARS [11].

The DWT series provides machines needed to perform high energy impact tests, ranging from 20 kJ to 100 kJ. In this series, the machine that performs the highest energy impact tests is the DWT 100-5, which allows a 2040 kg drop weight to be released from a height of 5 m. This type of high energy impact test machines is mostly used to study the fracture surface of ferritic steels [12].

Figure 2.8 - HIT series commercialized by Zwick Roell [11].

2.3.2. Instron – CEAST 9000 series

Instron is another company that also sells equipment for impact testing. Its CEAST 9300 series is composed by three machines, the CEAST 9310, the CEAST 9340 and the CEAST 9350. The CEAST 9310 is a table-top machine for low energy impact tests (from 0.15 to 20.4 J), while the others are large floor-mounted machines that allow high energy impact tests (up to 757 J on the CEAST 9350). The CEAST 9350 has multiple optional accessories like the high energy system, that increases its maximum impact energy up to 1800 J, the ARS and the environmental chamber, that changes the material´s surrounding conditions, like, for example, temperature and humidity. Table 2.3 presents the specifications for each CEAST 9000 series´ machines [13].

Table 2.3 - CEAST 9300 series´ machines specifications [13].

		CEAST 9310	**CEAST 9340**	**CEAST 9350**	**CEAST 9350 (with optional features)**
Energy (J)	Min.	0.15	0.3	0.59	0.59
	Max.	20.4	405	757	1800
Drop height (mm)	Min.	30	30	30	30
	Max.	700	1100	1100	1100
Drop mass (kg)	Min.	0.5	1	2	2
	Max.	3	37.5	70	70
Velocity on impact (m/s)	Min.	0.77	0.77	0.77	0.77
	Max.	3.7	4.65	4.65	24
ARS		No	No	No	Yes
Environmental chamber		No	No	No	Yes

2.3.3. Imatek – IM10 and DWTT series

Imatek is a relatively new company in the market, however it´s specialized in materials testing, particularly impact testing.

The IM10 series is composed of machines that can perform low and medium energy tests on materials and specimens of various geometries. Machines of this series can achieve a maximum energy on impact that ranges from 294 to 882 J, a drop height that ranges from 1000 to 3000 mm and a fixed maximum drop weight of 30 kg. All these machines have optional features like ARS, acceleration units and environmental chambers. If an acceleration unit is installed, the maximum energy on impact ranges from 500 to 2000 J and can achieve velocities up to 20 m/s [14].

Imatek also produces a series of high energy drop weight machines, designed to test the fracture characteristics on steel specimens, called DWTT series. On this series the maximum energy on impact ranges from 30625 to 101250 J, the maximum drop height ranges from 2500 to 4200 mm and the drop mass ranges from 1250 to 2500 kg. Although every standard drop weight machine of this series has a fixed drop mass, an optional feature that enables the drop weight to be variable is available, making the energy on impact range wider [15].

2.3.4. ADFEUP´s Drop Weight Machine

Before deciding to develop its own drop weight machine, ADFEUP used a Rosand IFW5 (Figure 2.9), which is located in FEUP´s testing laboratory, to carry out its studies. However, this drop weight machine proved too limited for the experiments that the group wanted to do, since its maximum energy is 300 J and its maximum velocity on impact is 4 m/s. The desire to design a drop weight machine grew, not only for the necessity of means to continue those experiments but also for academic purposes, enabling students to consolidate their knowledge during their master's in mechanical engineering

Like in every project, the initial point was to design the main structure of the machine according to the specifications needed, which were defined by Castro [3], Barbosa [4] and the ADFEUP´s members at that time. These specifications were as it follows:

- Maximum energy on impact of 700 J;
- Minimum energy on impact of 50 J (at maximum velocity);
- Maximum velocity of 5 m/s;
- Anvil positioning resolution of 1mm.

After the validation of the designed structure, Ramos [5] mounted the initial structure and implemented various important sub-systems. The sub-systems in question are an upper motor and transmission mechanism to move the carriage, a velocity acquisition sub-system and an anvil-impactor assembly. Ramos [5] also chose some sensors and made a pneumatic circuit to control the cylinder in charge of the drop weight release.

Figure 2.9 - FEUP´s Rosand IFW5 drop weight machine.

Sousa [6] was responsible for the initial electrical circuit assembly, a primordial command sequence to control the machine and the design of a PID controller that can position the carriage accurately. Sousa [6] also started the design of an ARS that would later be modified, validated and implemented by the work of this thesis, described in chapter 3.

Although a functioning machine was received in the beginning of this dissertation, there were still many implementations to be added and adjustments to be made in the electrical and pneumatic circuits, as well as in the control sequence. The final product of the four previous dissertations is presented in Figure 2.10.

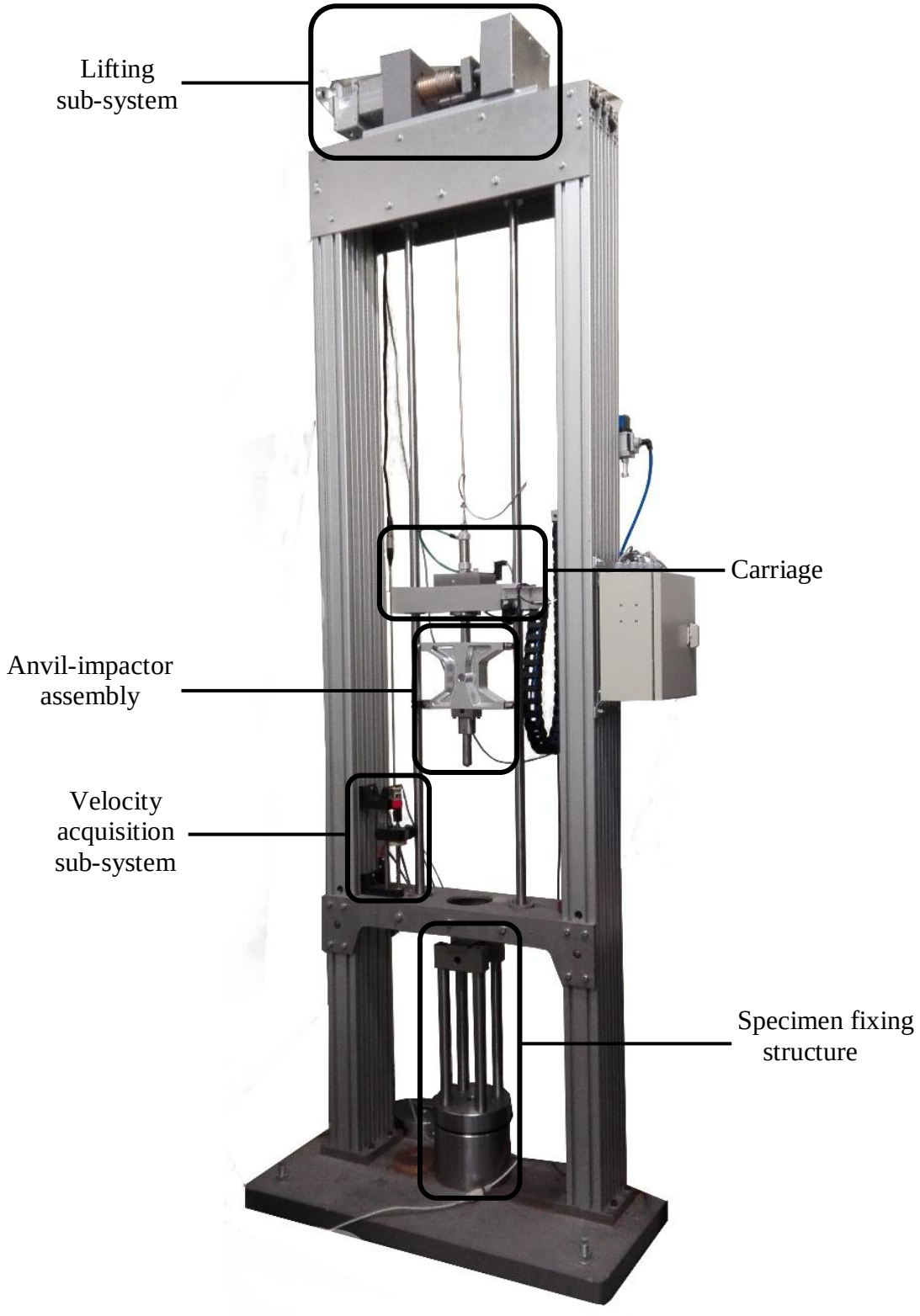

Figure 2.10 - ADFEUP´s drop weight machine initial state.

Chapter 3

Developed Sub-Systems

This chapter describes the designing and the validation process for two new implementations: the ARS and the anvil-impactor assembly.

3.1. Anti-rebound sub-system (ARS)

As it was previously said, Sousa [6] made an initial design of an ARS, however that mechanism had some flaws that had to be corrected. In addition, no mechanical parts´ drawings were made and no materials to fabricate the parts were chosen. As such, the initial tasks for this dissertation were to carefully analyse and correct his work, to make the mechanical parts´ drawings, that can be seen in Appendix A, and to choose all the materials for their fabrication. All these tasks were done with the help of *SolidWorks 2018* and the final design of the ARS can be seen in Figure 3.1.

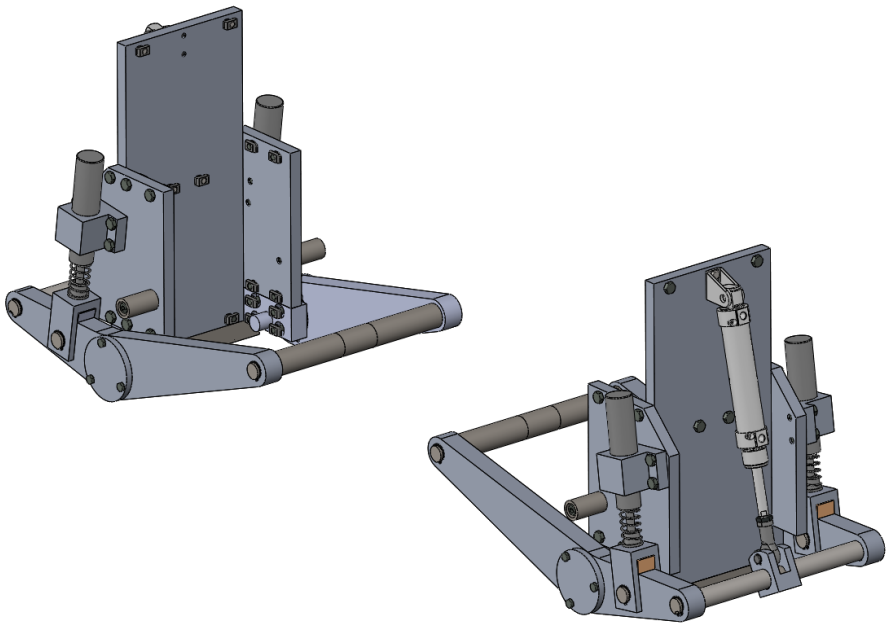

Figure 3.1 - Final model of the ARS, made in *SolidWorks 2018*.

This ARS is a mechanism that consists in two rotating arms, fixed at each column of the machine, that will hold the anvil-impactor assembly after the first impact on the specimen, preventing the test results to be influenced by consequent rebounds. This way, the tests performed on this drop weight machine can give accurate and useful data about the adhesive joint tested. The arms work on the principle of a lever and each one is actuated by one pneumatic cylinder fixed on the structure of the machine. When the cylinders are extended the ARS is considered in the active position and when they are retracted is considered in the inactive position, like shown in Figure 3.2. If, at any time, an emergency is declared, the ARS will act. For example, if an emergency button is pressed while the anvil is falling, the ARS will hold the anvil preventing it from damaging the specimen. To be able to do that, this mechanism also has a pair of shock-absorbers in each arm that should be able to dissipate all the energy when the heaviest drop mass is released from the highest point of the anvil´s stroke. In case of energy failure the springs of the shock absorber will force the rotation of the arms to a safe position.

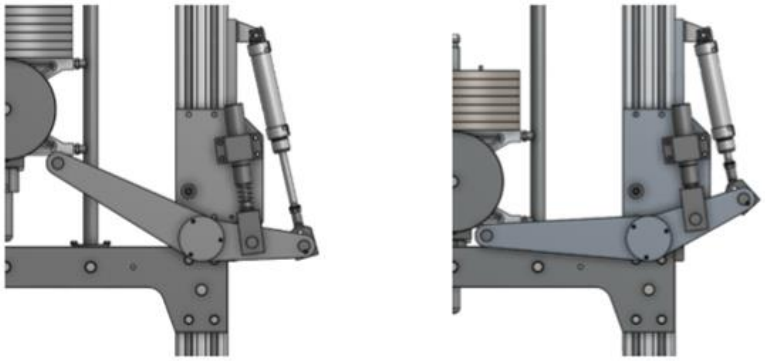

Active (safety) position Inactive (test) position

Figure 3.2 - The two positions of the ARS.

3.1.1. Rotating Structure

The rotating structure of the ARS is responsible for stopping the anvil and, because of that, is going to be positioned where the most stress concentrates. Therefore, the designed structure needs to be strong enough to withstand impact loads of the falling anvil and light weighted so it has a reduced inertia and can be quickly positioned. The main parts that assemble this structure are presented in Figure 3.3.

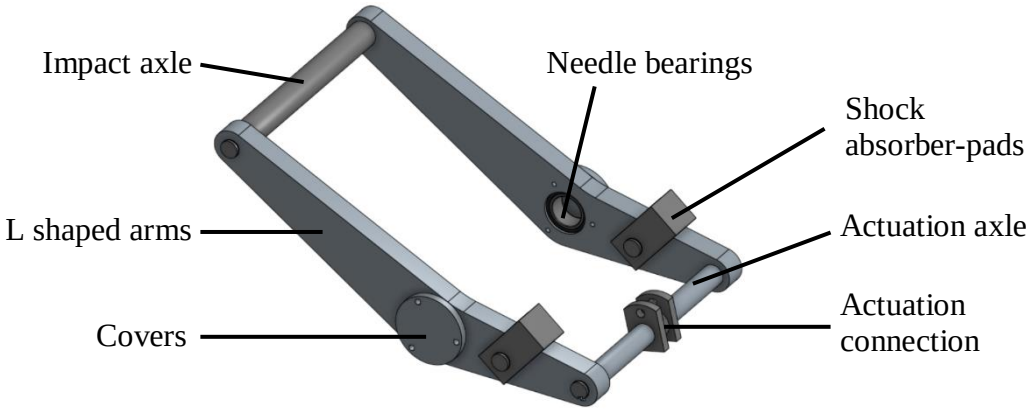

Figure 3.3 - Rotating structure of the ARS.

3.1.1.1. Main Body

The main body´s parts are the ones that contribute the most for the weight of the ARS, thus, to meet the light weight requirement, they were fabricated from aluminium alloy plates. Those aluminium alloy plates were the AW 7075 - T651 (used for the L shaped arms) and the AW 6082 - T651 (used for the covers), which were bought from KMS [16].

3.1.1.2. Needle Bearings

The rotating structure only contacts with the fixed structure by means of three components which are the shock-absorbers, the pneumatic actuators and the bearings. Since the shock-absorbers can´t always follow the arm´s rotating movement, they break contact with it and, when that occurs, only the bearings and the pneumatic actuator contact with the fixed structure. To try to preserve the pneumatic actuator, the chosen bearings must withstand the full impact load capacity of the machine, which Ramos [5] calculated to be 66.88 kN. This value represents the transmitted force to the levelling foots and although this will not be the load applied on the bearings, it was the one used because it´s the highest value found in the structure of the machine. So, considering this value, a safety coefficient of 3.5 and that the ARS has 4 bearings, each bearing should withstand a load around 60 kN.

In addition to being able to handle the high impact loads mentioned above, the chosen bearings should also be compact, due to the geometry of the parts that assemble the ARS. The SKF® NKI 35/20 TN needle bearings [17], shown in Figure 3.4, were chosen because they combine a high radial static load rating with the possibility to be mounted in a compact volume. The characteristics of these needle bearings are shown in Table 3.1 and their implementation can be seen in the ARS assembly´s drawings in Appendix A.

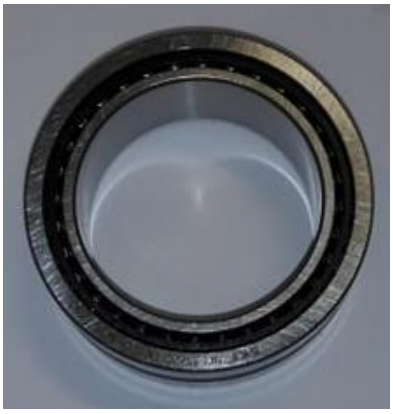

Figure 3.4 - SKF® NKI 35/20 TN needle bearing [17].

Table 3.1 - NKI 35/20 TN needle bearing properties [17].

m (kg) **Mass**	**C_r (kN)** **Radial dynamic load rating**	**C_{0r} (kN)** **Radial static load rating**	**P_u (kN)** **Radial fatigue limit load**
0.12	29.7	60	7.5

3.1.1.3. Impact and Actuation Axles

The impact axle, as the name suggests, is the component that directly collides with the falling anvil, whether during a rebound or a fall from one of the points of its stroke. Therefore, in order to choose the material from which this axle is going to be fabricated, one has to consider the worst-case scenario, which happens when the anvil falls from the highest point with the heaviest drop mass attached and collides with the said axle. Thus, it must be considered that the drop mass of the anvil is 56 kg and is going to fall from 1.27 m. The selected material was the N540 stainless steel from UniversalAfir [18], since it´s a material capable of withstand high loads and also because it´s not very influenced by corrosion over time. Since the actuator axle doesn't require such a high-performance material, the M310 RD stainless steel from UniversalAfir [18] was chosen.

To validate the choice made, a simulation, based on a finite element analysis, using *SolidWorks 2018* had to be made. However, before doing such, the maximum impact force, $F_{A,max}$, had to be calculated by making a dynamic study of the interaction between the ARS and the anvil impactor assembly.

To initiate this dynamic study, a free body diagram (see Figure 3.5) was defined to identify all the forces at stake in this interaction.

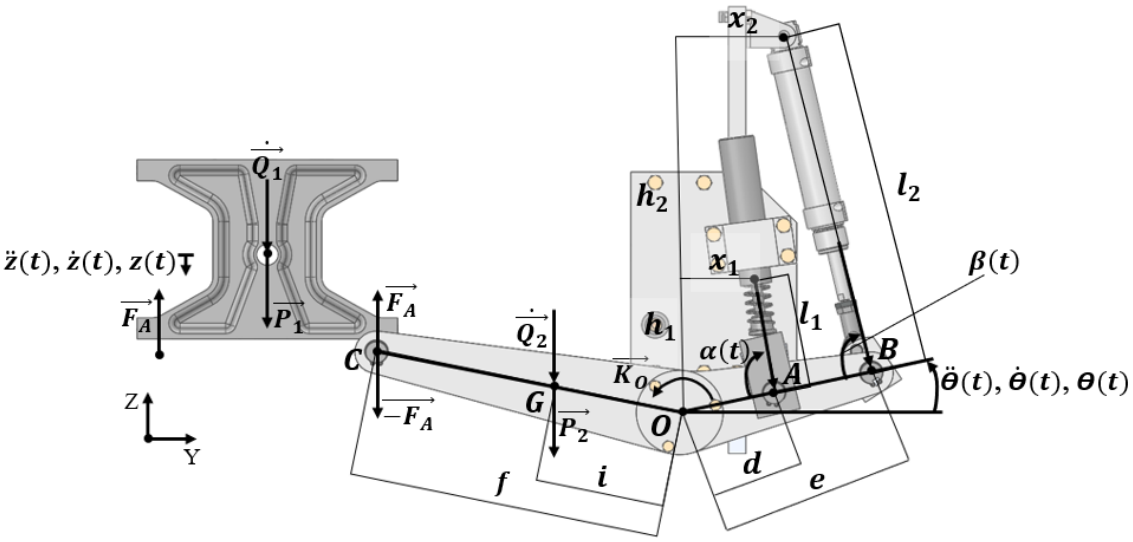

Figure 3.5 - Free body diagram for the dynamic study of the interaction between anvil and ARS.

By analysing both bodies separately, starting by the anvil-impactor assembly and knowing

$$\overrightarrow{P_1} = \begin{bmatrix} 0 \\ 0 \\ -m_1 \cdot g \end{bmatrix}; \quad \overrightarrow{\dot{Q}_1} = \begin{bmatrix} 0 \\ 0 \\ -m_1 \cdot \ddot{z}(t) \end{bmatrix}; \quad \overrightarrow{F_A} = \begin{bmatrix} 0 \\ 0 \\ 2F_A \end{bmatrix}; \tag{3.1}$$

Where m_1, g, $\ddot{z}(t)$ and F_A represent the drop mass, the gravity´s acceleration, the drop mass acceleration throughout time and the absolute value of the force transmitted to each of the ARS´ arms, respectively.

Knowing that the sum of the external forces ($\sum \overrightarrow{F^{ext}}$) equals the sum of the quantities of acceleration ($\sum \dot{\vec{Q}}$):

$$\sum \overrightarrow{F^{ext}} = \sum \dot{\vec{Q}} \Leftrightarrow \overrightarrow{P_1} + \overrightarrow{F_A} = \dot{\overrightarrow{Q_1}} \tag{3.2}$$

We can easily achieve the following expression:

$$F_A = \frac{m_1 \left(g - \ddot{z}(t)\right)}{2} \tag{3.3}$$

Now, analysing the ARS sub-system we obtain the following vectors for the displacements of the represented points (A, B, C and G):

$$\overrightarrow{OA} = \begin{bmatrix} 0 \\ d \cdot \cos\left(\theta(t)\right) \\ d \cdot \text{sen}\left(\theta(t)\right) \end{bmatrix}; \ \overrightarrow{OB} = \begin{bmatrix} 0 \\ e \cdot \cos\left(\theta(t)\right) \\ e \cdot \text{sen}\left(\theta(t)\right) \end{bmatrix}; \tag{3.4}$$

$$\overrightarrow{OC} = \begin{bmatrix} 0 \\ -f \cdot \cos\left(\frac{\pi}{6} - \theta(t)\right) \\ f \cdot \text{sen}\left(\frac{\pi}{6} - \theta(t)\right) \end{bmatrix}; \ \overrightarrow{OG} = \begin{bmatrix} 0 \\ -i \cdot \cos\left(\frac{\pi}{6} - \theta(t)\right) \\ i \cdot \text{sen}\left(\frac{\pi}{6} - \theta(t)\right) \end{bmatrix}; \tag{3.5}$$

Where d, e, f and i are the distances between the arm´s axle and the points A, B, C and G, respectively, and $\theta(t)$ represents the angular position of the arm throughout time, being the main degree of freedom in this sub-system.

It´s possible to define the vectors for the velocities and accelerations that will later be needed by deriving some of the previous vectors:

$$\dot{\overrightarrow{OA}} = \begin{bmatrix} 0 \\ -d \cdot \dot{\theta}(t) \cdot \text{sen}\left(\theta(t)\right) \\ d \cdot \dot{\theta}(t) \cdot \cos\left(\theta(t)\right) \end{bmatrix}; \ \dot{\overrightarrow{OG}} = \begin{bmatrix} 0 \\ -i \cdot \dot{\theta}(t) \cdot \text{sen}\left(\frac{\pi}{6} - \theta(t)\right) \\ -i \cdot \dot{\theta}(t) \cdot \cos\left(\frac{\pi}{6} - \theta(t)\right) \end{bmatrix}; \tag{3.6}$$

$$\ddot{\overrightarrow{OG}} = \begin{bmatrix} 0 \\ -i \cdot \ddot{\theta}(t) \cdot \text{sen}\left(\frac{\pi}{6} - \theta(t)\right) + i \cdot \dot{\theta}^2(t) \cdot \cos\left(\frac{\pi}{6} - \theta(t)\right) \\ -i \cdot \dot{\theta}(t) \cdot \cos\left(\frac{\pi}{6} - \theta(t)\right) - i \cdot \dot{\theta}^2(t) \cdot \text{sen}\left(\frac{\pi}{6} - \theta(t)\right) \end{bmatrix}; \quad (3.7)$$

Where $\dot{\theta}(t)$ and $\ddot{\theta}(t)$ are the first and second derivate of $\theta(t)$, which also means that they represent the angular velocity and the angular acceleration of the ARS arm throughout time, respectively.

The forces applied on the ARS are its own weight ($\overrightarrow{P_2}$), the impact force ($\overrightarrow{F_A}$), cylinder´s force ($\overrightarrow{F_{Cyl.}}$), shock-absorber force ($\overrightarrow{F_{Abs.}}$) and the dynamic momentum ($\overrightarrow{K_O}$):

$$\overrightarrow{P_2} = \begin{bmatrix} 0 \\ 0 \\ -m_2 \cdot g \end{bmatrix}; \ \overrightarrow{F_A} = \begin{bmatrix} 0 \\ 0 \\ -F_A \end{bmatrix}; \ \overrightarrow{F_{Cyl.}} = \begin{bmatrix} 0 \\ F_{cyl} \cdot \cos\left(\beta(t)\right) \\ -F_{cyl} \cdot sen\left(\beta(t)\right) \end{bmatrix}; \quad (3.8)$$

$$\overrightarrow{F_{Abs.}} = \begin{bmatrix} 0 \\ F_{abs} \cdot \cos(\alpha(t)) \\ -F_{abs} \cdot \text{sen}(\alpha(t)) \end{bmatrix}; \quad (3.9)$$

$$\dot{\overrightarrow{Q_2}} = m_2 \times \ddot{\overrightarrow{OG}} =$$

$$\begin{bmatrix} 0 \\ -m_2 \cdot i \cdot \ddot{\theta}(t) \cdot \text{sen}\left(\frac{\pi}{6} - \theta(t)\right) + m_2 \cdot i \cdot \dot{\theta}^2(t) \cdot \cos\left(\frac{\pi}{6} - \theta(t)\right) \\ -m_2 \cdot i \cdot \ddot{\theta}(t) \cdot \cos\left(\frac{\pi}{6} - \theta(t)\right) - m_2 \cdot i \cdot \dot{\theta}^2(t) \cdot \text{sen}\left(\frac{\pi}{6} - \theta(t)\right) \end{bmatrix}; \quad (3.10)$$

$$\overrightarrow{H_G} = \begin{bmatrix} I_{xx} \cdot \dot{\theta}(t) \\ 0 \\ 0 \end{bmatrix}; \ \overrightarrow{K_G} = \dot{\overrightarrow{H_G}} = \begin{bmatrix} I_{xx} \cdot \ddot{\theta}(t) \\ 0 \\ 0 \end{bmatrix}; \quad (3.11)$$

$$\overrightarrow{K_O} = \overrightarrow{K_G} + \overrightarrow{OG} \times \dot{\overrightarrow{Q_2}} = \begin{bmatrix} I_{xx} \cdot \ddot{\theta}(t) + m_2 \cdot i^2 \cdot \ddot{\theta}(t) \\ 0 \\ 0 \end{bmatrix}; \quad (3.12)$$

Where m_2, F_{cyl}, F_{abs}, I_{xx}, $\alpha\,(t)$ and $\beta(t)$ represent the ARS´s mass, the cylinders force, the shock-absorbers force, the moment of inertia in the ARS centre of mass, the

angle between the shock-absorbers and the ARS´s arm and the angle between the cylinder and the ARS´s arm, respectively.

It is also known that the shock absorber force is proportional to the velocity, so $\overrightarrow{F_{Abs.}}$ can also be defined as:

$$\overrightarrow{F_{Abs.}} = \begin{bmatrix} 0 \\ -c \cdot d \cdot \cos(\alpha(t)) \cdot \operatorname{sen}(\theta(t)) \cdot \dot{\theta}(t) \\ -c \cdot d \cdot \operatorname{sen}(\alpha(t)) \cdot \cos(\theta(t)) \cdot \dot{\theta}(t) \end{bmatrix} \tag{3.13}$$

After defining all these vectors and knowing that the sum of the external momentums ($\sum \overrightarrow{M_O^{ext}}$) equals the sum of the dynamic momentums ($\sum \overrightarrow{K_O}$), it´s possible to use the following expression:

$$\sum \overrightarrow{M_O^{ext}} = \sum \overrightarrow{K_O} \Leftrightarrow$$
$$\overrightarrow{OA} \times \overrightarrow{F_{Abs.}} + \overrightarrow{OB} \times \overrightarrow{F_{Cyl.}} + \overrightarrow{OC} \times \overrightarrow{F_A} + \overrightarrow{OG} \times \overrightarrow{P_2} = \overrightarrow{K_O} \tag{3.14}$$

That leads to:

$$\begin{aligned} &(I_{xx} + m_2 \cdot i^2) \cdot \ddot{\theta}(t) = \\ &c \cdot d^2 \cdot F_{abs} \left(\operatorname{sen}(\theta(t))^2 \cdot \cos(\alpha(t)) - \cos(\theta(t))^2 \cdot \operatorname{sen}(\alpha(t)) \right) \cdot \dot{\theta}(t) \\ &-e \cdot F_{cyl} \left(\cos(\theta(t)) \cdot \operatorname{sen}(\beta(t)) + \operatorname{sen}(\theta(t)) \cdot \cos(\beta(t)) \right) \\ &\quad + f \cdot F_A \cdot \cos\left(\frac{\pi}{6} - \theta(t) \right) + i \cdot m_2 \cdot g \cdot \cos\left(\frac{\pi}{6} - \theta(t) \right) \end{aligned} \tag{3.15}$$

In order to simplify this expression, the geometric relations between the different degrees of freedom must be defined.

$$\begin{cases} d \cdot \cos(\theta(t)) = x_1 + l_1(t) \cdot \cos(\alpha(t)) \\ d \cdot sen(\theta(t)) = h_1 - l_1(t) \cdot \operatorname{sen}(\alpha(t)) \end{cases} \Leftrightarrow$$
$$\begin{cases} \alpha(t) = tan^{-1}\left(\dfrac{d \cdot sen(\theta(t)) - h_1}{-(d \cdot \cos(\theta(t)) - x_1)} \right) \\ l_1(t) = \dfrac{d \cdot \cos(\theta(t)) - x_1}{\cos\left(tan^{-1}\left(\dfrac{d \cdot sen(\theta(t)) - h_1}{-(d \cdot \cos(\theta(t)) - x_1)} \right) \right)} \end{cases} \tag{3.16}$$

$$\begin{cases} e \cdot \cos(\theta(t)) = x_2 + l_2(t) \cdot \cos(\beta(t)) \\ e \cdot sen(\theta(t)) = h_2 - l_2(t) \cdot \operatorname{sen}(\beta(t)) \end{cases} \Leftrightarrow$$

$$\begin{cases} \beta(t) = tan^{-1}\left(\dfrac{e \cdot sen(\theta(t)) - h_2}{-(e \cdot \cos(\theta(t)) - x_2)}\right) \\ l_2(t) = \dfrac{e \cdot \cos(\theta(t)) - x_2}{\cos\left(tan^{-1}\left(\dfrac{e \cdot sen(\theta(t)) - h_2}{-(e \cdot \cos(\theta(t)) - x_2)}\right)\right)} \end{cases} \tag{3.17}$$

Where x_1, x_2, h_1, h_2, l_1 and l_2 are geometric parameters that can be seen in Figure 3.5.

$$z(t) = f \cdot \theta(t) \tag{3.18}$$

$$\dot{z}(t) = f \cdot \dot{\theta}(t) \tag{3.19}$$

$$\ddot{z}(t) = f \cdot \ddot{\theta}(t) \tag{3.20}$$

Substituting Expression (3.20) in Expression (3.3) leads to:

$$F_A = \frac{m_1 \left(g - f \cdot \ddot{\theta}(t)\right)}{2} \tag{3.21}$$

Finally, substituting Expression (3.21) in Expression (3.15) it´s possible to obtain the following expression:

$$\begin{aligned} \ddot{\theta}(t) = & \\ & \frac{c \cdot d^2 \cdot F_{abs}\left(\operatorname{sen}(\theta(t))^2 \cdot \cos(\alpha(t)) - \cos(\theta(t))^2 \cdot \operatorname{sen}(\alpha(t))\right) \cdot \dot{\theta}(t)}{I_{xx} + m_2 \cdot i^2 + \dfrac{f^2 \cdot m_1}{2} \cdot \cos\left(\dfrac{\pi}{6} - \theta(t)\right)} \\ & + \frac{\dfrac{f \cdot m_1 \cdot g}{2} \cdot \cos\left(\dfrac{\pi}{6} - \theta(t)\right) + i \cdot m_2 \cdot g \cdot \cos\left(\dfrac{\pi}{6} - \theta(t)\right)}{I_{xx} + m_2 \cdot i^2 + \dfrac{f^2 \cdot m_1}{2} \cdot \cos\left(\dfrac{\pi}{6} - \theta(t)\right)} \\ & - \frac{e \cdot F_{cyl}\left(\cos(\theta(t)) \cdot \operatorname{sen}(\beta(t)) + \operatorname{sen}(\theta(t)) \cdot \cos(\beta(t))\right)}{I_{xx} + m_2 \cdot i^2 + \dfrac{f^2 \cdot m_1}{2} \cdot \cos\left(\dfrac{\pi}{6} - \theta(t)\right)} \end{aligned} \tag{3.22}$$

Expression (3.22) was, then, implemented in *Matlab Simulink* to create a dynamic model of the interaction between the ARS and the anvil-impactor sub-system, which can be viewed in Appendix C at its full extent, as well as the results. Notice that Expressions (3.16) and (3.17) weren´t substituted, so that that Expression (3.22) can be better precepted, although they were taken into consideration in *Matlab Simulink* model. However, before running the model, it´s still needed to attribute values to the parameters at stake. Most of the parameters can be obtained by consulting the *SolidWorks 2018´s* drawings, such as the distances between the arm´s axle and the forces´ actuation points or the moment of inertia of the arm. The force applied by the pneumatic cylinder is indicated in its data sheet, which is 482.5 N when the air is pressurized at 6 bar. In the case of the shock-absorber chosen by Sousa [6], ACE MC3350EUM-0 [19] (see Figure 3.6), there is no indication about its damping coefficient or its force, however the manufacturer informs that the force of this component is constant along the whole stroke, as it can be seen in Figure 3.7.

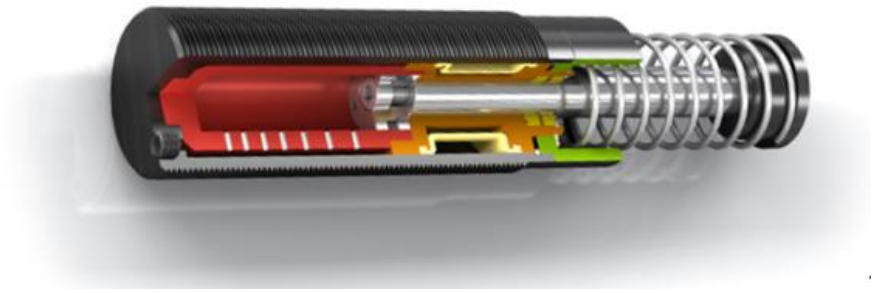

Figure 3.6 - ACE MC3350EUM-0 [19].

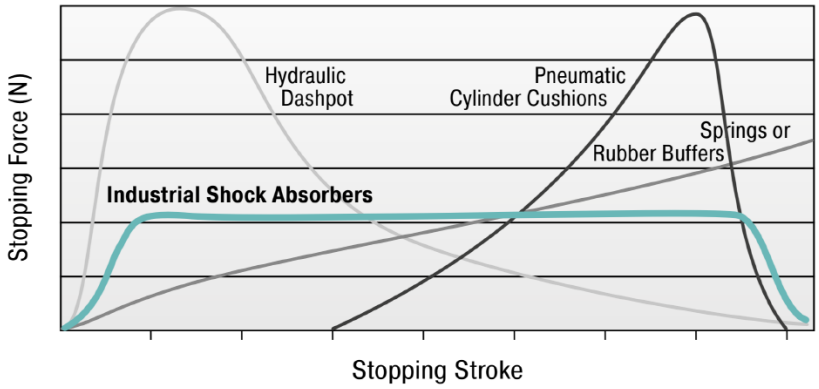

Figure 3.7 - Stopping force along industrial shock-absorber´s stroke [20].

Knowing this, we can achieve the following expression:

$$E_{Abs.} = \int_0^x F_{Abs.}(s) \cdot ds \Leftrightarrow E_{Abs.} = F_{Abs.} \cdot x \Leftrightarrow \frac{E_{Abs.}}{x} = F_{Abs.} \tag{3.23}$$

Where $E_{Abs.}$ is the dissipated energy by the shock-absorbers per cycle and x is the shock-absorbers´ stroke.

As it was previously said, the shock-absorber force is proportional to the velocity:

$$F_{Abs.} = c \cdot \dot{x} \tag{3.24}$$

By combining both expressions, the damping coefficient can now be estimated by:

$$c = \frac{E_{Abs.}}{x \cdot \dot{x}} \tag{3.25}$$

Consulting the shock absorbers data sheet, the values for $E_{Abs.}$ and x are found and applied like shown in Expression 3.26:

$$c = \frac{2 \cdot 330}{0.0486 \cdot \dot{x}} = \frac{2 \cdot 330}{0.0486 \cdot d \cdot \dot{\theta}} \tag{3.26}$$

This coeficient is then used in the first term of the Simulink model of Expression 3.22.

Now that the values for all parameters are known, they are inserted in the developed *Matlab Simulink* model, like shown in Figure 3.8. By running the model, the results for the angular acceleration throughout time, $\ddot{\theta}(t)$, are obtained. Those results can be consulted in Figure 3.9.

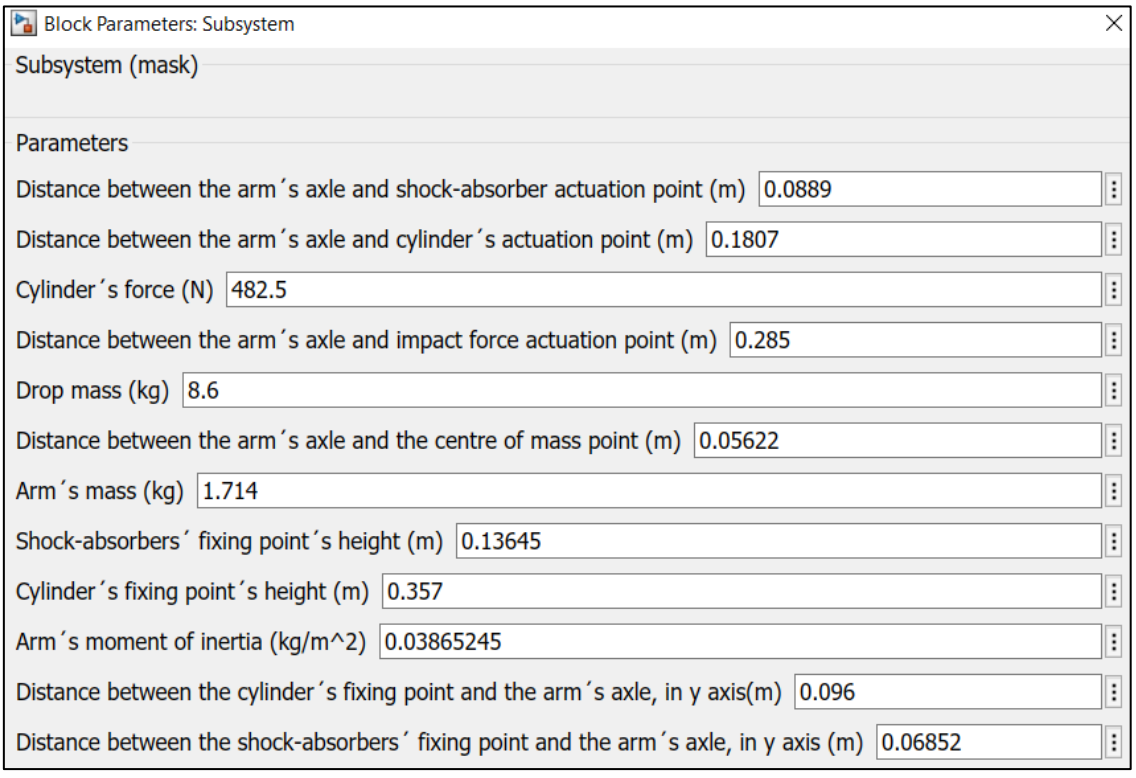

Figure 3.8 - Parameters´ values inserted in the developed Matlab Simulink model, considering the maximum drop weight.

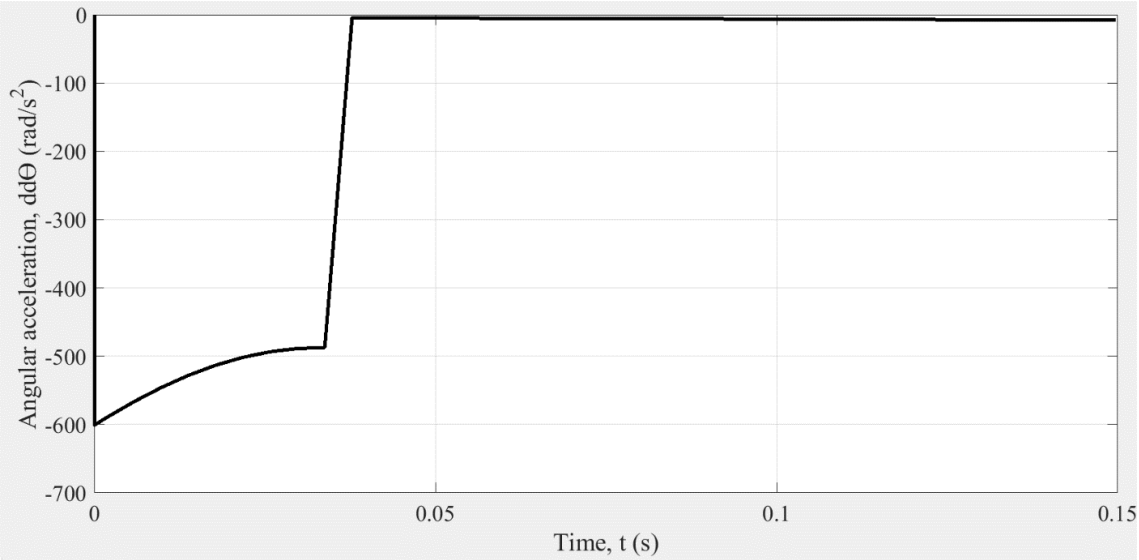

Figure 3.9 - Angular acceleration obtained in the developed Matlab Simulink model, considering the maximum drop weight.

Now, it is finally possible to calculate $F_{A,max}$, using Expression (3.3), needed to run the simulation on *SolidWorks 2018*, and confirm if the material for the impact axles was correctly chosen.

$$F_{A,max} = \frac{m_1 \times (g - f \cdot \ddot{\theta}_{max}(t))}{2} = \frac{56 \times (9.81 - 0.285 \times (-600))}{2} = 5062.68\ N \quad (3.27)$$

Inserting this value in *SolidWorks 2018´*s simulation parameters, it´s possible to obtain the results for the factor of safety, shown in Figure 3.10. The minimum value found for the factor of safety was 6.46, granting that the material will keep its integrity with the impacts.

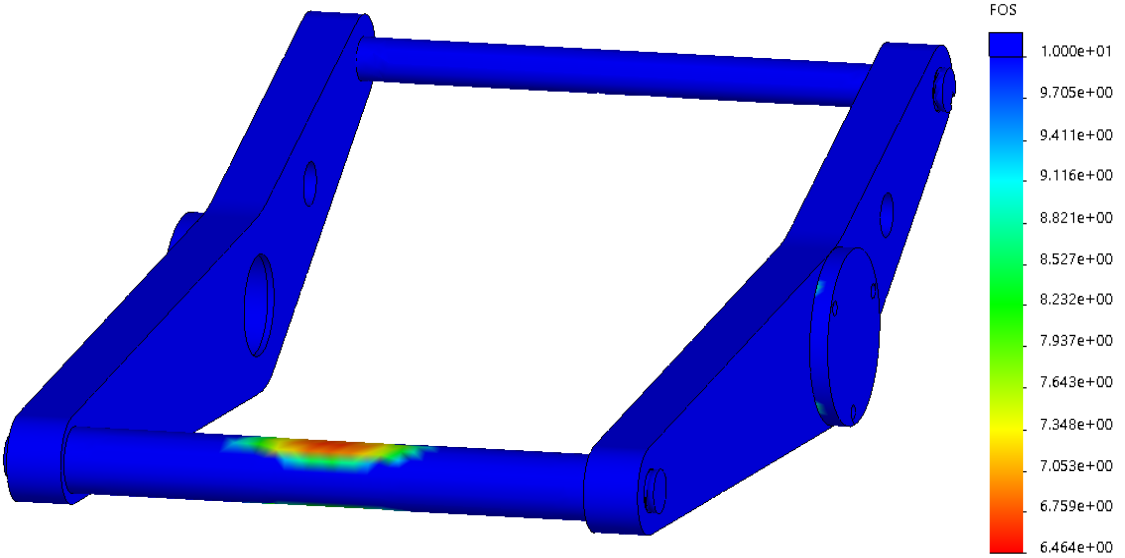

Figure 3.10 - Factor of safety obtained when a $5063\ N$ is applied to the ARS´ rotating structure, recurring to *SolidWorks 2018*.

3.1.1.4. Actuation Axle Connector

In order to move the ARS, the pneumatic cylinder must act on the actuator axle, however the rod eyes that Festo provides do not meet the diameter needed for this axle. To solve this problem, an intermediary part had to be designed by Sousa [6], but it had to be modified because this designed part would interfere with the rod eye, meaning that there wasn't enough space for both. The final design of this part is shown in the Figure 3.11.

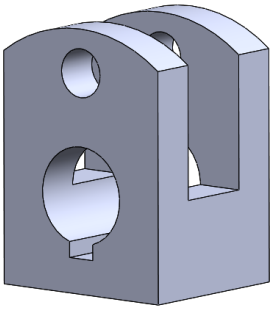

Figure 3.11 - New design of the actuation axle connector, made in *SolidWorks 2018*.

It consists in an aluminium alloy part, fabricated from an aluminium alloy plate, AW 6082 - T651, obtained from KMS [16]. It is comprised by two holes, the smallest one is for the axle of the rod eye, which has a 10 mm diameter, and the largest one is for the actuation axle. To guarantee that this part wouldn't rotate and that it would transmit the force to the actuation axle, this component has a slot to allocate a parallel key.

3.1.1.5. Shock-Absorbers Pads

The contact points between the ARS´s arms and the shock-absorbers are where most of the stress will build up and it´s important that the damping force always acts perpendicularly to the arms. To be able to do this, special pads (Figure 3.12) were designed and fabricated from AW 6082 - T651, bought from KMS [16].

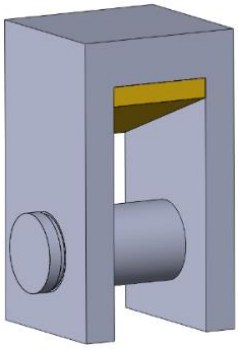

Figure 3.12 - Designed shock absorber pad, made in *SolidWorks 2018.*

Since the cylinders can extend faster than the shock-absorbers, the alignment pads could rotate and be misplaced, making the damping force impossible to act

perpendicularly. To avoid this from happening, polyurethane parts with a specific geometry were made to be placed under the pads, in order to force them to be aligned with the shock-absorbers when the mentioned components break contact. As the shock-absorbers act on the pads, the polyurethane parts are easily compressed and, therefore, don't interfere with the functioning of the machine.

3.1.2. Fixed Structure

The fixed structure, represented in Figure 3.13, is the link between the ARS and the main structure of the drop weight machine. It is composed by three aluminium alloy plates, two of them to mount the mechanical stoppers, that prevent the rotation of the arm to a certain angle, and the shock-absorbers and the other is to mount the pneumatic actuator.

All these plates are fixed on the structure of the drop weight machine using screws and T-nuts. Although this type of mechanical connection can hold the plates against the profiles, they shouldn't be subjected to vertical forces because they are likely to slip. This problem was solved by designing three steel blocks that will discharge the vertical forces to the main structure of the machine. Additionally, two of these blocks will position the axles to mount the needle bearings.

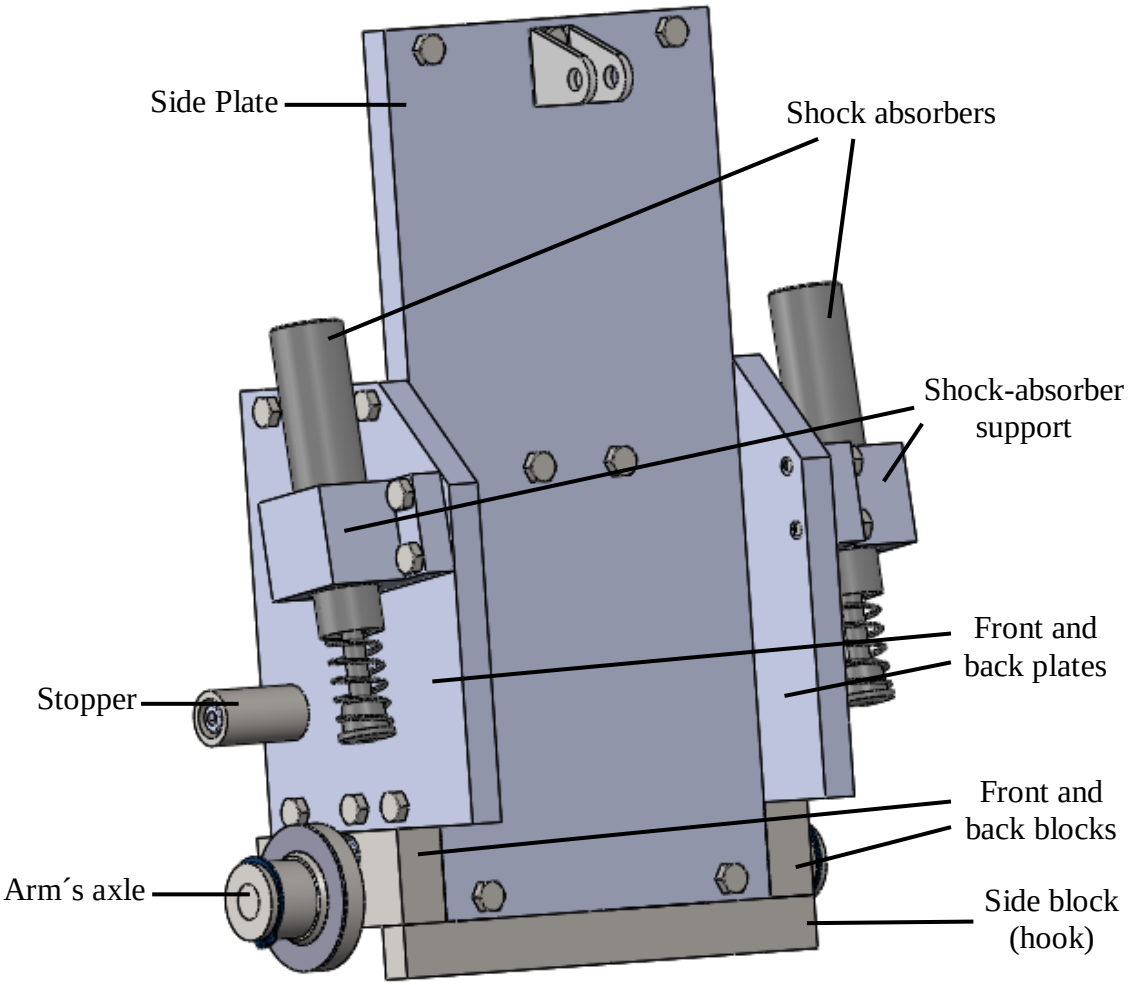

Figure 3.13 - Final design of the ARS´ fixed structure, made in *SolidWorks 2018*.

To connect all the parts that assemble the ARS, the materials presented in Table 3.2 are used.

Table 3.2 - Fasteners used to assemble the ARS.

Element	**Norm**	**Qt.**
Keys	C ISO/R773 6x6x25	4
	A ISO/R773 6x6x32	2
Screws	ISO 4017 - M8X30 -12.9	24
	ISO 4762 - M6x30 - 12.9	6
	ISO 4762 - M8x25 - 12.9	16
	ISO 4017 - M6x20 - 12.9	12
	ISO 4762 - M8x50 - 12.9	4
	ISO 4017 - M8x25 - 12.9	28
	ISO 4017 - M6x16 - 12.9	4
Circlips	DIN 471 - 20x1.2	16
	DIN 471 - 35x1.5	4
	DIN 471 - 10x1	4
Galvanized T-nuts	Bosch´s norm	44

After the mechanical drawings and materials of the parts that comprise the ARS were defined, it was possible to manufacture them and to mount this mechanism. However, it´s not completely assembled, since it still lacks the shock-absorbers in its construction, which haven´t yet been delivered. For this reason, this sub-system´s functioning is yet to be tested. The currently implemented ARS´s arrangement can be seen in Figure 3.14.

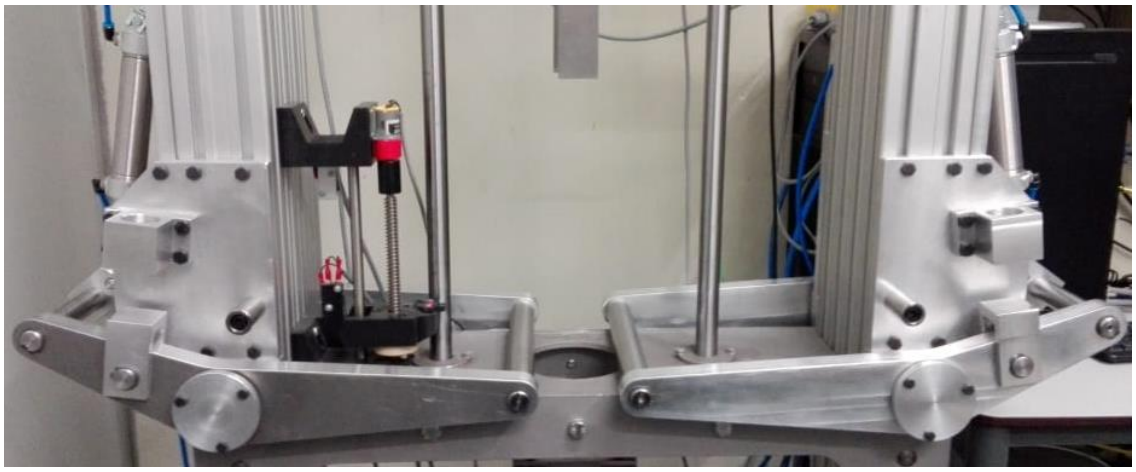

Figure 3.14 - Currently implemented ARS´s arrangement.

3.2. Anvil-impactor sub-system

The anvil-impactor sub-system assembles all the components that contribute for the drop mass. Initially, the designed assembly was only comprised by an impactor, in form of a puncture, and the anvil, as shown in Figure 3.15. However, there was the need to implement a new impactor to adapt to a new and more rigid specimen fixing structure (see Figure 3.16), designed by one of the ADFEUP´s members, and a pair of piezoelectric sensors, that will measure the evolution of acceleration and force throughout time.

Normally, drop weight machines have one sensor to either measure the force or to measure the acceleration, since one can be deducted from the other. However, most of those machines don´t use pre-calibrated sensors, meaning that they have to be recalibrated before each usage, like what happens with Rosand IFW5 machine. Since that process is made by the operator, who can´t guarantee the same reference for each calibration, the associated error of the measurement increases, which will influence the results obtained. To avoid that source of error in the impact test´s results, this drop weight machine will use pre-calibrated sensors. However, if only one of these sensors is used, in long term, it can lose its reference and provide wrong data without the user´s knowledge. So, to ensure that the collected data is reliable, this drop weight machine uses a pre-calibrated piezoelectric accelerometer and a pre-calibrated piezoelectric load cell. This way, the obtained results on both sensors can be compared and, if their information matches, it can be assumed that the measurements are reliable.

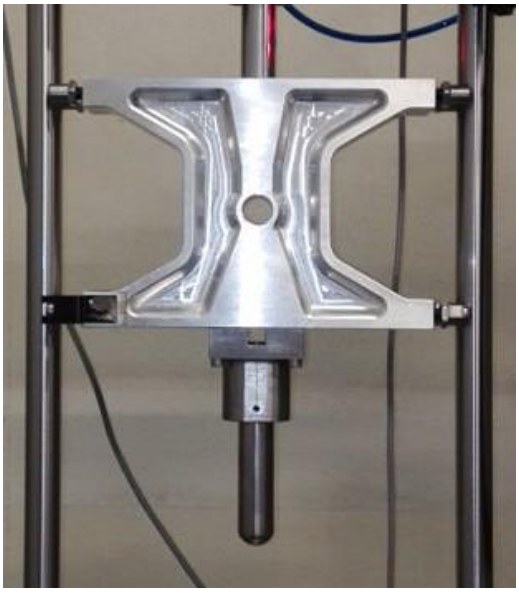

Figure 3.15 - Initial anvil-impactor assembly.

In order to completely characterize an adhesive joint under impact conditions, one should measure the force and the displacement. The force can be obtained directly by the load cell or by multiplying the drop mass by the accelerometer´s measured impact acceleration. The displacement could be obtained by double integrating the measured acceleration, using either sensor. However, since we are dealing with AC coupled sensors, which have an intrinsic decaying function when integrating data in real time, there is an associated error leading to wrong calculated displacements [21].

There are other ways to measure the displacement, like using a high-speed camera, however, for this kind of solution, the target should be very illuminated, which is hard to implement due to the specimen fixing structure.

For these reasons, the displacement will be obtained after the test is done, integrating the resulting acceleration data, gathered by both sensors. This is a temporary solution, since, in the future, a new tool, equipped with sensors that can directly measure the displacement (LVDT or linear potentiometer), will be attached to the new specimen fixing structure.

After considering the mounting of the sensors, a solution for the new anvil-impactor assembly was designed in *SolidWorks 2018*, Figure 3.17. The mechanical parts´ drawings for this assembly are presented in Appendix B.

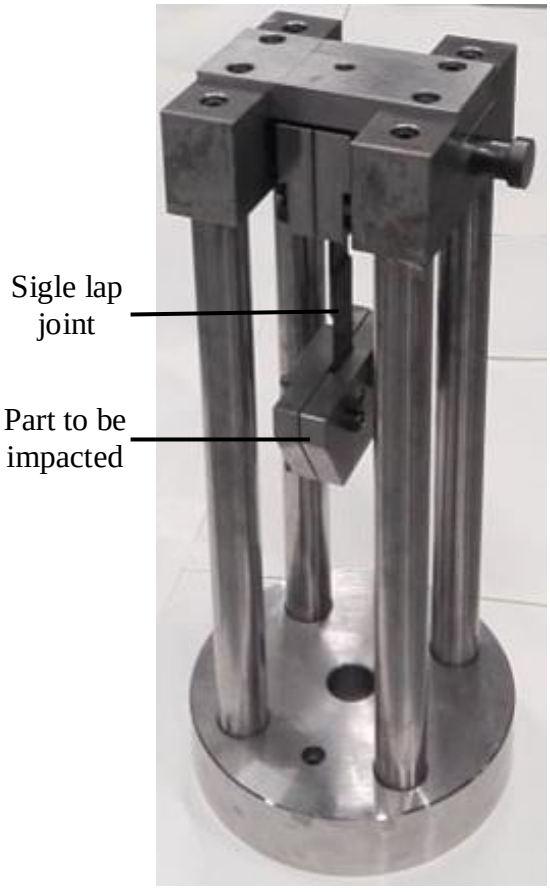

Figure 3.16 - New specimen fixing structure.

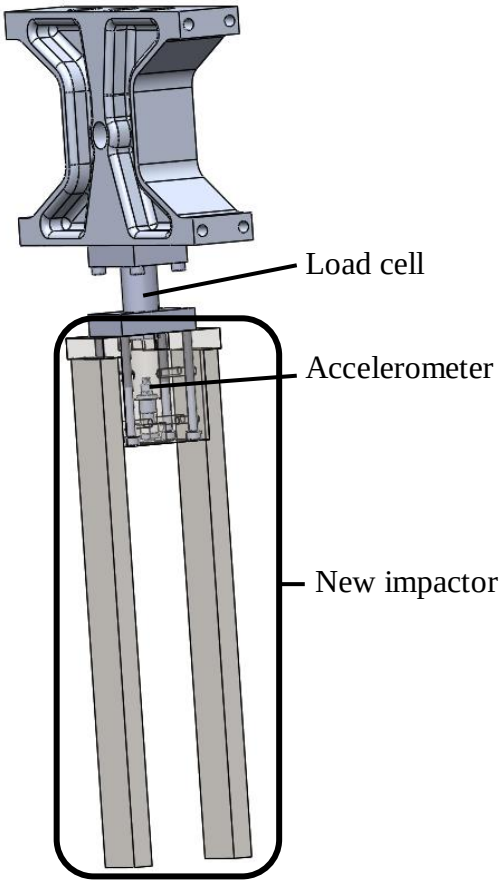

Figure 3.17 - New anvil-impactor assembly design, made in SolidWorks 2018.

To validate the new anvil-impactor assembly proposed, it´s important to have some considerations in mind. The most important one is to know what´s the measuring range needed for each sensor. The other aspects to consider are explained in section 4.2.

When considering which accelerometer is to be chosen, one should think that accelerations that result from an impact can be somewhat unpredictable. Furthermore, it may be needed to test materials other than adhesive joints, which have different rigidities, resulting in different impact behaviours. So, in order to not limit this drop weight machine in terms of what materials can be tested, the selected accelerometer must be able to withstand and measure high impact accelerations.

Now, in what the load cell concerns, there are two possible ways that this sensor is going to be loaded: The anvil-impactor assembly hits the specimen, subjecting the load cell to compressive forces, or is grabbed by the ARS, subjecting the load cell to tensile forces. After gathering information about the highest recorded impact load on adhesive joints tested by ADFEUP´s members, it was concluded that this value was close to 35 kN, as Figure 3.18 demonstrates. So, the load cell should be able to measure compressive forces higher than the mentioned value.

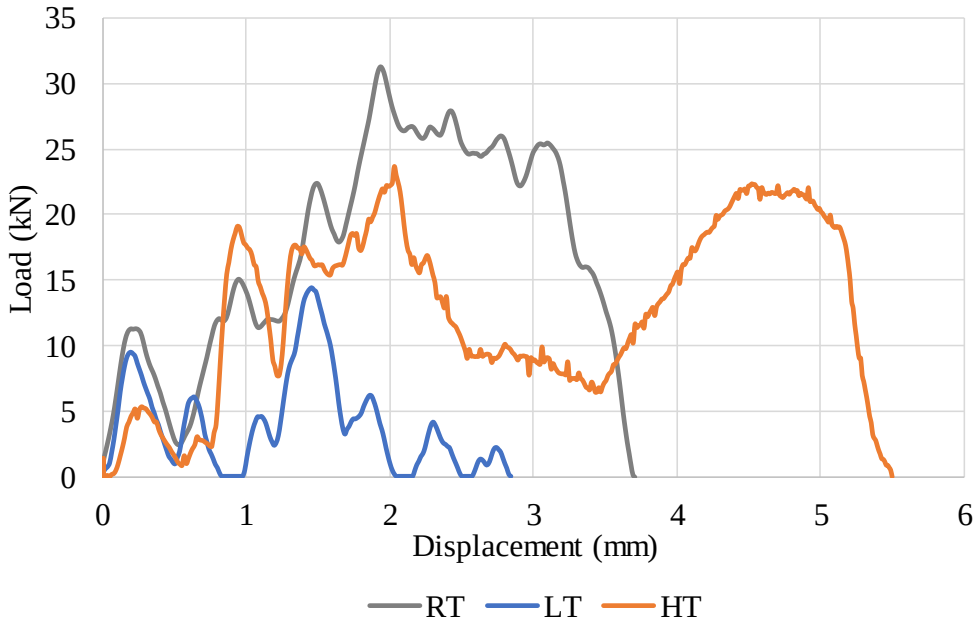

Figure 3.18 - Graph of the displacements-load of carbon fibre reinforced polymer (CFRP) substrates tested under impact at different temperatures: room temperature (RT), low temperature (LT) and high temperature (HT) [22].

To know the tensile forces that the load cell should withstand, the linear acceleration, $\ddot{z}$, of the anvil-impactor assembly when it collides with the ARS´s axle must be known. Using the maximum angular acceleration, $\ddot{\theta}_{max.}$, previously calculated in the dynamic study and Expression (3.20), $\ddot{z}_{max.}$ comes:

$$\ddot{z}_{max.} = 0.285 \times (-600) = -171\ m/s^2 \tag{3.28}$$

The forces that contribute to the tensile load that the press force sensor will be subjected are the quantity of acceleration forces and the weight forces of the impactor and one steel plate, so it´s calculated by:

$$F_{Tens.} = \dot{Q}_{Imp.} + P_{Imp.} + \dot{Q}_{Plate} + P_{Plate}$$

$$= m_{Imp,} \times \left(\ddot{z}_{Imp.} + g\right) + m_{Plate} \times \left(\ddot{z}_{Imp.} + g\right)$$

$$= 5.495 \times (-171 - 9.81) + 0.039 \times (-171 - 9.81) \approx -1000\ N \tag{3.29}$$

However, the maximum value of the angular acceleration, $\ddot{\theta}_{max.}$, was obtained when a drop mass of 56 kg is released from the highest point of the stroke and it´s also important

to run the simulation when the minimum drop mass is released, 8.5 kg, since the energy at stake is lower, taking less time for the shock-absorbers to dissipate it and creating a higher linear acceleration, $\ddot{z}$. To do that, the drop mass parameter in the *Matlab Simulink* model was changed and the dynamic simulation was run again, obtaining the following results (Figure 3.19):

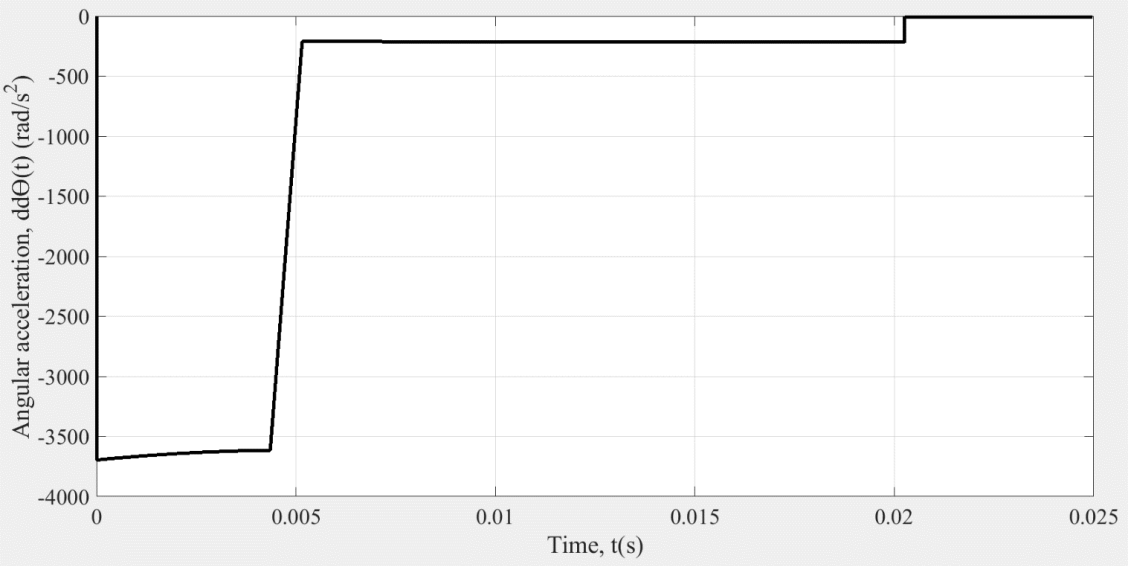

Figure 3.19 - Results for the angular acceleration obtained in the developed Matlab Simulink model, considering the minimum drop weight.

So, the new resultant maximum linear acceleration, $\ddot{z}_{max.}$, will come:

$$\ddot{z}_{max.} = 0.285 \times (-3700) = -1055\ m/s^2 \tag{3.30}$$

And will lead to a tensile force of:

$$\begin{aligned} F_{Tens.} &= \dot{Q}_{Imp.} + P_{Imp.} + \dot{Q}_{Plate} + P_{Plate} \\ &= m_{Imp,} \times \left(\ddot{z}_{Imp.} + g\right) + m_{Plate} \times \left(\ddot{z}_{Imp.} + g\right) \\ &= 5.495 \times (-1055 - 9.81) + 0.039 \times (-1055 - 9.81) \approx -5893\ N \end{aligned} \tag{3.31}$$

So, when selecting the load cell, the maximum admissible tensile force should be higher than the calculated value.

Since the load cell was specifically dimensioned to test adhesive joints, when testing other types of materials, the operator should consider dismounting it from the assembly and only rely upon the values measured by the accelerometer, which is over dimensioned and, therefore, can withstand higher impact loads without the risk of damaging it.

To assemble the anvil-impactor sub-system, the fasteners described in Table 3.3 are used.

Table 3.3 - Fasteners used to assemble the new anvil-impactor assembly.

Element	Norm	Qt.
Screws	ISO 4762 - M4x12 -12.9	8
	ISO 4762 - M6x25 - 12.9	4
	ISO 4762 - M6x85 - 12.9	4
Nuts	ISO 4032 - M8 - 12.9	1
	ISO 4035 - M8 - 12.9	1

The final arrangement of the anvil-impactor assembly is shown in Figure 3.20.

Figure 3.20 - Final arrangement of the anvil-impactor assembly.

Chapter 4

Actuation and Control Logic

This chapter is divided in three sections: section 4.1 addresses the hardware used in the pneumatic circuit, section 4.2 describes and explains the currently implemented electrical circuit´s components and section 4.3 focuses on the control logic and interface to operate the machine.

4.1. Pneumatic circuit

In order to take advantage of FEUP´s compressed air network, some sub-systems of the drop weight machine are actuated by converting the pressurized air into forces that will perform a desired action, like the release of the anvil-impactor assembly and the positioning of the ARS.

The implemented pneumatic circuit, represented in Figure 4.1, is composed by an air treatment unit (comprised by components 1, 2, 3 and 4) that feeds the cylinder that releases the anvil (6) and two cylinders that actuate the arms of the ARS (8 and 9). To control the air flow that enters the cylinder that releases the anvil, a 3/2 directional valve (5) is used, while for the other two cylinders a 5/2 directional valve (7) is used. Each component of this pneumatic circuit is going to be described in the following sections.

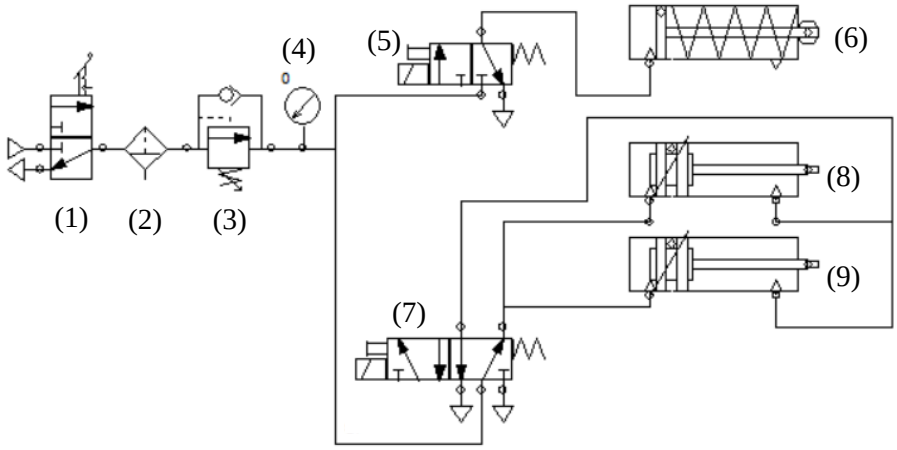

Figure 4.1 - Diagram of the implemented pneumatic circuit.

At the starting point of this dissertation, only the pneumatic cylinder to release the anvil and its actuating valve were already acquired.

4.1.1. Cylinders

Both cylinders used in the drop weight machine had already been chosen. Ramos [5] had chosen a SMC C85N25-25S [23], responsible for the anvil release, and Sousa [6] had chosen two FESTO DSNU-32-100-PPV-A [24] that actuate the two arms of the ARS.

The SMC C85N25-25S [23] is a single acting linear round cylinder with a 25 mm diameter and 25 mm stroke. To choose this cylinder, Ramos [5] had to consider that it had to support a maximum weight of 56 kg and, in order to be a safe mechanism, was intentionally over dimensioned. At the end of the cylinder a special clamp, designed by Castro [3], is used. This clamp allows the carriage to easily attach to the anvil´s pivot by fitting spheres in the pivot´s gap, like shown in Figure 4.2 - stage 1, 2 and 3. When being released, the pneumatic actuator´s linear movement pushes a sleeve (represented in green) that will then free the spheres that were previously holding the drop mass, Figure 4.2 - stage 4.

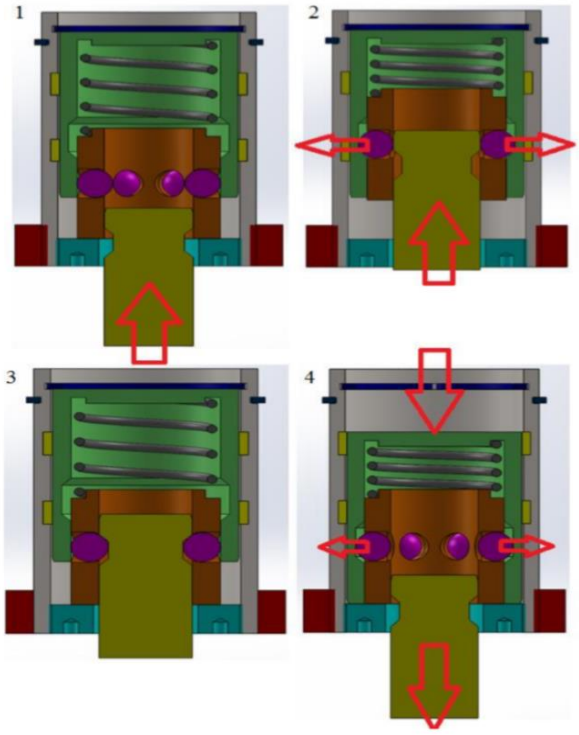

Figure 4.2 - Stages of the clamp of the carriage´s cylinder functioning [5].

The FESTO DSNU-32-100-PPV-A [24] (see Figure 4.3) is a double acting linear round cylinder with a 32 mm diameter and 100 mm stroke. Its functioning was carefully dimensioned so that it could hold and lift half of the weight of the drop mass, since there is one of this type of cylinders in each arm of the ARS. This type of cylinder also has adjustable pneumatic damping and a magnet, so it is possible to implement a proximity

sensor. To go along with these two cylinders the accessories demonstrated in Table 4.1 were chosen.

Figure 4.3 - FESTO DSNU-32-100-PPV-A [24].

Table 4.1 - Selected FESTO DSNU-32-100-PPV-A´s accessories [24].

Accessories	Designation	Description	Qt.
Clevis foot mounting	LBN-32	Part to fix the cylinder	2
Rod eye	SGS-M10x1.25	Part for the rod end	2
Proximity sensor	SME-8M-DS-24V-K-0,3-M8D	Magnetic sensor of type Reed	1
Proximity sensor support	SMBR-8-32	Clamp to hold sensor near the cylinder	1
Cable extension	NEBU-M8G3-K-2.5-LE3	Cable extension for sensor of 2,5 m	1

Since both of FESTO DSNU-32-100-PPV-A [24] cylinders are actuated in parallel and there´s only two possible positions for the cylinders (extended or retracted), only one proximity sensor is needed to inform their position at any given moment.

4.1.2. Directional valves

To control the compressed air that feeds the SMC C85N25-25S [23], a PARKER B3R5BXXXXH [25] (Figure 4.4 - a) valve was used. It is a 3/2-way electrically activated valve with spring return, like shown in Figure 4.4 - b. However, this valve didn´t have a solenoid equipped, so Sousa [6] had to choose one. The selected solenoid was the PARKER P2E-KV32C1 [26].

a) b)

Figure 4.4 - a) PARKER B3R5BXXXXH; b) PARKER B3R5BXXXXH symbol [25].

As it was previously said, this directional valve and the cylinder that it feeds were already implemented when this dissertation started, but its implementation was not correct and caused some malfunctions on the drop weight machine. The problem was that when deactivating the computer software´s variable responsible for the actuation of the solenoid, a voltage peak was created. This voltage peak was responsible for an instantaneous actuation of all the components connected to the signal conditioning board, forcing, for example, the emergency situation to be declared, as if an emergency button was pressed. This would always stop the correct functioning of the machine in the test sequence. This problem was solved by simply implementing a freewheeling diode in parallel with the solenoid.

For the actuation of both cylinders of the type FESTO DSNU-32-100-PPV-A [24] a fast-acting 5/2-way valve was needed. But, in order to select this valve, it was first required to know the air flow that each cylinder needs to fully extend. This was made by first obtaining the volume of air that each cylinder needs:

$$V_{Cyl.} = \Delta x \times \pi \times r^2 = 100 \times \pi \times 16^2 = 80425\ mm^3 \tag{4.1}$$

Where Δx is the cylinder´s stroke and r is the cylinders radius.

Now, with the time that the cylinders have to fully extend (Δt), which was calculated by Sousa [6], it´s possible to obtain the air flow that the valve needs to provide:

$$\dot{V}_{Cyl.} = \frac{2 \times V_{Cyl.}}{\Delta t} = \frac{2 \times 80425}{0.11} \times \frac{60}{10^6} = 87.74\ dm^3/min \tag{4.2}$$

With the obtained result, it´s now possible to select the required valve. The chosen valve was a FESTO MHE2-MS1H-5/2-M7-K [27] (Figure 4.5 - a), that provides a 100 L/min air flow. The chosen valve´s implementation was made considering that if, for any reason, the electrical circuit fails, the ARS will always act, because the spring forces that specific position. This valve has an integrated solenoid and has protection against transients that result in a voltage peak, which means that doesn't needs the diode, like in the previous valve. The associated symbol of the valve is shown in Figure 4.5 - b.

a) b)

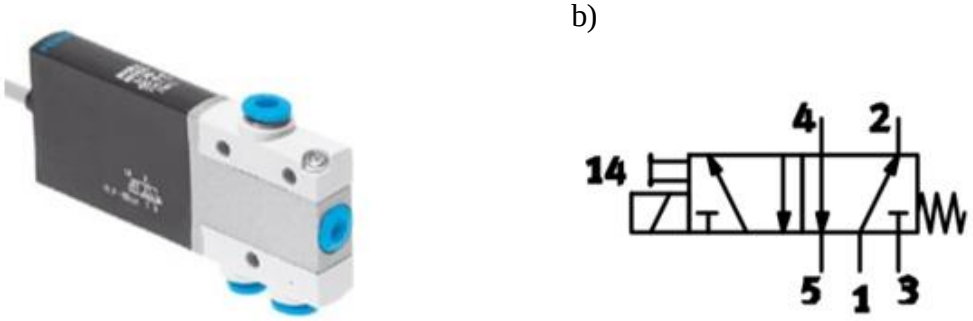

Figure 4.5 - a) FESTO MHE2-MS1H-5/2-M7-K; b) FESTO MHE2-MS1H-5/2-M7-K symbol [27].

4.1.3. Air treatment unit

The chosen feeding unit was a FESTO MSB4-AGA:C4:H3:N3-WP [28], Figure 4.6. This component is comprised by an on/off manual valve with silencer, a 5 μm filter with manual condensate drain and a pressure regulator that ranges from 0.5 bar to 12 bar with a pressure gauge incorporated.

Figure 4.6 - FESTO MSB4-AGA:C4:H3:N3-WP [28].

4.1.4. Pneumatic accessories

In order to completely assemble all the mentioned pneumatic parts some connection accessories had to be chosen. Table 4.2 summarizes those chosen accessories.

Table 4.2 - Pneumatic circuit accessories.

Accessories	Designation	Description	Qt.
T connections for Φ6-Φ6	QSMT-6	Easy connection (T shape) with 3 ports to connect the 6 mm tubing	3
L connections for G1/8- Φ6	QSML-G 1/8-6	Easy connection (L shape) between a G1/8 port and the 6 mm tubing	5
L connections for G1/8- Φ8	QSML-G 1/8-8	Easy connection (L shape) between a G1/8 port and the 8 mm tubing	1
L connections for M7- Φ6	QSML-M7-6	Easy connection (L shape) between a M7 port and the 8 mm tubing	3
Tube of Φ6 mm	PUN-6X1-BL	50 m of tube of Φ6 mm	-
Silencer M7	UC-M7	Silencer with a M7 screw	2

4.2. Electronics

In order to be able to control the drop weight machine, an electric circuit is needed. This circuit should provide the means to power the various components that are part of it and also serve as interface between the computer and the various sensors and actuators. It is, therefore, important that this circuit is carefully assembled so that, when creating the control logic, the system works as expected, preventing the damaging of its components.

As it was previous stated in section 2.3.4, an initial electrical circuit had already been implemented by Sousa [6], who also provided the circuit´s schematic and some documentation about the implemented components. With the help of this information, a thorough revision was made to verify if everything was connected as it was supposed to and what changes had to be done. The current implemented circuit´s schematic is presented in Appendix D and can be useful to consult it for a better understanding of the upcoming sections, where a description of the implemented hardware is performed.

4.2.1. Lifting sub-system

The lifting sub-system, Figure 4.7, is the mechanism that moves the carriage up or down by wrapping a cable around a motorized worm. The worm has a particular geometry that enables the cable to always be wrapped with the same diameter, so that the relation between the carriage´s velocity and the motor´s velocity is kept constant. Additionally, this sub-system also has a mechanical part that ensures that the cable is always centered with the hole where it passes through, by forcing the worm to move along the axis. This solution was proposed by Castro [3] and then assembled by Ramos [5].

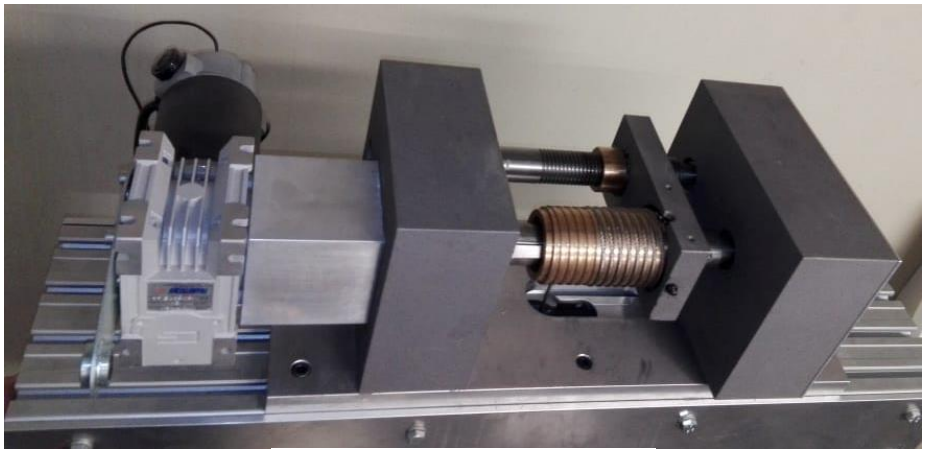

Figure 4.7 - Lifting sub-system.

The implemented motor is a Transtecno ECM-100/040 [29], Figure 4.8. It is a worm gear DC motor capable of producing 140 W and a maximum velocity of 100 min^{-1}. To control it the Electromen EM-115 [30] driver was chosen, demonstrated in Figure 4.9. This PWM driver converts the feeding signal into an adequate voltage signal that powers the motor, enabling it to rotate at a proportional speed. The feeding signal can be provided

in various ways, but the chosen method was to directly connect to an external 0-10 V reference given by an analog output of the data acquisition (DAQ) board. To select the rotation´s direction, two digital inputs, also given by the DAQ board, are used.

Figure 4.8 - Transtecno ECM-100/040 [29].

Figure 4.9 - Electromen EM-115 [30].

4.2.2. Velocity acquisition sub-system

Theoretically, the velocity on impact can be obtained by knowing the drop height, Expression 4.3, however it´s just an estimate that ignores some effects like the air resistance or the friction on the guiding columns. This can lead to results that don´t correspond to the reality of the test made, thus a velocity-acquisition sub-system is implemented in the drop weight machine, Figure 4.10.

$$V_{imp.} = \sqrt{2 \cdot g \cdot h} \tag{4.3}$$

Figure 4.10 - Velocity acquisition sub-system.

This sub-system assembly was created and implemented by Ramos [5] and works by detecting the two combs of a small part that is attached to the anvil. When each of the combs passes through the optical detector, a variable on Simulink (t1 for the first comb and t2 for the second comb) is associated with the time instant that detection occurs. With those two time instants it´s possible to calculate the time between each detection, which associated with the distance between the two combs gives the impact velocity of the falling anvil.

Since the specimens to be tested in this machine are going to have different lengths, it´s also important that the optical detector can be moved according to the different impact points. For this reason, a small DC motor, connected to a screw-drive, moves the platform where the optical detector is fixed. The selected motor for this function is a Como Drills 918D100112 [31].

To be able to reverse the direction of the motor´s rotation, a board with an L298N integrated circuit [32] was chosen, which has two built-in H-bridges, although only one is used. This type of circuit is widely used in making small DC motor controllers and this specific one also contains protection circuits and voltage regulators. Originally, this board comes prepared to be implemented with 12 V motors, however if a jumper pin is removed the board will accept 24 V motors, like the one being used.

Table 4.3 shows how the connections in the L298N board are made, considering that only one motor is connected.

Table 4.3 - L298N board connections to the electrical circuit lines.

Pin	Line	Description
GND	GND24	Board´s ground
5 V	5 VDC_PS3	5 V supply
12 V	24 VDC_PS1	24 V supply
ENA	Port B0	Enables the motor
IN1	Port B7	Direction selector
IN2	Port B6	Direction selector
OUT1	-	Motor powerline
OUT2	-	Motor powerline

4.2.3. Sensors

Currently, there are seven different types of sensing elements applied in the drop weight machine:

- One optical detector;
- Two microswitches;
- One inductive detector;
- One photoelectric detector;

- One proximity detector;
- One piezoelectric accelerometer;
- One piezoelectric press force sensor.

Each one has a different working principle and a specific function in the machine, issues to be discussed in the following sections.

4.2.3.1. Optical detector

The optical detector is the sensing element responsible for the detection of the combs of the mechanical part that is fixed on the anvil, as briefly mentioned in the previous section. This detector is an OMRON EE-SX670-WR [33], shown in Figure 4.11. It´s a slot-type microsensor that works by the same principle as a light barrier, which means that a light beam is being transmitted by an emitter to a receiver and whenever that light beam is interrupted, a positive signal is sent by the sensor. This particular sensor has an NPN configuration, which means that it works in inverted logic and, in order to implement it, it needs to be associated with a relay (K12) that inverts it back.

Figure 4.11 - OMRON EE-SX670-WR [33].

To correctly connect this sensor, one has to consider that it has 4 leads, that can be identified by its colour: a brown one to feed 24 VDC, a blue one to connect the 0 VDC, a black one which works as the collector and a pink one used to select Dark On mode or Light On mode. So, the brown lead was connected to the relay´s coil´s positive lead and to the 24 VDC line, the black one to the relay´s coil´s negative lead, the blue one to the 0 VDC line and the pink one is connected to the blue lead, which selects the Dark ON mode. Figure 4.12 shows the mentioned connections. The relay´s normally open contact is then connected to the PCIN6 line, sending the input signal to the Software. The functioning of the Dark On mode can be better understood by consulting Figure 4.13.

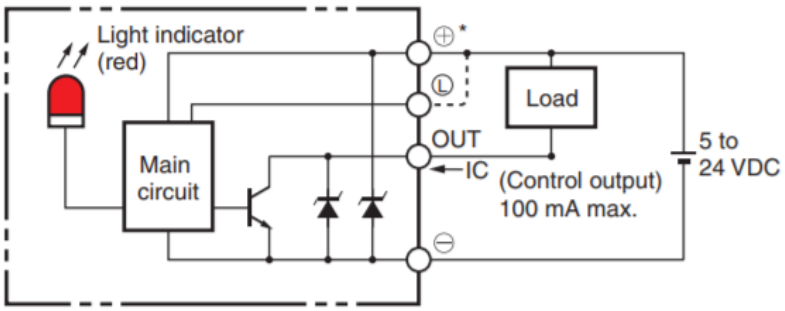

Figure 4.12 - OMRON EE-SX670-WR´s lead connections [33].

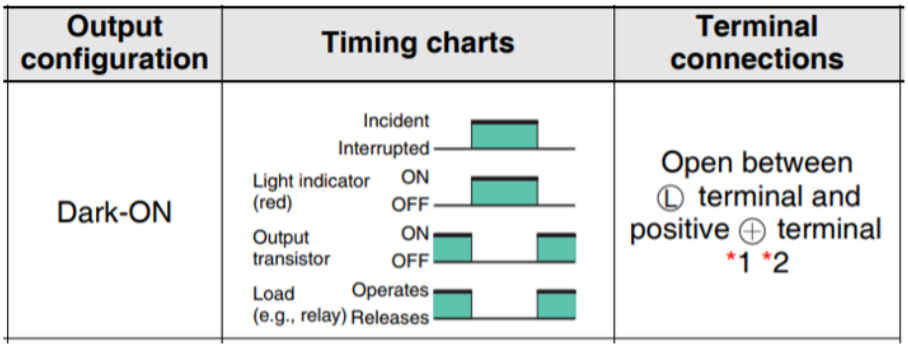

Figure 4.13 - OMRON EE-SX670-WR´s Dark-ON mode [33].

4.2.3.2. Microswitches

As mentioned in section 4.2.2, there is a moving platform on the velocity acquisition sub-system that positions the optical detector depending on the length of the specimen to be tested. Thus, it is important to limit the stroke of this moving platform by using two microswitches.

The selected model is the Cherry D459-V3RD [34] (see Figure 4.14) that has a 3-way switch, which means that it has one normally open contact and one normally closed contact for the same input. Therefore, when the switch is pressed both contacts change their state and each one can perform an action. Recurring to this information, the normally closed contacts are used to send an input signal to the computer (PCIN2 for the upper microswitch and PCIN3 for the lower microswitch) and the normally open contacts are used to send a signal to relays´ coils (K5 for the upper microswitch and K6 for the lower microswitch) that will then cut the power from the ports IN1 and IN2 of the L298N board [32] and consequently stop the motor´s rotation in that direction.

Figure 4.14 - Cherry D459-V3RD [34].

4.2.3.3. Inductive detector

As a way of preventing the lifting sub-system´s motor to lift the carriage beyond the possible height, a sensor that limits its stroke is attached to the carriage. The chosen sensor is an RS Pro 701-8253 [35], shown in Figure 4.15, which consists in an inductive detector that senses a small metallic part fixed on the drop weight machine´s structure at a defined height. When the sensor performs a detection, sends a signal to the software using PCIN5

line, which forces the software to enter the emergency state, and also triggers a normally closed relay (K8) that breaks the powering of the lifting sub-system´s motor.

Figure 4.15 - RS Pro 701-8253 [35].

Notice that, if this sensor breaks the contact for the motor movement when it detects the metallic part, this would mean that the carriage would be stuck in that position, because it stops right in front of that metallic part. However, a parallel normally open contact, triggered by a signal sent via software (PCOUT5) to the associated relay (K9), is used to move the motor freely.

This sensor has 3 leads, distinguished by colour: The brown and blue leads are connected to the 24 VDC and 0 VDC terminals of the power supply (PS1), respectively, and the black lead is connected to PCIN5 line and to the relay´s coil (K8).

4.2.3.4. Photoelectric detector

In order to make the desired command logic, that is discussed in section 4.3, the anvil has to go thru a stage where it will be attached to the carriage. Thus, there must be a method of making the software know that the anvil is, in fact, attached. It was with this intention that a photoelectric detector of the type OMRON E3FA-DN23 [36] (see Figure 4.16) was used. It´s a defuse reflective sensor, meaning that it emits a light and triggers a signal when an object is in front of its beam and reflects it back. Knowing this, the said sensor is fixed on the carriage, pointing directly to where the anvil´s pivot is going to attach. Thus, when the carriage is being lifted and the anvil keeps reflecting the sensor´s light beam back, it is concluded that the anvil is attached to the carriage.

Figure 4.16 - OMRON E3FA-DN23 [36].

Just like what happens with the optical detector, subject of section 4.2.3.1, the selected photoelectric sensor has an NPN configuration and, therefore, will work in an inverted logic, so it will also require an associated relay (K11). The line that the relay´s contact feeds is the PCIN4. Since its number of leads and respective functions are also the same as the optical detector, demonstrated in Figure 4.17, both sensor´s lead connections are identical. This means that this sensor is also working in Dark On mode (see Figure 4.18).

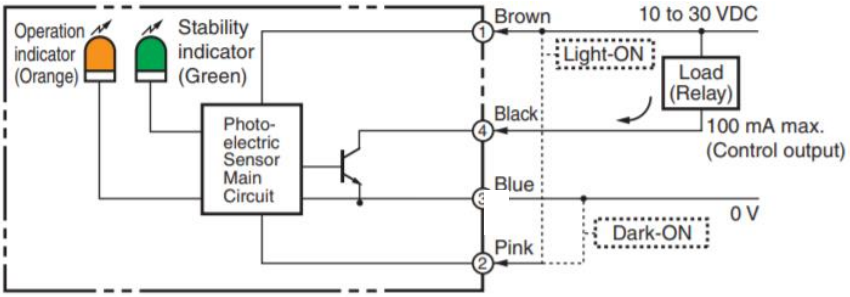

Figure 4.17 - OMRON E3FA-DN23´s lead connections [36].

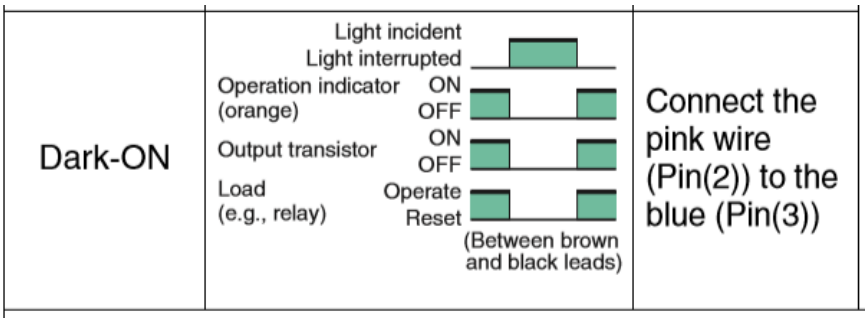

Figure 4.18 - OMRON E3FA-DN23´s Dark-ON mode [36].

4.2.3.5. Proximity sensor

The drop weight machine´s software should always be aware in which position the ARS is, at any given moment. For that reason, when buying the pneumatic cylinders from Festo, the recommended proximity sensor, a FESTO SME-8M-DS-24V-K-0,3-M8D [37] (see Figure 4.19), was also obtained. This is a sensor that works by the magnetic Reed principle and has a normally open contact. So, when this sensor detects the presence of the magnetic field created by the cylinder´s magnet, its contact changes state (closes), letting current pass through and feeding the PCIN7 line, which will then change the state of the associated variable in the software.

Figure 4.19 - FESTO SME-8M-DS-24V-K-0,3-M8D [37].

To implement it, the brown and blue leads must be connected to the 24 VDC and 0 VDC, respectively, and the black lead connected to the PCIN7 line.

4.2.3.6. Accelerometer

The accelerometer is the sensor responsible for measuring the accelerative forces of the anvil-impactor assembly during the fall. The highest expected values for the linear acceleration will happen at the moment of impact. Like it was stated in section 3.2, accelerations on impact are unpredictable, not only because of the system dynamics but also because of the great variety of materials that can be tested in this drop weight machine. So, as a way of trying not to limit the drop weight machine in terms of what materials can be tested, an accelerometer with a vast measuring range must be selected.

Another aspect to consider, when selecting the accelerometer, is its frequency range, which depends on the type of application, like Figure 4.20 shows.

Application	Piezoelectric	Capacitive MEMS	Piezoresistive
Static Acceleration (0 Hz, 1 g) Gravity, Sensor Orientation		✓	✓
G- Force (0 Hz, <25 g) Rocket, Centrifugal, Aircraft		✓	✓
Seismic (<1 Hz, <1 g) Earthquake, Waves, Bridges	✓		
Low Frequency Vibration (<5 Hz, <25 g) Human Motion, Robotics	✓	✓	✓
General Vibration (5 Hz to 500 Hz, <25 g) Electric Motor, Car Suspension	✓	✓	
High Frequency Vibration (>500 Hz, <25 g) Gear Noise Analysis, Turbine Monitoring	✓		
General Shock (<100 Hz, <200 g) General Testing, Shock Absorber Testing	✓	✓	✓
High Impact Shock (<250 Hz, >200 g) Drop Testing	✓		✓
Extreme Shock (>1,000 Hz, >2,000 g) Vehicle Crash Testing, Metal on Metal	✓		✓

Figure 4.20 - Different types of accelerometer per application [21].

Based on the information given in Figure 4.20, it´s possible to conclude that the drop weight impact test application is categorized as a high impact shock. However, considering the unpredictable behaviour of impact loads, one has to guarantee that the sensor has a frequency range higher than the 250 Hz shown. Therefore, it was concluded that the needed accelerometer for ADFEUP´s drop weight machine should be one considered to be for extreme shock applications.

To meet the mentioned requirements, the KISTLER 8704B5000 [38] accelerometer (see Figure 4.21) was selected. This sensor has a measuring range that goes from -5000g up to 5000g (the widest range of its series) and a frequency range from 1 to 10000 Hz. This is an Integrated Eletronic PiezoElectric (IEPE) sensor, meaning that it contains a crystal (Quartz) structure that, when stressed by accelerative forces, creates a proportional charge output signal. Despite this sensor´s signal having high voltages, it produces almost no current, meaning that the sensor is a high impedance source of electricity, which makes it susceptible to signal degradation. Also, high impedance signals are very vulnerable to all kinds of noise, which is bad for precise measurements. In order to convert the high impedance to a low impedance and to power the accelerometer, a charge amplifier must be selected.

Figure 4.21 - KISTLER 8704B5000 [38].

A LabAmp of the type KISTLER 5165A [39] (Figure 4.22) was the chosen charge amplifier to connect to the accelerometer. It has four input channels and four output channels, although the latter aren´t used. This hardware provides two rj45 ports which allow stablishing an ethernet network between other LabAmps, if needed, and a computer.

Figure 4.22 - LabAmp of the type KISTLER 5165A [39].

Additionally, along with the LabAmp, Kistler also provides a computer software that shows the measured data in real time. In this software one can define how the acquisition

of that data is performed, like the sampling rate, the number of samples or duration of the acquisition. Knowing that the sampling frequency should be, at least, 10 times greater than the accelerometer´s frequency, its value can be calculated by Expression 4.5:

$$f_{sampling} > 10 \times f_{accelerometer} = 10 \times 10000 = 100000\ Hz \qquad (4.5)$$

The chosen sampling rate was 200000 Hz, because it was the maximum sampling rate that wouldn´t cause trouble to the computer post-process analysis.

This software also provides the possibility to create virtual channels that can calculate other measurands in real time, like the displacement. However, this functionality isn´t very useful because, as it was said in section 3.2, the displacement would be obtained affected by an error. Figure 4.23 shows the accelerometer configuration in the provided software.

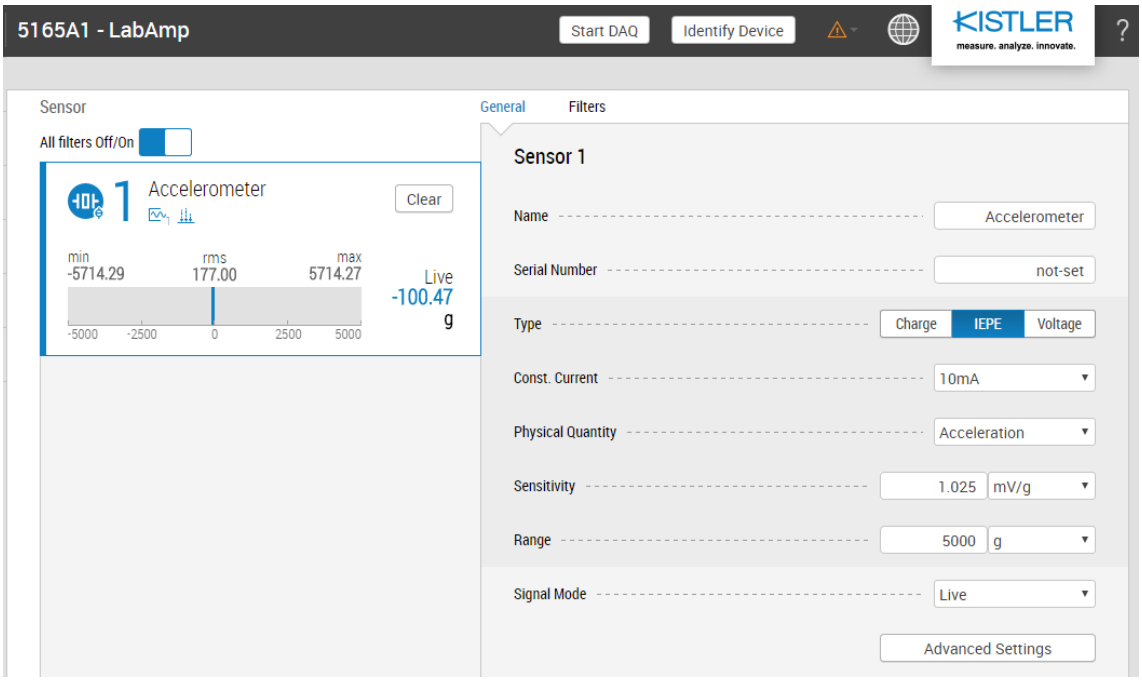

Figure 4.23 - Accelerometer configuration in the provided Kistler´s software.

4.2.3.7. Press force sensor

The load cell is the element responsible for measuring the impact loads applied on the specimens. Like it was stated in section 3.2, the way that this sensor is implemented in the anvil-impactor assembly makes it susceptible to both compressive forces (known to be lower than 35 kN) and tensile forces (calculated to be around 5.9 kN), so the sensor to be selected must withstand these loads. Additionally, the selected sensor should have a frequency range similar to the accelerometer (1 to 10000 Hz) in order to obtain matching measurement results.

Considering the mentioned requirements, the KISTLER 9333A [40] press force sensor was selected, shown in Figure 4.24. Just like the accelerometer, this sensor is also based on the piezoelectric measuring principle, meaning that it creates a charge output signal that is proportional to the load applied to its crystal quartz. It is specially designed to measure compressive forces, up to 50 kN, which meets the requirements of at least being able to measure 35 kN. However, the maximum tensile force allowed is 5 kN, lower than the 5.9 kN calculated in section 3.2. To avoid these tensile loads on the press force sensor, the operator can adjust the test parameters (increasing the drop weight and decreasing the impact velocity), in order to obtain the same impact energy that would be obtained when releasing a drop mass of 8.5 kg of the highest point.

Figure 4.24 - KISTLER 9333A [40].

One of the most important things to have in mind, to guarantee that the press force sensor is taking good measurements, is its mounting. The mounting of the press force sensor must guarantee that all the load is transferred to its flanges, so, considering the anvil-impactor assembly proposed in section 3.2, it is concluded to be the correct implementation.

To help this sensor operate, another input channel of the LabAmp is used. This will allow both sensors to start the data acquisition at the same time, resulting in data that can be directly compared. For this type of sensor, the configuration is slightly different, as shown in Figure 4.25.

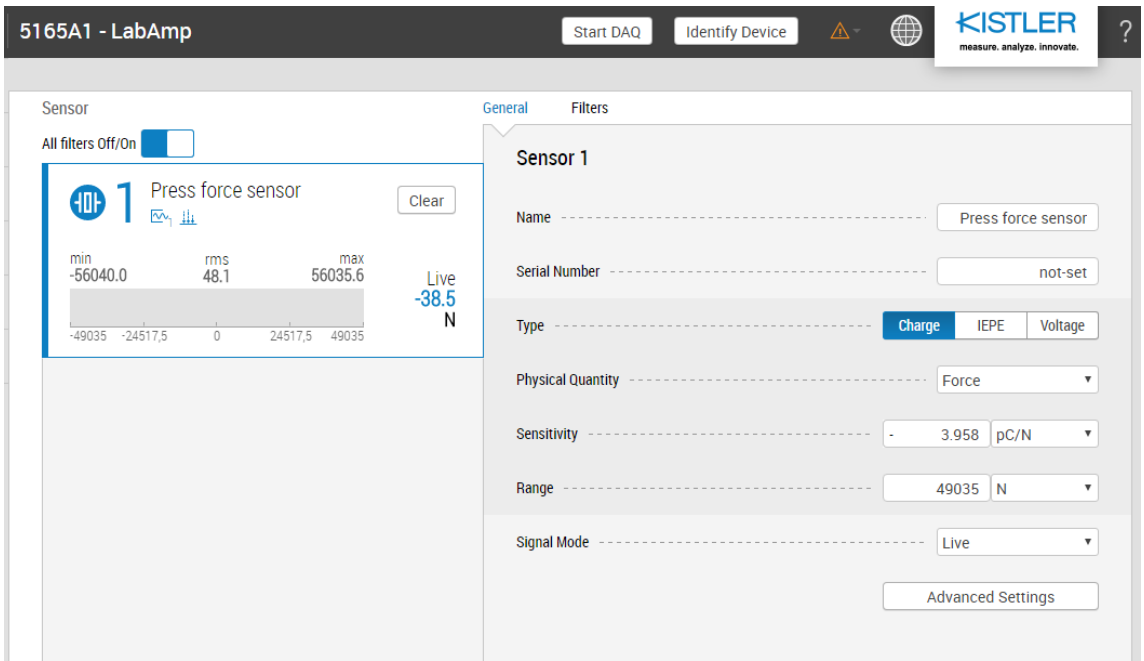

Figure 4.25 - Press force sensor configuration in the provided Kistler´s software.

4.2.4. Boards

The control of the drop weight machine is made possible via a MATLAB® add-in running on a computer, which is Simulink®. Therefore, to make the set of sensors and actuators be able to communicate with the computer, a DAQ board was installed on the latter. However, all sensors and actuators work with 24 VDC, while the computer digital logic works with 5 VDC, making it impossible for the computer to receive inputs or provide outputs as it is. To make this communication compatible, a printed circuit board (PCB) was designed, made and implemented by Sousa [6]. This means that this PCB is able to convert the detectors´ 24 VDC signals into 5 VDC signals to feed to the computer´s DAQ board and to convert 5 VDC signals coming from the computer´s DAQ board into 24 VDC signals to feed the motors and solenoids. Additionally, a second board had to be chosen so that the computer could decode the data collected from the encoder of the lifting sub-system´s motor and send it to the software.

4.2.4.1. DAQ board

The selected DAQ board is a Measurement Computing´s PCIM-DDA06/16 [41] (represented in Figure 4.26), which has 6 analog output channels and 24 bits of digital input/output. The 24 bits of digital input/output are divided into 3 channels (A, B and C), each one with 8 bits (1 byte). Each channel can be defined as a set of inputs or outputs, but individual bits can´t. A was defined as an input channel, while B and C were chosen to be output channels. While channel A and B were fully used, channel C is only used to send a reset signal to the encoder of the lifting sub-system´s motor (explained in next sub-section) and to change the lifting sub-system´s motor rotating direction. Table 4.4 shows the association between the bits in each channel and the line they feed.

Figure 4.26 - Measurement Computing´s PCIM-DDA06/16 [41].

Table 4.4 - Bit channels and the respective electrical circuit line association.

Channel	Bit	Line	Description
A (Input channel)	A1	PCIN7	Proximity sensor
	A2	PCIN6	Optical detector
	A3	PCIN5	Inductive detector
	A4	PCIN4	Photoelectric detector
	A5	PCIN3	Velocity acquisition sub-system´s lower microswitch
	A6	PCIN2	Velocity acquisition sub-system´s upper microswitch
	A7	PCIN1	Emergency buttons
B (Output channel)	B0	ENA	L298N Board Enable
	B1	PCOUT5	Inductive detector override
	B2	PCOUT4	Velocity acquisition sub-system´s motor powering
	B3	PCOUT3	Virtual emergency button
	B4	PCOUT2	ARS control
	B5	PCOUT1	Anvil release signal
	B6	IN2	Select ascending direction for velocity acquisition´s motor
	B7	IN1	Select descending direction for velocity acquisition´s motor
C (Output channel)	C0	INDEX	Reset encoder of the lifting sub-system´s motor
	C1	PCOUT6	Select ascending direction to move the carriage
	C2	PCOUT7	Select descending direction to move the carriage

4.2.4.2. Encoder board

As a way of knowing the position of the sub-system´s motor and, consequently, knowing the position of the carriage, this motor is equipped with an incremental optical encoder, namely an Intecno ME22-300-6.000-2-LS1 [42]. This is a high-resolution optical encoder that has two square wave output channels (A and B) plus an index channel (I) and can count 300 pulses per revolution. Whenever the encoder turns a certain angle (360/300=1.2º), channel A gives a pulse and channel B gives the same pulse, but phase-

shifted by 90º, in order to know the direction of the motor´s rotation. Every time the encoder performs a complete revolution, channel I gives a pulse, although this channel is not used for this purpose, as it will be posteriorly explained. Figure 4.27 illustrates the encoder´s signals throughout time.

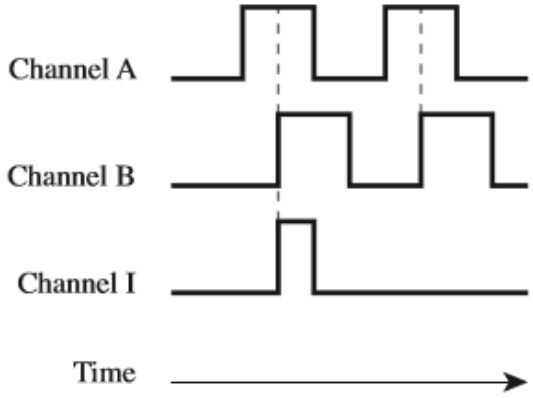

Figure 4.27 - Intecno ME22-300-6.000-2-LS1´s signals throughout time.

To convert the pulses generated by the encoder into useful information that can be interpreted by the software, a Measurement Computing´s PCI-QUAD04 [43] (Figure 4.28) is used. This is a quadrature encoder board that has the particularity of reading both channels´ (A and B) rising and falling edges. This functionality increases the resolution by a factor of four (4*300=1200), since the board reads four pulses per encoder count. Thus, whenever the motor´s shaft turns 0.3º (resulting from 360/1200) the encoder board increases its counting by one.

Figure 4.28 - Measurement Computing´s PCI-QUAD04 [43].

One thing the encoder lacks is a way of resetting its counting at will, which is needed just before the carriage starts to position itself to release the anvil-impactor assembly. However, the encoder allows resetting the counting when channel I is activated. Recurring to this functionality and using an output signal from de DAQ board (C0), instead of the actual channel I, the desired functionality is achieved.

4.2.4.3. PCB

As discussed in section 4.2.4, a PCB was designed and implemented as a way to convert 24 VDC signals into 5 VDC signals, and vice-versa. The approach taken to make this component work as pretended was to use optocouplers. The concept of the optocouplers functioning is very similar to the relays´ one: when a current passes through one of the lines of the optocoupler, a led (a coil, in relay analogy) is activated, which will close the other line´s circuit because a phototransistor (a contact, in relay analogy) is receiving the led´s light beam. Since both lines are completely isolated, there is no risk in feeding the computer a 24 VDC signal, which could damage its internal circuit. Due to the number of inputs and outputs needed, four PS2502-4 were implemented in the PCB, because each one of this type of component provides four individual integrated optocouplers, allowing for multiple connections at once. Two PS2502-4 were used for the inputs and the other two for the outputs. A PS2502-4´s circuitry can be seen in Figure 4.29.

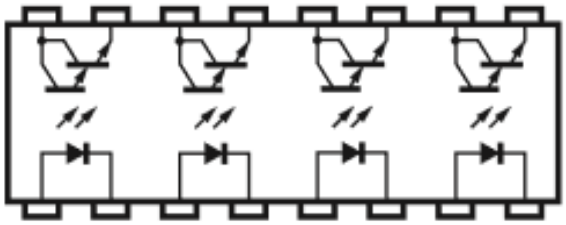

Figure 4.29 - PS2502-4.

Since the communication is made both ways (sensors to computer and computer to actuators), two distinct types of circuits had to made, one for the input conversion and one for output conversion, as shown in Figure 4.31 and Figure 4.30, respectively.

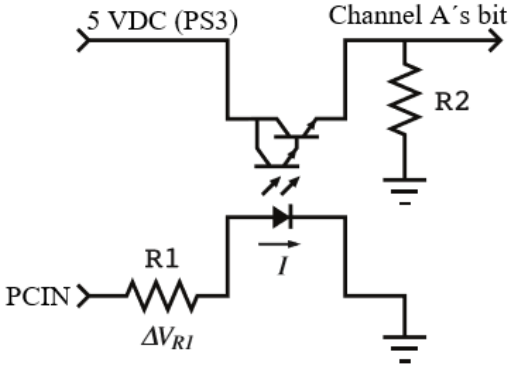

Figure 4.31 - Computer input conversion for a single line.

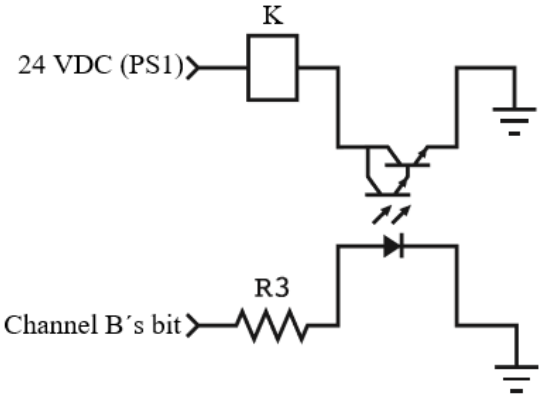

Figure 4.30 - Computer output conversion for a single line.

The values for the implemented resistors, as calculated by Sousa [6], are $R1 = 1200\ \Omega$, $R2 = 390\ \Omega$ and $R3 = 390\ \Omega$. The final PCB design, in *gerber* format, can be seen in Figure 4.32.

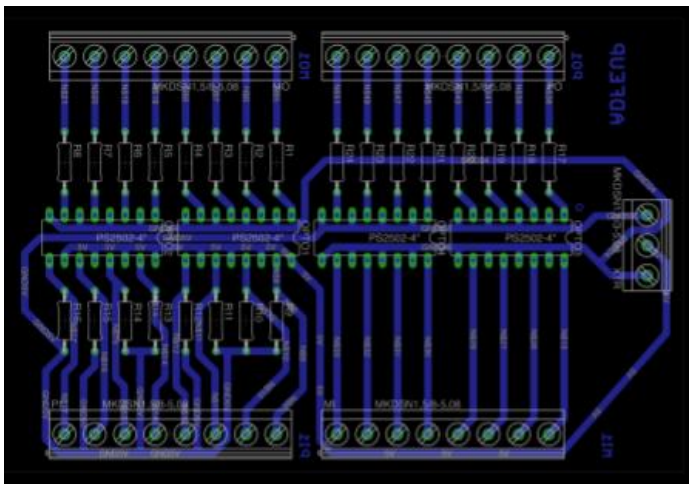

Figure 4.32 - Designed printed circuit board, in *gerber* format [6].

4.2.5. Power circuit´s hardware

The electric power source for the drop weight machine is directly obtained from the mains, which means that it comes in the form of 230 VAC. Since all of the electrical hardware described in previous sections is powered by 5 or 24 VDC, power supplies were used. Considering that, there are no analog signals with the exception of the driver reference, which is given by the DAQ board, there´s no need to worry about signal´s noise. For this reason and because they are cheaper, three switch power supplies were chosen by Sousa [6].

The lifting sub-system´s motor has its own power supply, because it has a crucial role in the drop weight machine and also because it needs a lot of power. At max power, the current intensity it will require is 6 A, as calculated by Sousa [6], using Expression 4.6.

$$P = V \cdot I \Leftrightarrow I = \frac{P}{V} = \frac{140}{24} \approx 6\ A \tag{4.6}$$

Since 6 A power supplies weren´t found, a 10 A power supply was chosen, namely a RS Pro 240W DRP240 Series [44], demonstrated in Figure 4.33 - a. In the electrical circuit´s diagrams, this power supply is referenced as PS2.

To power the various sensors and relays present in the drop weight machine´s circuitry a RS Pro 96W MDR-100 Series [45] was chosen (see Figure 4.33 - b). This power supply provides 24 VDC and has a current of 4 A. The value of the needed current was obtained by adding the required current for every component that is fed 24 VDC and adding an extra for safety and future implementations. In the electrical circuit´s diagrams, this power supply is referenced as PS1.

The last power supply is used to power the signal condition board (or PCB) and the L298N board with 5 VDC. The selected power supply was a RS Pro 10W MDR-10 Series [46], shown in Figure 4.33 - c. It has 2 A of current, which is much higher than what these

components really need. In the electrical circuit´s schematics, this power supply is referenced as PS3.

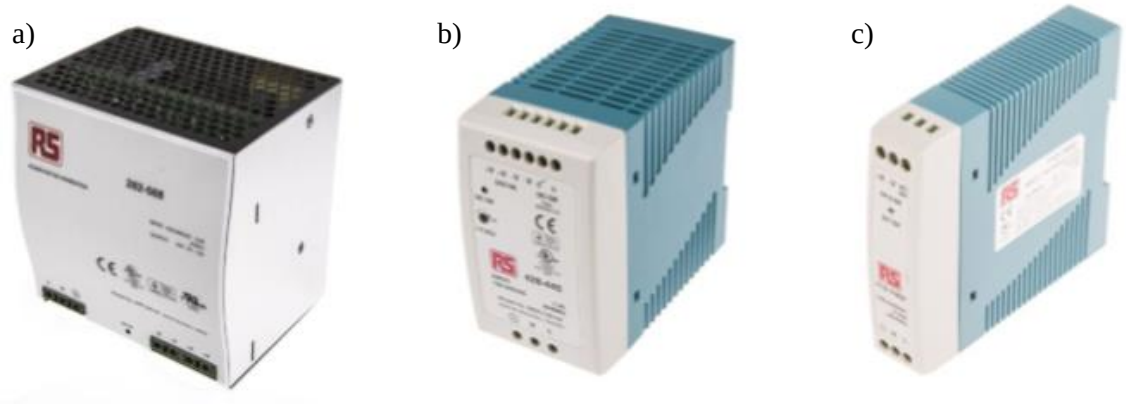

Figure 4.33 - a) RS Pro 240W DRP240 Series [44]; b) RS Pro 96W MDR-100 Series [45]; c) RS Pro 10W MDR-10 Series [46].

As what happens with most machines, circuit protection had to be implemented. The implemented components responsible for this protection are:

- General manual power switch;
- Residual-current circuit breaker for the 230 VAC part of the electrical circuit, SIEMENS 5SM3312-0 [47], represented in Figure 4.34 - a;
- Circuit breaker for the 230 VAC part of the electrical circuit, Schneider Electric´s Tesys GB2DB21 [48], represented in Figure 4.34 - b;
- Circuit breaker for the 24 VDC PS1´s power lines of the electric circuit, Schneider Electric´s Tesys GB2CB09 [49], represented in Figure 4.34 - c;
- Circuit breaker for the 24 VDC PS2´s power line of the electric circuit, ABB SH201T-C10 [50], represented in Figure 4.34 - d;
- Fuse for the 5 VDC PS3´s power line of the electrical circuit.

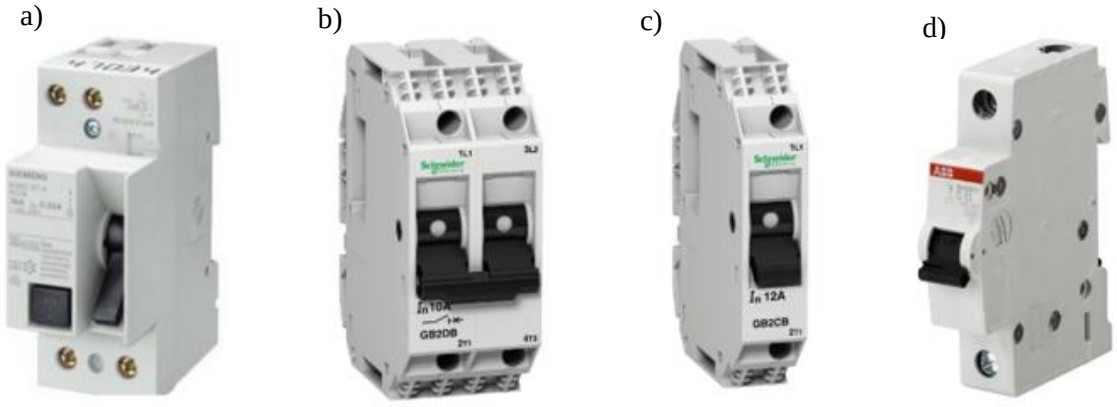

Figure 4.34 - a) SIEMENS 5SM3312-0 [47]; b) Schneider Electric´s Tesys GB2DB21 [48]; c) Schneider Electric´s Tesys GB2CB09 [49]; d) ABB SH201T-C10 [50];

4.2.6. Emergency circuit´s hardware

When designing any machine, it´s important to consider that things can go unexpectedly wrong and that there should be a way of preventing this type of situations to cause some major damage. For this reason, all machines have an emergency state, that, when active, immediately interrupts the machine´s actions in that moment and intervenes in a way of trying to protect its components and operators.

Currently, there are three ways that make this drop weight machine enter an emergency situation: To press one of the two physical buttons (one fixed at the machine structure and other near the computer), to press the virtual button in the interface or when the carriage passes thru its stroke´s limit. In the future, there could be more ways of doing so, like, for example, if some safety barriers are installed and they are opened at the moment of a test.

The implemented physical emergency buttons are the Schneider Electronics´s XALK178E [51] (see Figure 4.35). Each button has two associated contacts, one normally closed and one normally open. The normally closed contacts are connected in series with solenoid of the valve that controls the pneumatic cylinder that releases the anvil, while the normally open contacts are connected to two relays´ coils (K3 and K10). These relays will have normally closed contacts in series with several components´ power lines that need their power shut down when emergency situations happen, except for the ARS, which has normally open contacts in series.

Figure 4.35 - Schneider Electronics´s XALK178E emergency button [51].

In the virtual emergency button case, when pressed, it will send an output signal via PCOUT3 line that, after passing through the PCB, will feed a relay´s coil (K4). Like what happens with the physical buttons´ relays, also this relay will have normally closed contacts in series with components that should shut down in emergencies, while having a normally open contact in series with the ARS.

To summarize, when an emergency situation is declared, the cylinder that releases the anvil as well as both installed motors are deactivated, stopping any possible action that the machine is performing. However, the ARS will be activated, preventing the damaging of the specimen, even if the emergency situation occurred when the anvil is falling.

The software is always listening to all components that can trigger the emergency situation and no matter what state the machine is at the moment, it can always switch to

that state. In order to exit the emergency state, the software waits for an user input that informs that the emergency situation is solved.

4.3. Command Sequence and Interface

As stated in previous sections, the command sequence is controlled by a program running in a MATLAB® add-in, Simulink®. Simulink® offers a great variety of functionalities that allow the communication between the computer and the drop weight machine, like Simulink Real-Time™ toolbox (used to connect the software to the DAQ board and the encoder board) and Simulink Stateflow® (used to program states and transitions of the machine´s behaviour). Ramos [5] and Sousa [6] had already started to create a command sequence, however, since there were some new implementations in the machine, it had to modified. Additionally, it was necessary to create an interface so that any operator could easily work with the drop weight machine. The interface was created using another MATLAB® add-in, GUIDE®, that stands for graphical user interface developing environment.

In a way, Simulink Stateflow® works similarly to Grafcet, since block states are used to perform a set of actions and to go from block to block the conditions of a transition must be validated, as Figure 4.36 exemplifies. Figure 4.36 also shows other common transitions, like the "start" transition (represented by an arrow with a circle at the other end) and the "end" transition (represented by a white arrow). Simulink Stateflow® can be accessed through the use of a Chart in Simulink®. Chart is a type of block that receives the inputs from Simulink® and, after running the state machine, provides the outputs to Simulink® in real time. Charts also have local variables that help in the logic sequence between states. A list of all variables can be consulted in Appendix E.

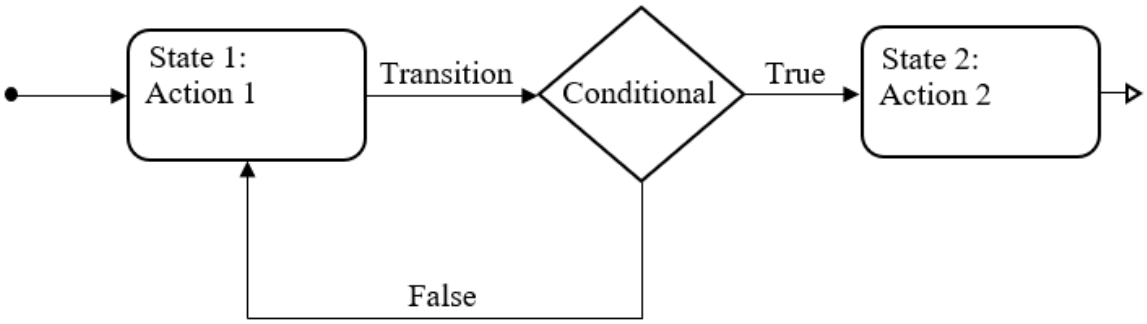

Figure 4.36 - How transitions are processed in Simulink Stateflow®.

In state blocks, actions can be performed when entering, during or when exiting the block, which can be useful for a better performance of the developed program. In addition, state blocks can contain other state blocks within themselves, in order to stablish a hierarchy of importance. This means that sub-routines can be created inside a higher-level hierarchic routine. Transitions between higher-level state blocks always take precedence over the lower-level ones.

In the next sections, each level of the implemented command sequence, as well as the associated interface, will be described and explained, so that the functioning of the drop weight machine is completely understood.

4.3.1. Highest-level routine

The highest-level of the Simulink® Stateflow diagram only has two states, as depicted in Figure 4.37: the MAIN state and the SOS state. The MAIN state is where the normal functioning of the machine takes place, while the SOS state runs when an emergency situation is declared. The reason why this is done is because, as it was previously said, higher-level transitions take precedence over lower-level transitions, meaning that, even if the machine is performing some action or transition within the MAIN state, it´s always ready to enter in the SOS state and interrupt what is doing at any given moment.

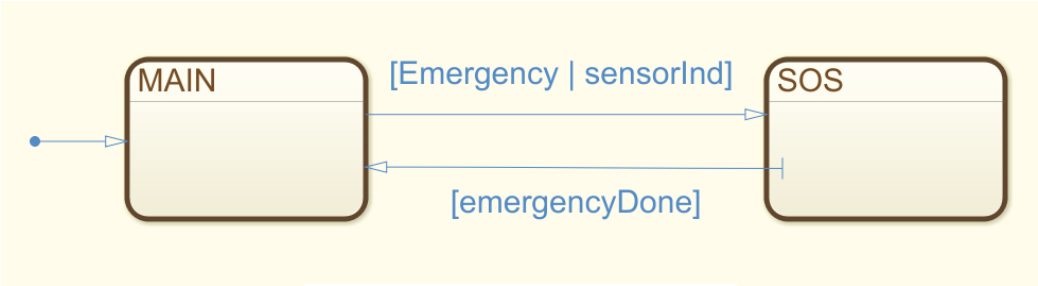

Figure 4.37 - Highest-level routine.

4.3.2. MAIN sub-routine

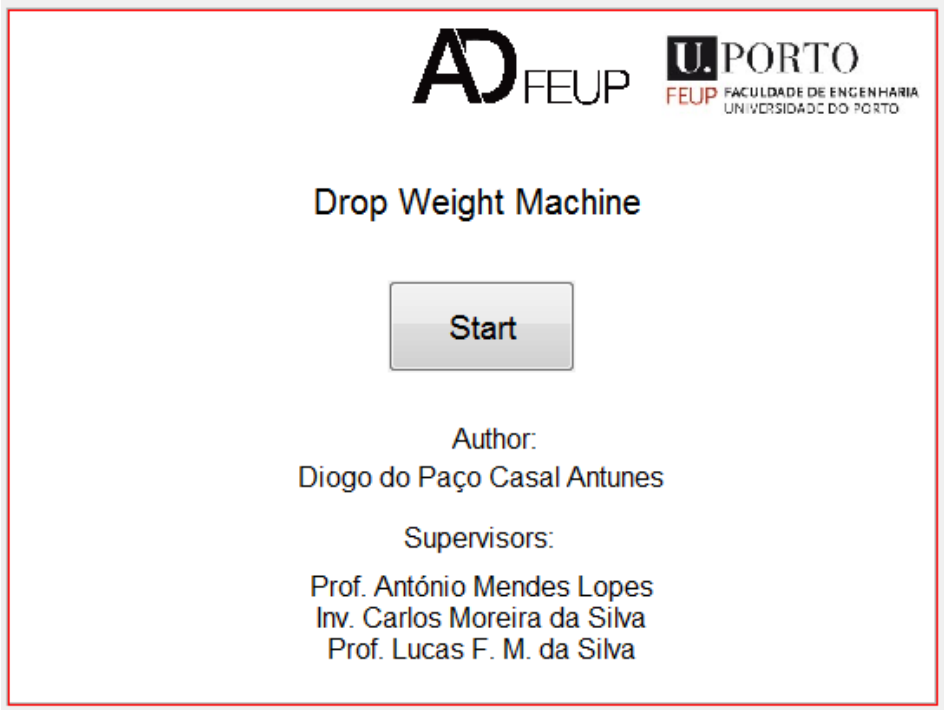

Figure 4.38 - Initial interface window.

When starting the program, by pressing the "Start" button of the interface (represented in Figure 4.38), the machine automatically enters the MAIN state (Figure 4.39). Within the MAIN state, there are three important sub-routines which are the INIT sub-routine, the TEST sub-routine and the MANUAL sub-routine. The INIT sub-routine takes care of the initialization of the machine, while the others are two possible modes to control the machine. Additionally, there is an IDLE state that resets some variables of the program and also is a middle state that waits for the operator to select in between the TEST mode and the MANUAL mode.

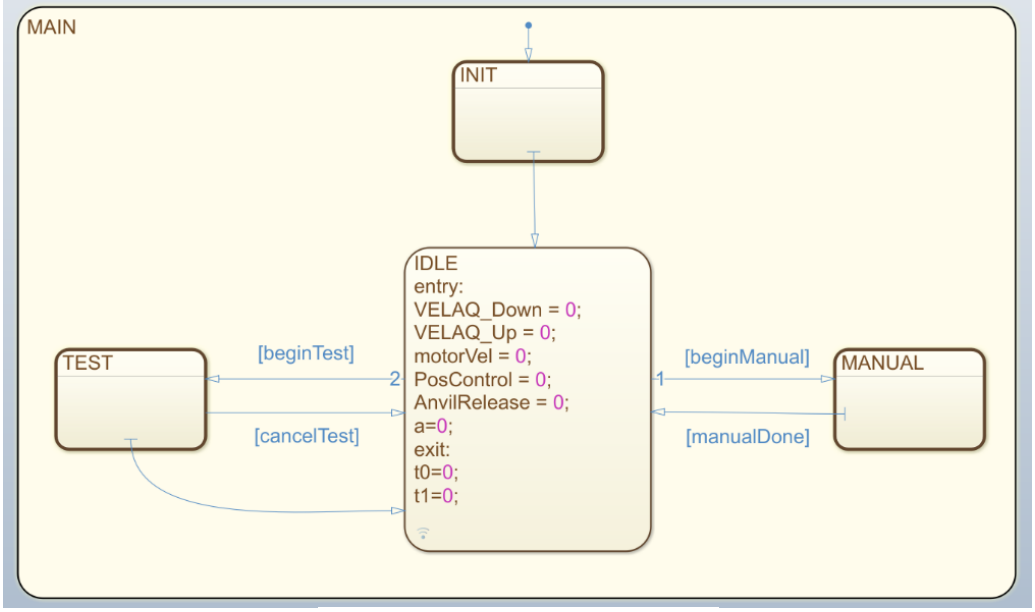

Figure 4.39 - MAIN sub-routine.

To select the mode in which the machine operates, the operator has to press the button that corresponds to that mode in the interface window shown in Figure 4.40.

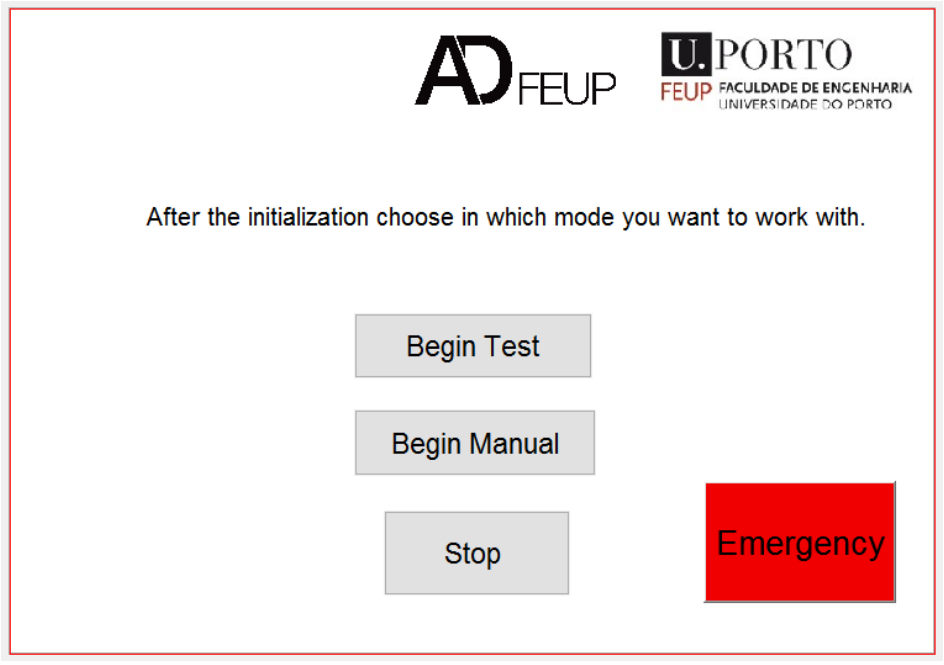

Figure 4.40 - Select operating mode interface window.

4.3.3. INIT sub-routine

The INIT sub-routine is a very simple one, being composed by three blocks, as shown in Figure 4.41, two of which are sub-routines: the FIND_VELAQ, responsible for positioning the moving platform of the velocity acquisition sub-system to its lowest point, and the CHECK_ANVIL, that verifies if the anvil is attached to the carriage. Additionally, in the INIT sub-routine, the initial value of most of the variables is assigned.

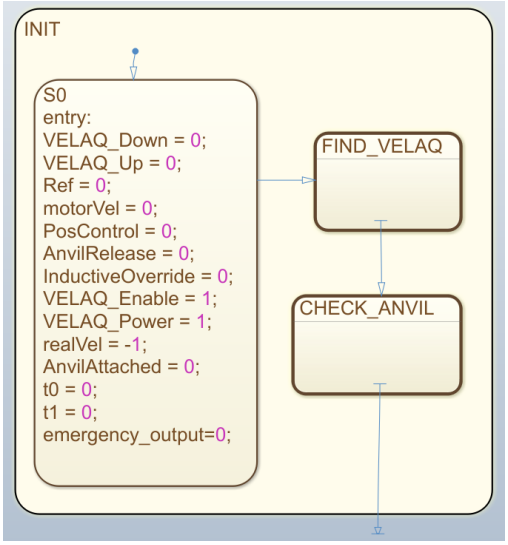

Figure 4.41 - INIT sub-routine.

4.3.4. FIND_VELAQ sub-routine

This sub-routine is essentially used to position the moving platform of the velocity acquisition sub-system to its lowest point, as it was already stated. The logic behind this sub-routine is very simple: if the lower microswitch is not being pressed (given by the condition not(FDC_Inf)) the velocity acquisition sub-system´s motor forces the moving platform to go downwards until the mentioned microswitch is pressed. An overview of this sub-routine can be seen in Figure 4.42.

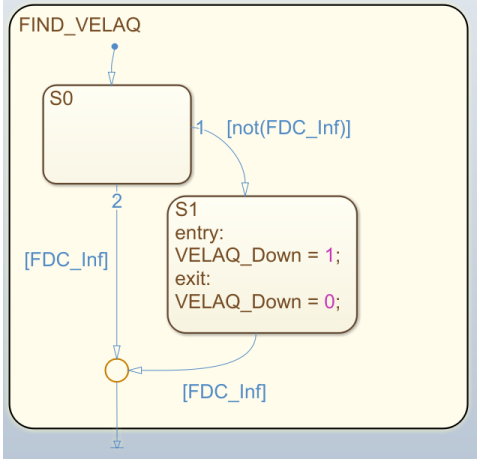

Figure 4.42 - FIND_VELAQ sub-routine.

4.3.5. CHECK_ANVIL sub-routine

The CHECK_ANVIL sub-routine, shown in Figure 4.43, is used to verify if the anvil is attached to the carriage. This sub-routine starts to check whether the photoelectric detector´s light beam is being interrupted or not. If the light beam is not being interrupted the program assumes that the anvil is not attached. If, on the other hand, the light beam is being interrupted, the carriage will be lifted to a defined height. If the light beam stays interrupted during that lift, the program assumes that the anvil is attached, if not, it is assumed that the anvil is disattached from the carriage.

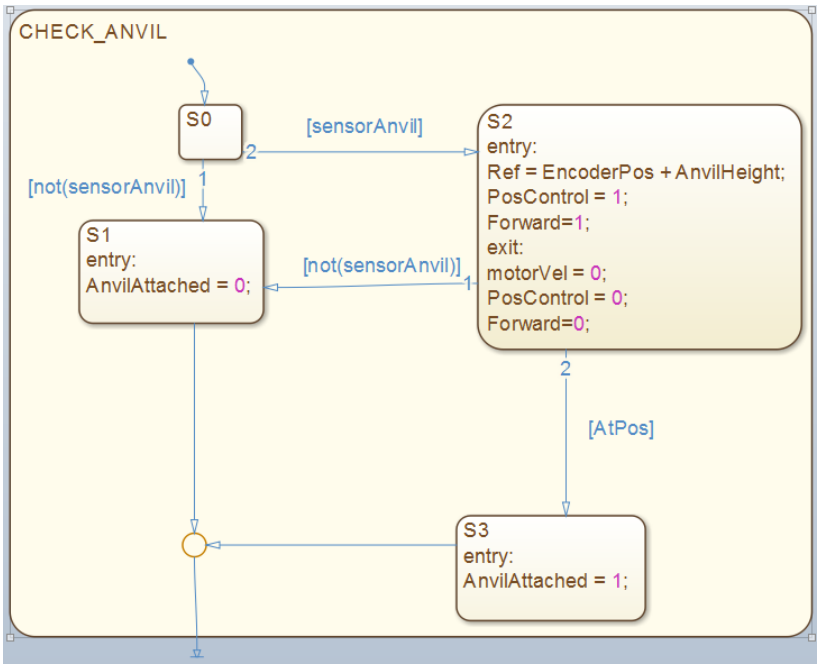

Figure 4.43 - CHECK_ANVIL sub-routine.

4.3.6. TEST sub-routine

The TEST sub-routine, like the name implies, is where tests with specific parameters are performed. Therefore, before the TEST sub-routine itself starts, it´s important to define the pretended values for the parameters of the test, which can be done by filling the fields in the interface window shown in Figure 4.44. Since the weights that attach to the anvil were already fabricated, the values for drop mass are discretized (lower value is 8.5 kg and higher value is 56 kg), thus, the operator must always give that information. This means that the operator just needs to define the value of one more parameter, since all others can be calculated from the two given ones. So, there are three ways to define the parameters:

- Type 1 - Drop mass and velocity on impact (ranging from 0.5 to 5 m/s);
- Type 2 - Drop mass and impact energy (ranging from 1 to 700 J);
- Type 3 - Drop mass and drop height (ranging from 0.012 to 1.274 m);

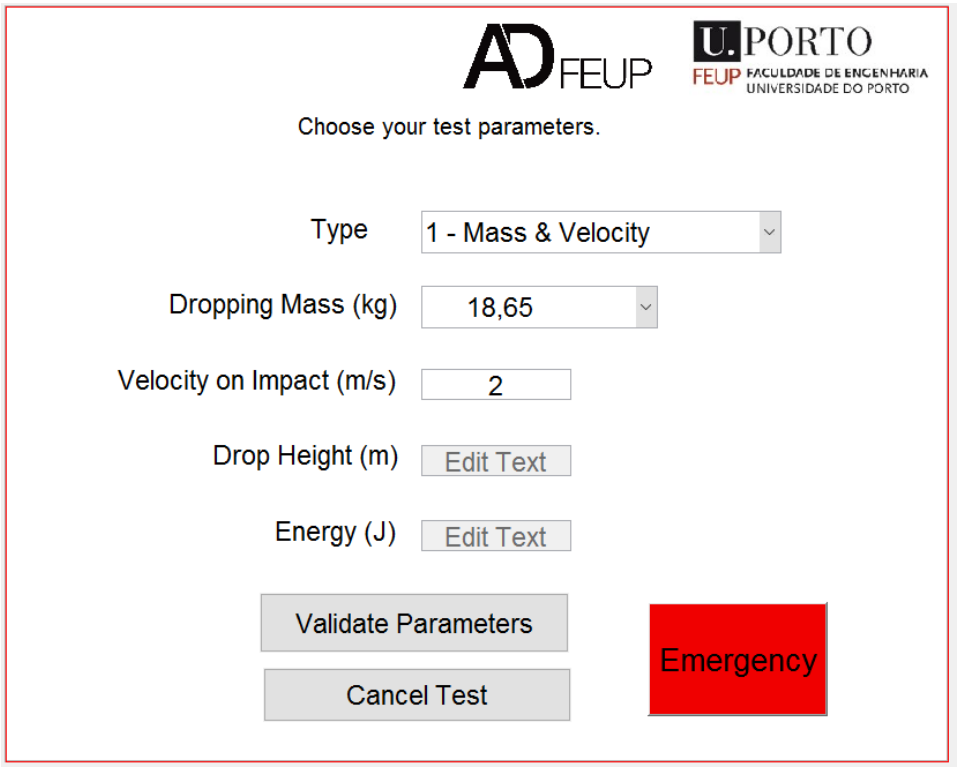

Figure 4.44 - Set parameters interface window.

After the definition of the pretended parameters, an interface window asking for the confirmation of those values will pop-up, like Figure 4.45 shows.

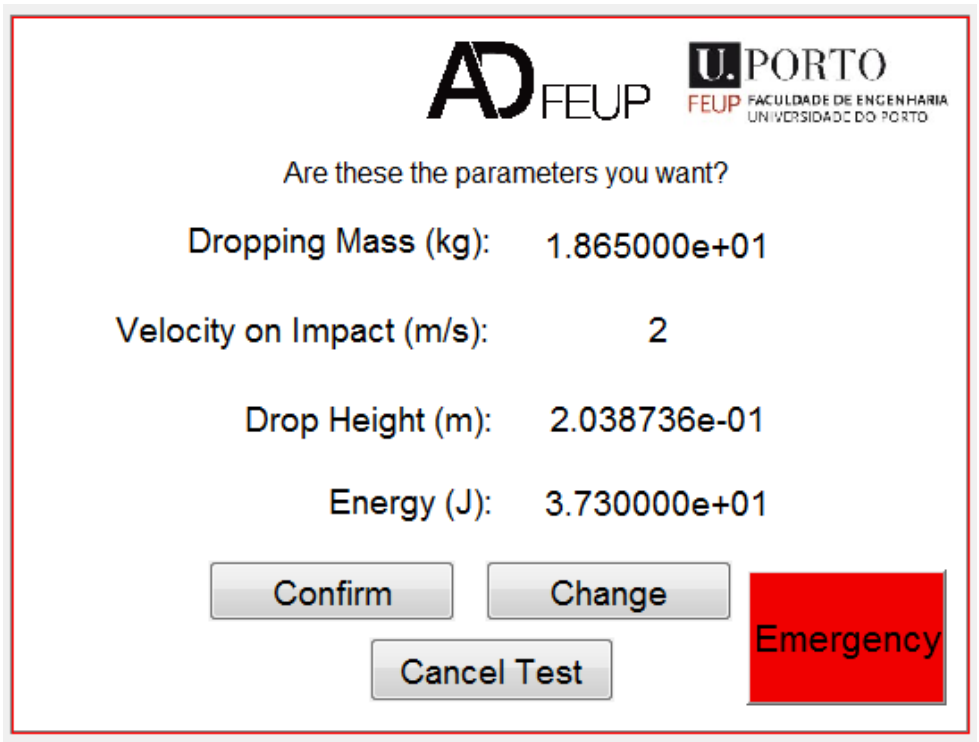

Figure 4.45 - Confirmation of the chosen parameters interface window.

If the presented values are not the desired ones, the operator has the possibility to go back to the previous interface window and reinsert the parameters´ values, by pressing the "Change" button. If, on the other hand, the parameters´ values are confirmed, a new interface window will open (see Figure 4.46). This new window will inform the operator which set of weights should be attached to the anvil.

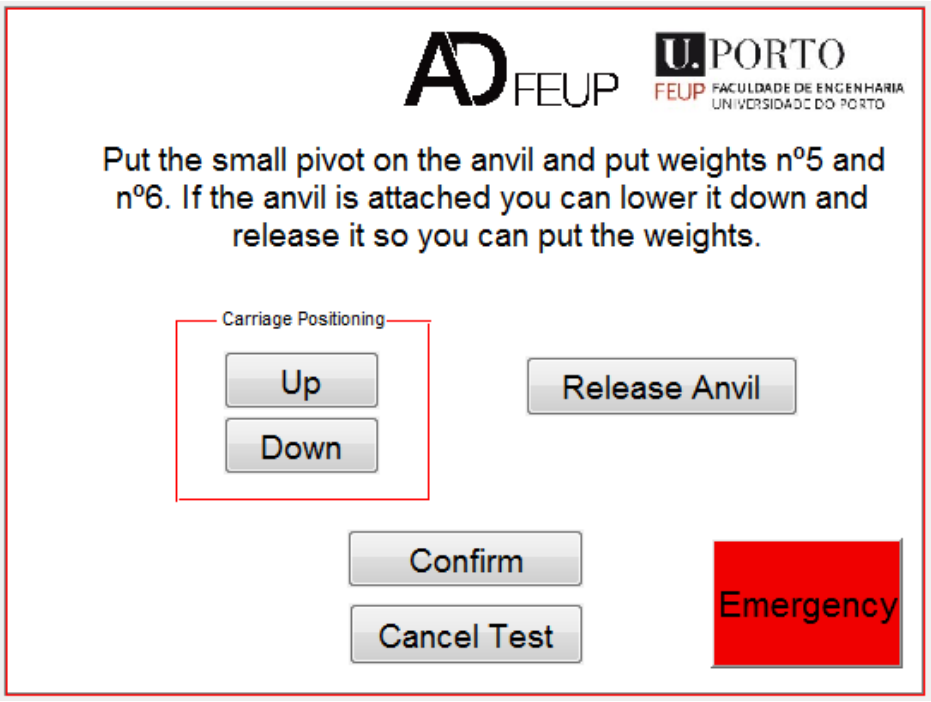

Figure 4.46 - Set weights interface window.

After attaching the indicated set of weigths and letting the program know that this action was done by clicking on the "Confirm" button, the TEST sub-routine´s sequence can finally be started. Notice that, when this state is active it´s because the machine has already been through the INIT sub-routine at least once, meaning that the software is aware if the anvil is attached or not, even if previous tests or a release of the anvil through the manual mode were performed. This is guaranteed because the program constantly tracks the state of the anvil attachment to the carriage using the boolean variable "AnvilAttached". So, if the machine knows that the anvil is not attached, it will start the TEST sub-routine by running the GRAB_ANVIL sub-routine. Contrarily, if the machine knows that the anvil is attached to the carriage, the sequence will continue without passing through the GRAB_ANVIL sub-routine.

The next stage of this sub-routine is to define the impact point, which is done in two separate steps. The first step is to manually position the anvil-impactor assembly in contact with the specimen and then press the "Manual Done" button of the interface window (see Figure 4.47). Once the "Manual Done" button is pressed, the second step is initiated. In this step, the moving platform of the velocity acquisition sub-system will automatically try to find the second comb of the mechanical part fixed to the anvil. This is essentially done by going through the velocity acquisition sub-system´s whole stroke.up and down, until the optical detector´s light beam is interrupted. If the light beam isn't interrupted, it means that the mechanical part is outside the velocity acquisition

system´s stroke, meaning that the specimen´s dimensions are not adequate, so it must be redesigned and adjusted to that stroke.

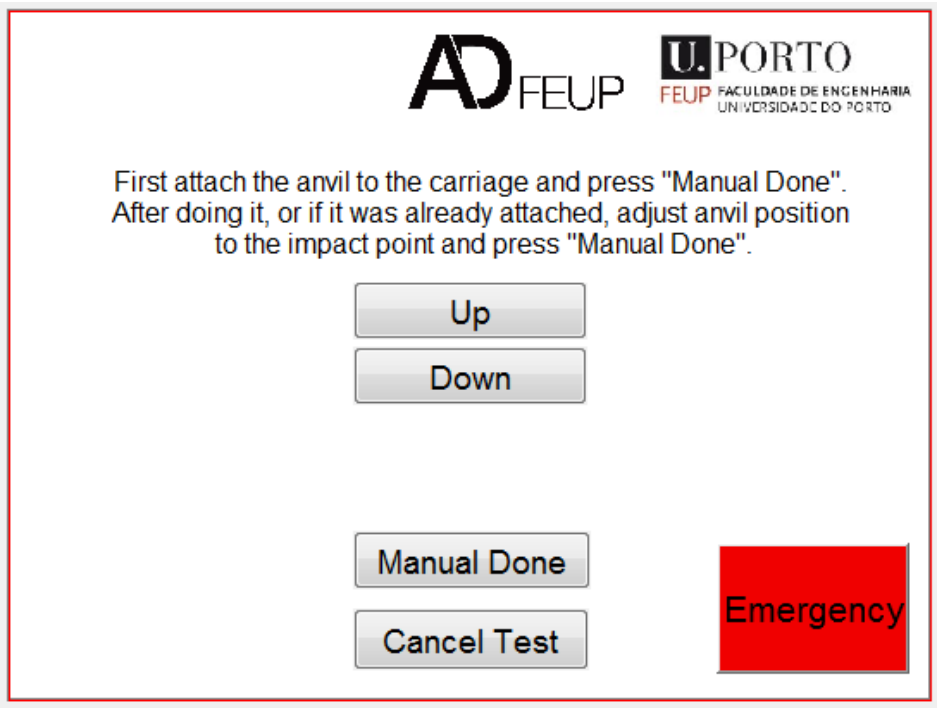

Figure 4.47 - Manual control (TEST sub-routine) interface window.

If the impact point was successfully found, it will be required that the “Manual Done” button is pressed a second time, so that a new interface window appears. This new window, that can be seen in Figure 4.48, will wait until the operator tells the carriage to lift the drop mass by pressing the “Begin Lift” button.

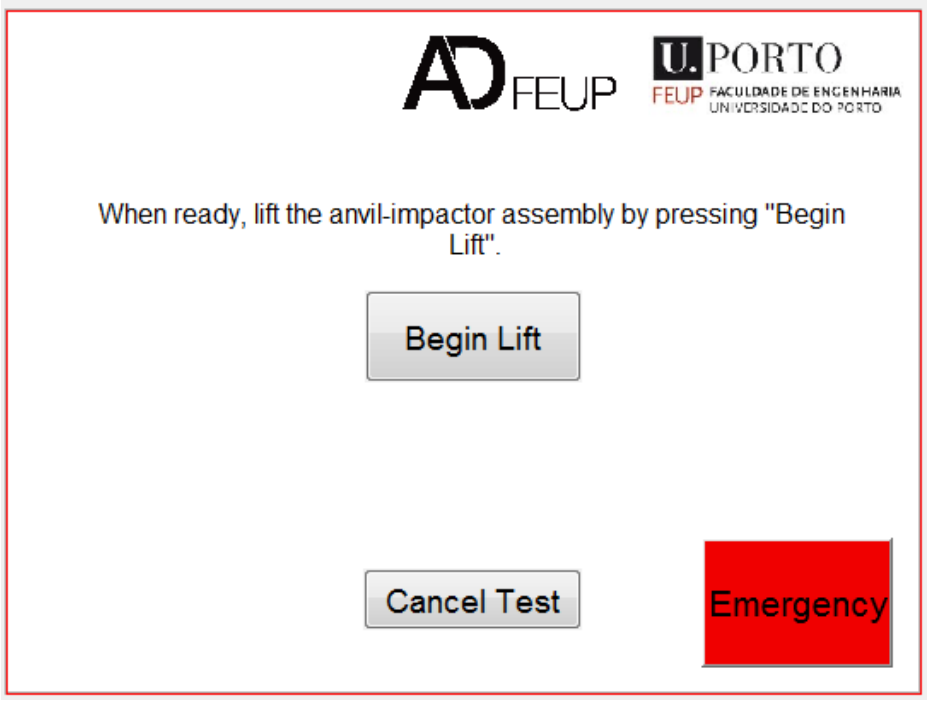

Figure 4.48 - Lift anvil-impactor assembly interface window.

Once the “Begin Lift” button is pressed, the carriage will lift the anvil-impactor assembly to the indicated, or calculated, height, given by the specified test parameters. After the carriage has arrived at the requested height, the TEST sub-routine will wait for the operator´s command of releasing the anvil. The releasing order is done by pressing the “Release” button in interface window shown in Figure 4.49.

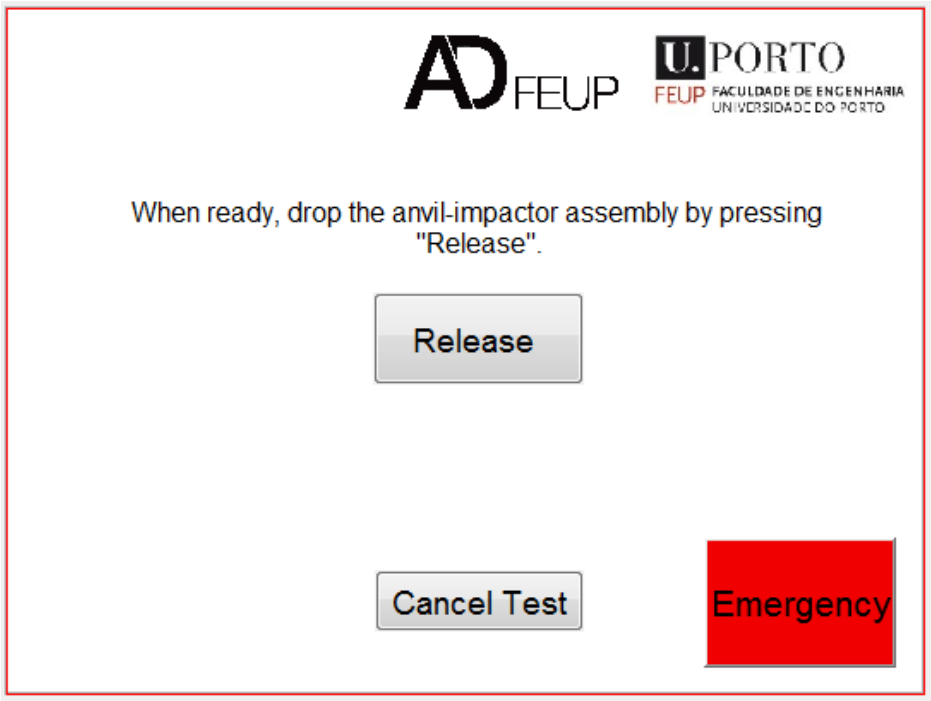

Figure 4.49 - Release anvil interface window.

After the anvil completes its fall and the ARS acts, a new interface window will show up, Figure 4.50, where the operator can obtain the velocity on impact.

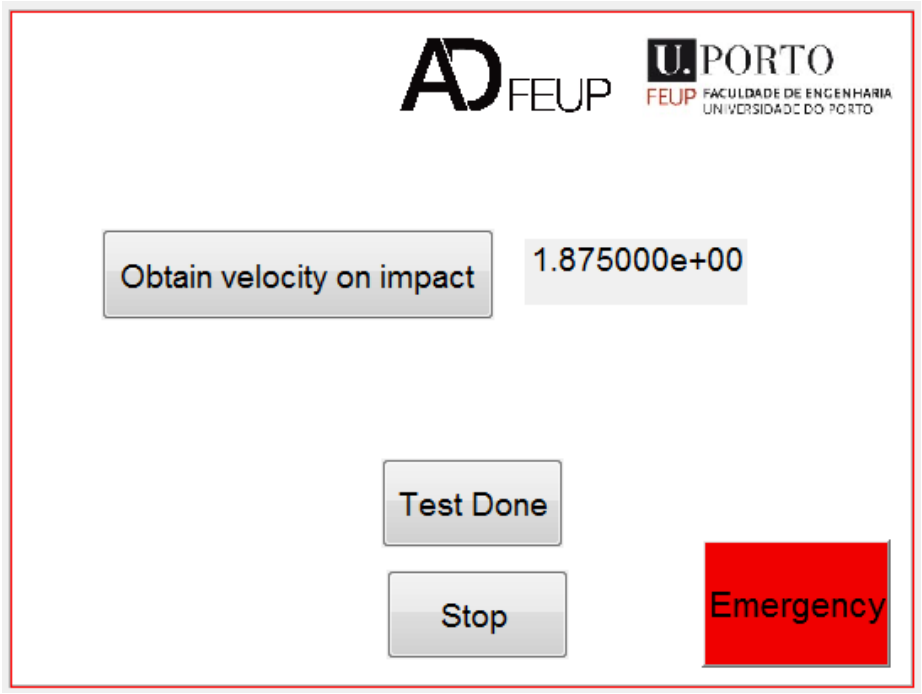

Figure 4.50 - Results interface window.

This velocity on impact is calculated by the Expression 4.7:

$$Vel_{real} = \frac{Velaq\ distance}{t_1 - t_0} \tag{4.7}$$

Where $Velaq\ distance$ is the distance between combs of the mechanical part fixed on the anvil (which has a constant value of 0.014 m), t_0 is the time instant when the first comb is detected and t_1 is the time instant when the second comb is detected.

To better understand the described TEST sub-routine´s sequence, the respective Stateflow´s diagram is presented in Figure 4.51.

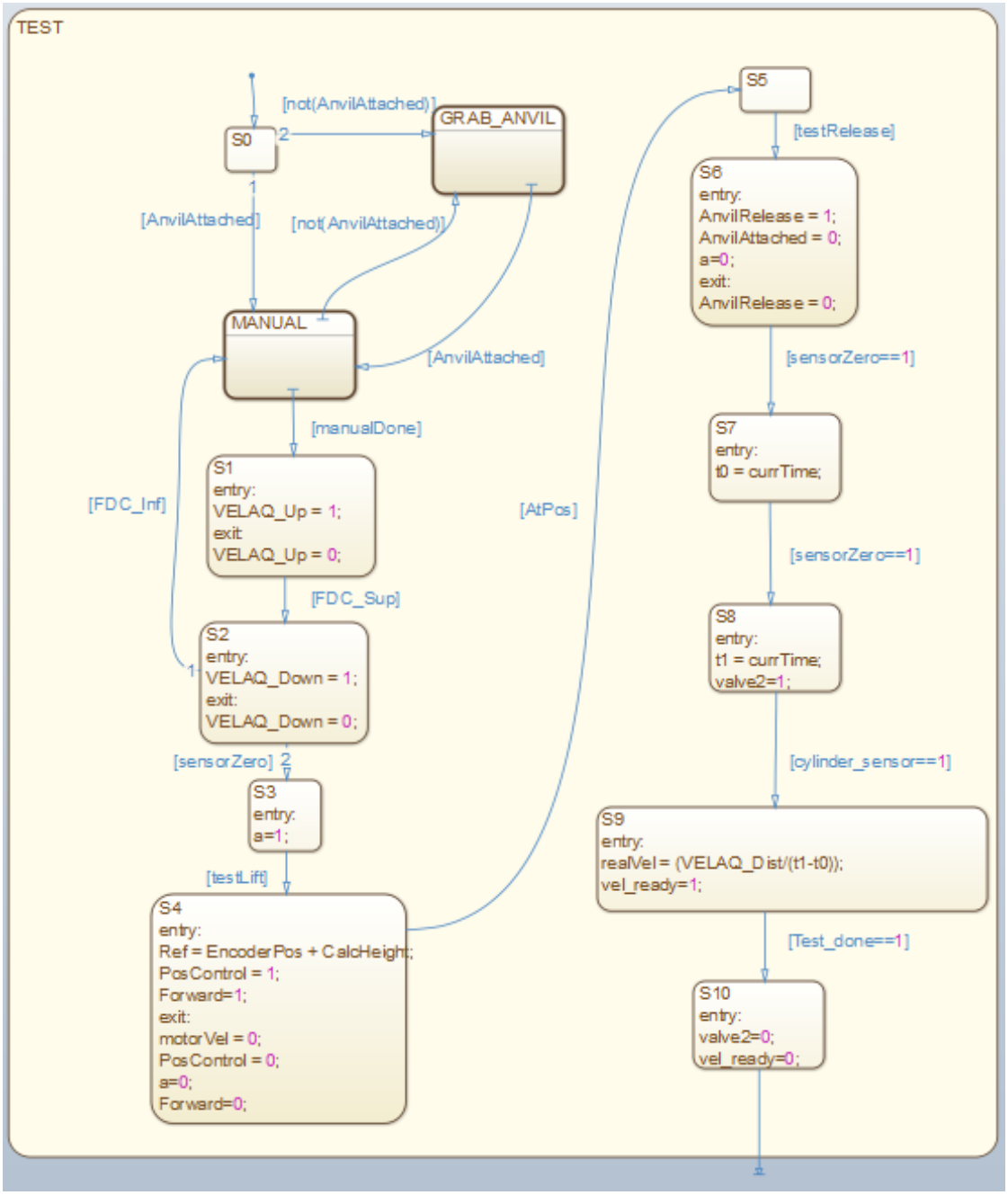

Figure 4.51 - TEST sub-routine.

4.3.7. GRAB_ANVIL sub-routine

The GRAB_ANVIL sub-routine (see Figure 4.52) allows the operator to manually move the carriage, so that it can attach to the anvil. To do so, the operator just has to softly descend the carriage towards the anvil´s pivot, since the weight of the carriage is enough to force the fitting inside the clamp. This sub-routine is also controlled in the interface window presented in Figure 4.47.

After pressing the "Manual Done" button, the program will check whether the anvil is attached or not by running the already explained CHECK_ANVIL sub-routine. If the anvil was not correctly fixed to the carriage, the program will return to the previous phase of this sub-routine, so that the attachment can be retried.

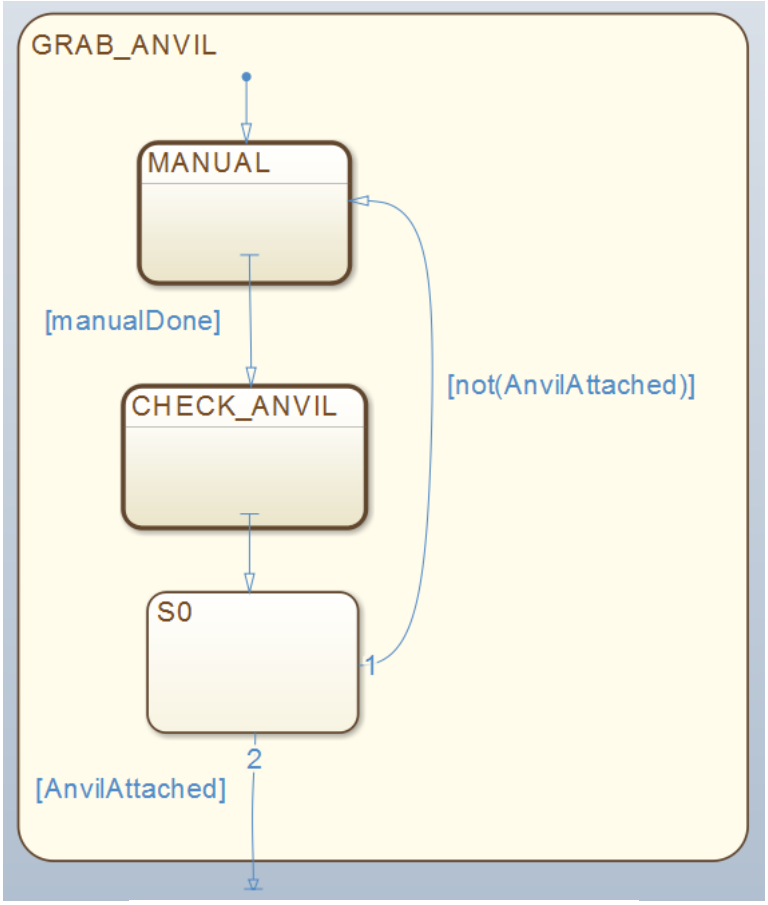

Figure 4.52 - GRAB_ANVIL sub-routine.

4.3.8. MANUAL sub-routine

When the "Begin Manual" button is pressed (present in the interface window shown in Figure 4.40), the manual control interface window (Figure 4.53) is made visible and the MANUAL sub-routine is initiated, allowing the control of each part of the machine independently from the others and from a logic sequence. This way, the operator can:

move the carriage up or down, move the velocity acquisition sub-system´s moving platform up or down, activate or deactivate the ARS and release the anvil. Therefore, the operator can control, with absolute freedom, all the sub-systems of the machine, allowing for a quick series of tests without having to fill the parameters´ values. This functionality can be useful for when the operator doesn't know the parameters´ values in which the tests should be done, giving him an idea to start with. The associated Stateflow´s diagram is shown in Figure 4.54.

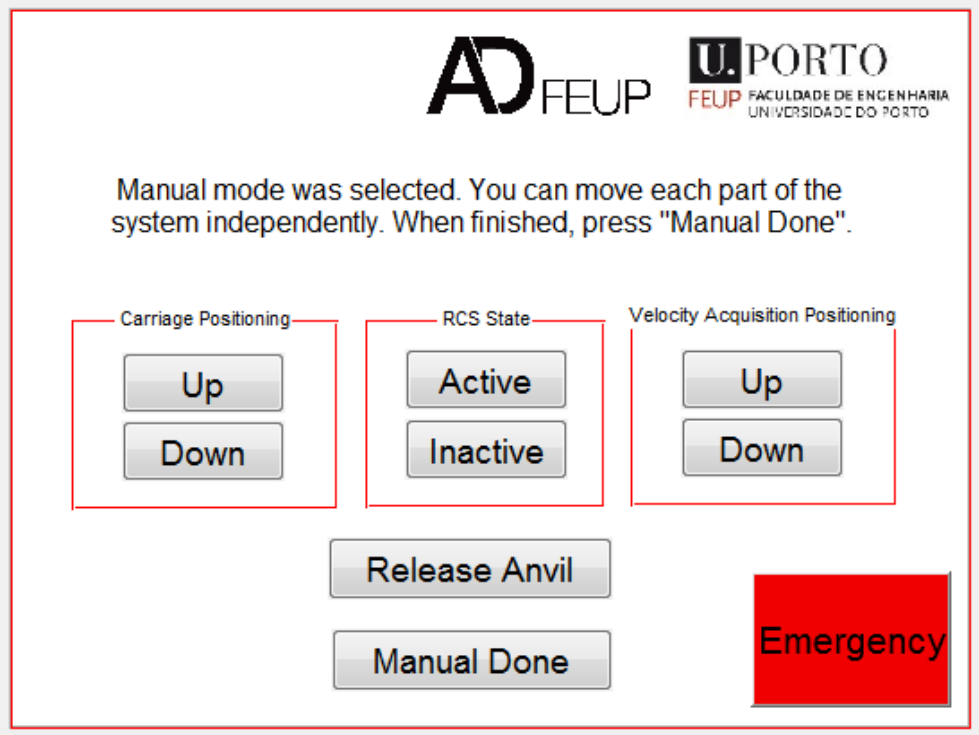

Figure 4.53 - Manual interface window.

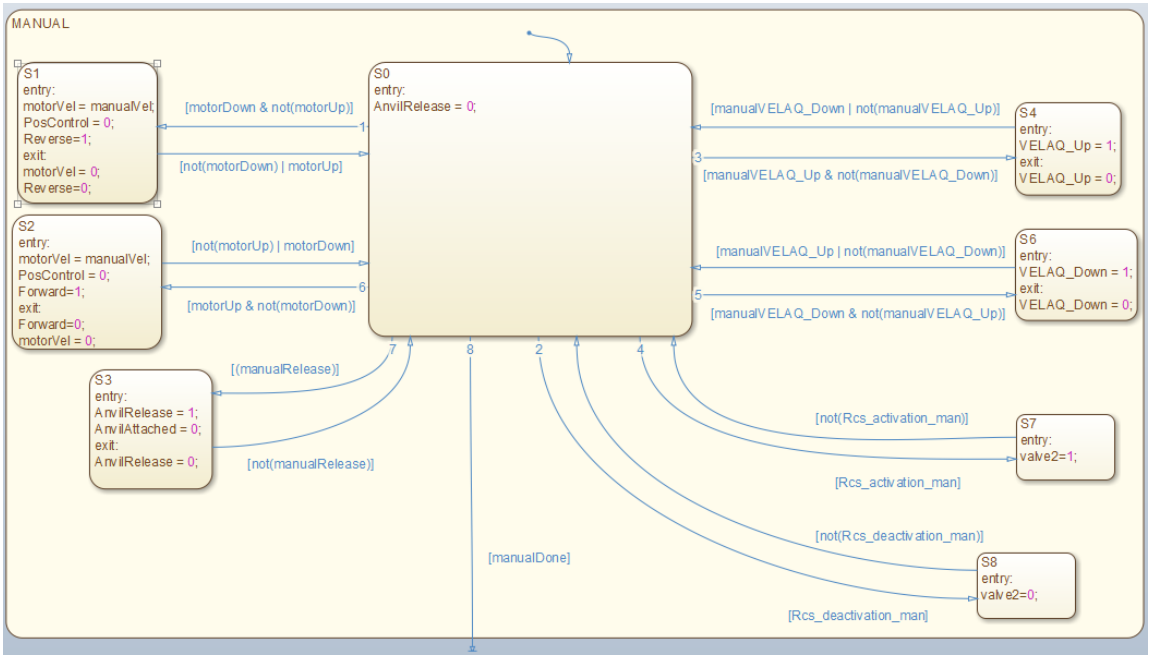

Figure 4.54 - MANUAL sub-routine.

4.3.9. SOS sub-routine

If, at any moment, a physical emergency button or a virtual emergency button (of any interface window) is pressed or the carriage passes through the upper limit of its stroke the SOS sub-routine is initiated. When this sub-routine is activated, all the current actions of the drop weight machine are interrupted, because its S0 state deactivates all output variables, except the variable that controls the ARS, which is activated (see Figure 4.55).

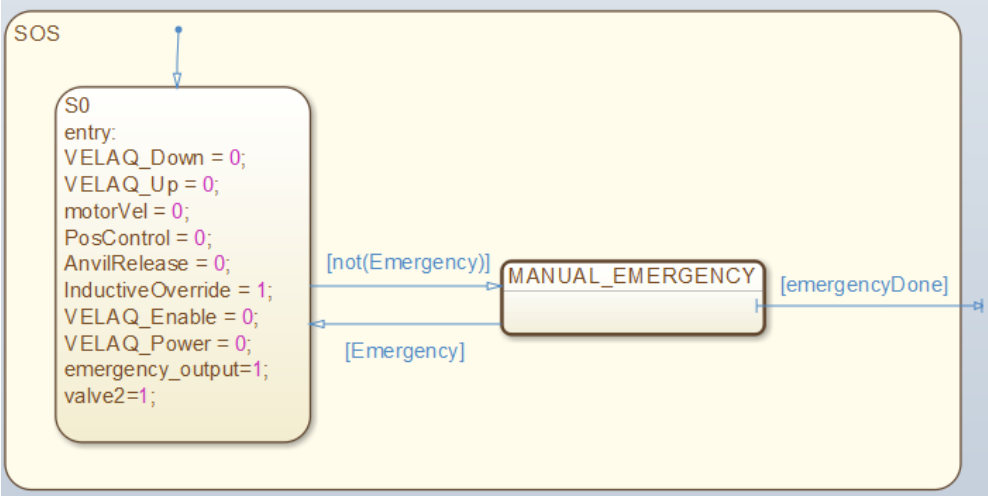

Figure 4.55 - SOS sub-routine.

After the S0 state, the machine enters the MANUAL_EMERGENCY sub-routine, that is equal to the MANUAL sub-routine, allowing the operator to move each sub-system independently, using the buttons in the emergency interface window presented in Figure 4.56. This enables the operator to solve the issue that triggered the emergency situation. When the problem is solved, the “Emergency Done” button should be pressed, and the program will return to the MAIN sub-routine (see Figure 4.39).

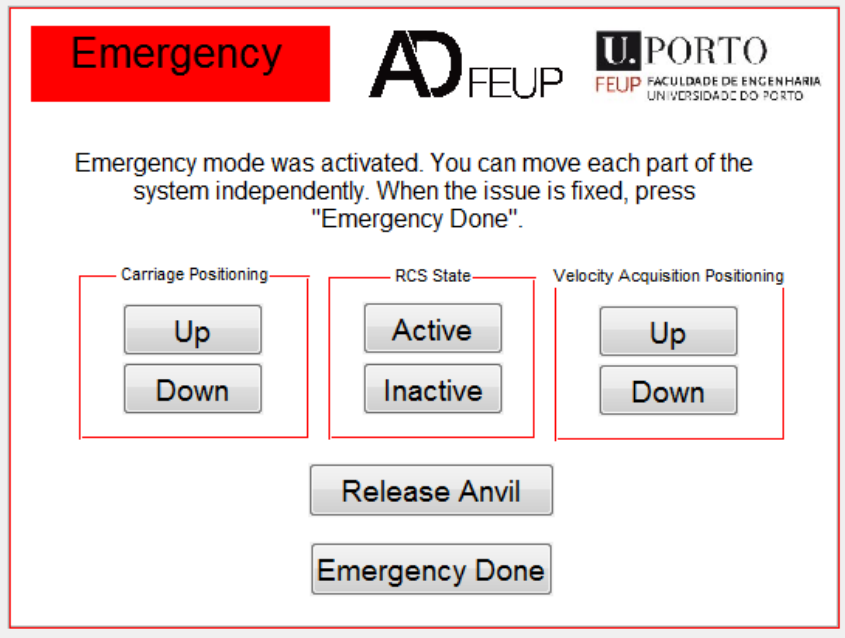

Figure 4.56 - Emergency interface window.

In a way of summarizing the drop weight machine´s functioning, Figure 4.57 shows a flow chart with a simplified command sequence.

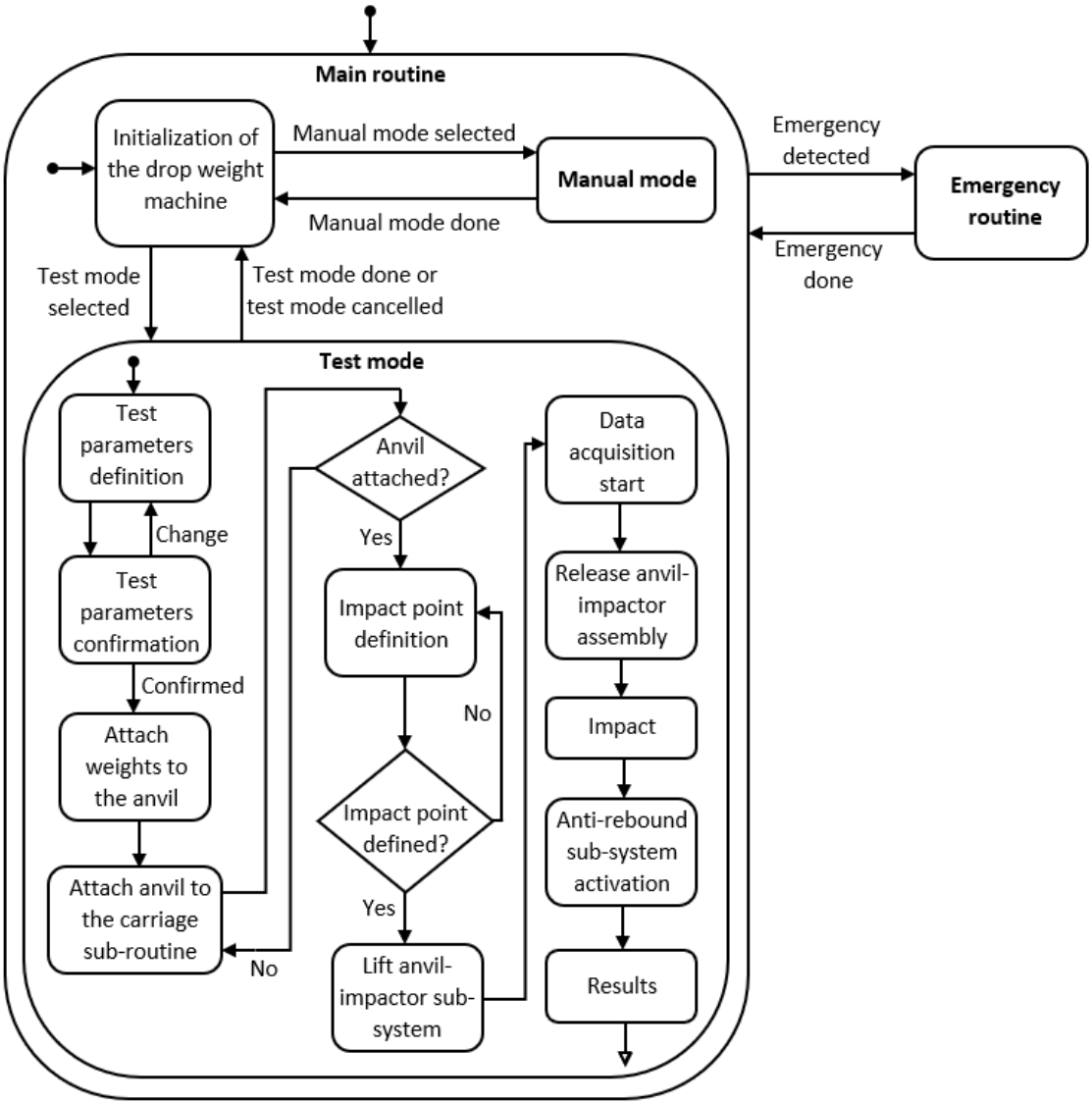

Figure 4.57 - Command sequence´s flowchart.

Chapter 5

Adhesive Joints Tests

In this chapter the validation of the drop weight machine is done by performing some impact tests on two different types of specimens. First, the operating conditions are defined, then, the results obtained in the Rosand IFW5 and in the ADFEUP´s drop weight machine are presented and compared. Additionally, these results are also compared with numerical data results obtained from simulations made on *Abaqus*. In these simulations, the same impact load is applied to a modelled adhesive joint, equal to the ones used on both machines.

At the time these tests were made, only a LabAmp with one input channel was available, instead of the pretended 4 channels LabAmp, due to a delivery mistake. For this reason and because there was a lack of specimens of each type, the tests made can´t contemplate the results of both implemented piezoelectric sensors. It was decided that the tests would only be performed to validate the press force sensor, since it would be a direct comparison with Rosand IFW5 machine, which also uses a load cell.

5.1. Test parameters

Since Rosand IFW5´s results were already acquired for previous research projects of ADFEUP´s members, the test parameters for the different specimens were already defined. In the next sections, a description of the different tested specimens, as well as the test parameters, is presented.

5.1.1. Specimen of type 1

The first specimen to be tested is a single lap joint adhesively bonded with XNR6852 E−3 and in which both substrates are from carbon fibre reinforced epoxy.

The XNR6852 E−3 is an epoxy-based adhesive that combines high strength, ductility and impact resistance, which are important properties in the automotive industry. The carbon fibre reinforced epoxy is a material with anisotropic properties, meaning that it has good properties along the fibre direction (like strength and stiffness), but not when considering shear and transverse properties. For this reason, this type of materials is not frequently used in structural bonding. However, combining it with the mentioned adhesive, can achieve a joint capable of withstanding high impact loads in the fibre direction. An example of the described joint is presented in Figure 5.1.

Figure 5.1 - Single lap joint of type 1.

The test parameters used to test this joint were:

- Drop weight: 26.5 kg;
- Velocity on impact: 3.48 m/s;
- Temperature: 24 ºC.

5.1.2. Specimen of type 2

This specimen is very similar to the previous one, since it uses the same materials for the substrates and the same adhesive. The main difference between the two specimens is the bonded area, which in this specimen is half the area of the first. For this single lap joint, the test parameters used were slightly different in terms of velocity:

- Drop weight: 26.5 kg;
- Velocity on impact: 3 m/s;
- Temperature: 24 ºC.

5.2. Results and discussion

The results of the tests are depicted in Figure 5.2 and Figure 5.3. We verify that, for each type of specimen, the registered maximum forces are similar on both drop weight machines. In the case of the specimen of type 1, when comparing with the simulation results on *Abaqus*, a difference of 4.4 kN for the Rosand´s and 3.4 kN for ADFEUP´s machine is noticed. This leads to a deviation of 10 % of the expected value, but considering that this is the result of experiments that are affected by various factors, it is not a significant difference. In the case of the specimen of type 2, the results show that the maximum force obtained in the ADFEUP´s drop weight machine are very similar to what the simulation´s results predict. Rosand´s results show the same maximum force deviation as seen for the previous specimen and, although they are not significant

differences, they can be explained by the type of load cell used. The KISTLER 9333A [40] load cell applied to the ADFEUP´s machine is pre-loaded and pre-calibrated, which makes it relatively insensitive to the fastening torque. In contrast, the load cell installed in the Rosand machine does not have these characteristics and it´s assembled by a pass-through single bolt. This type of assembly means that the load cell is quite sensitive to the pre-load of the mounting screw and requires regular calibration after reassembly, which is a likely factor to explain these differences.

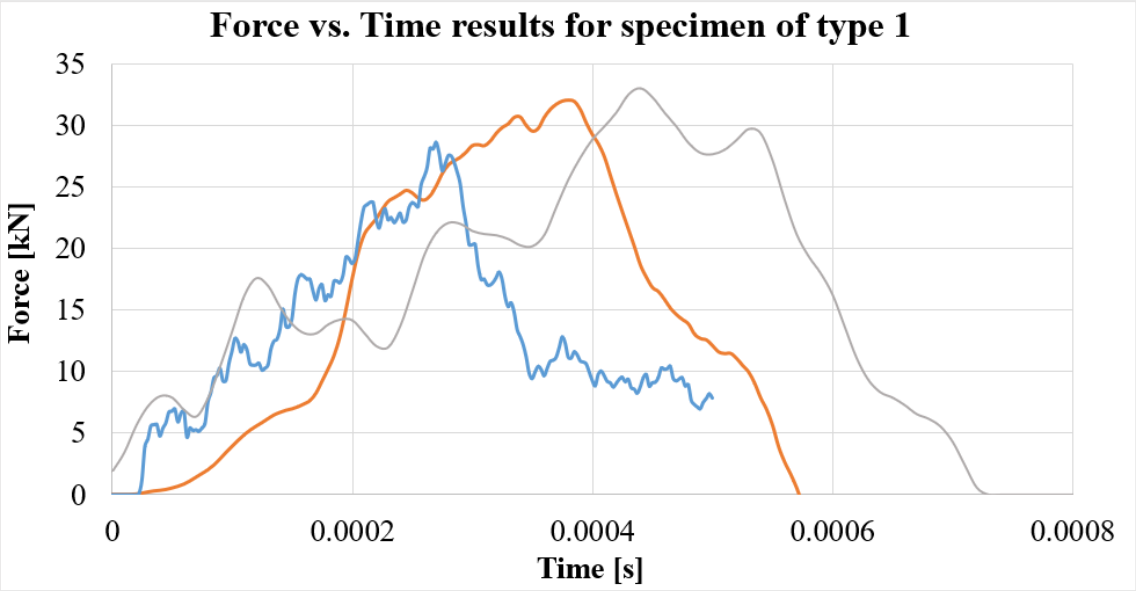

Figure 5.2 - Impact force versus time for the specimen of type 1 obtained in the ADFEUP´s drop weight machine (orange), Rosand´s machine (gray) and numerical data from *Abaqus* (blue).

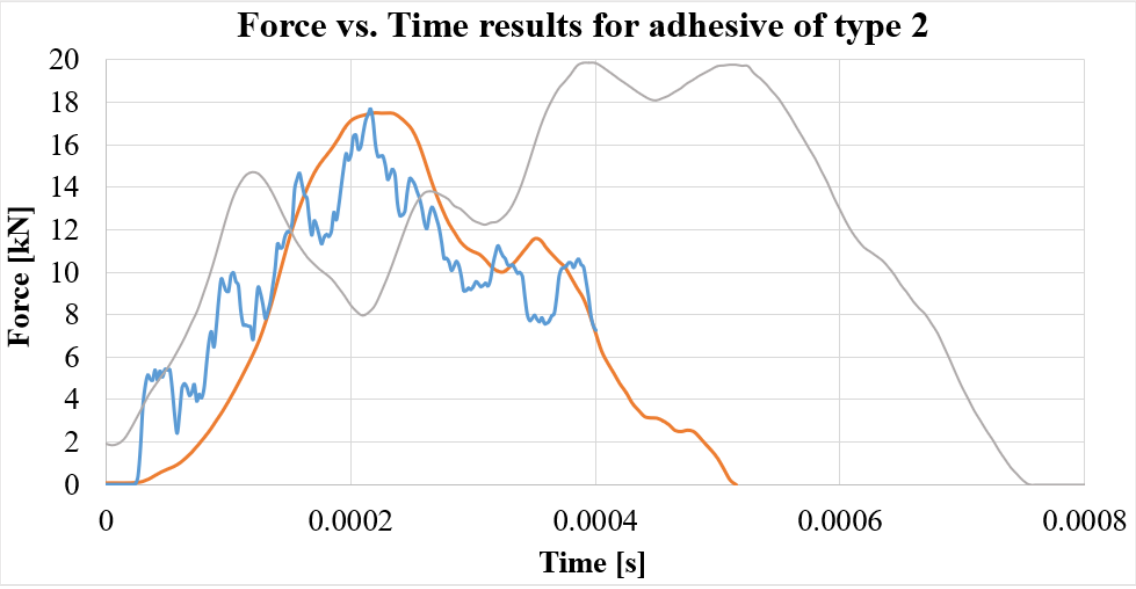

Figure 5.3 - Impact force versus time for the specimen of type 2 obtained in the ADFEUP´s drop weight machine (orange), Rosand´s machine (gray) and numerical data from *Abaqus* (blue).

Now, considering the duration of the impact, we observe significant differences between the results on the two machines and on both types of specimens. In the case of the specimen of type 1, the impact duration is 0.73 ms for the Rosand´s and 0.58 ms for the ADFEUP´s machine. In the case of the specimen of type 2, the impact duration is 0.755 ms for the Rosand´s and 0.55 ms for the ADFEUP´s machine. These differences can be explained by the way the specimens are fixed on the structure designed for that purpose in each machine. While in ADFEUP´s drop weight machine the specimen fixing structure has been purposely designed to be very rigid, presenting minimal deformation during the whole impact test, in the Rosand´s machine the specimen fixing structure (see Figure 5.4) is not aligned with the load path and can bend more easily, introducing deformations that can influence the final result. This specimen fixing structure is also relatively crude, using only two small screws to create clamping pressure in a small portion of the specimen, increasing the likelihood of specimen slippage during the test. These considerations are supported by the fact that Rosand machine´s impact force curve shows many irregularities in its shape, which, associated with the vibration of that structure, contributes to a longer impact.

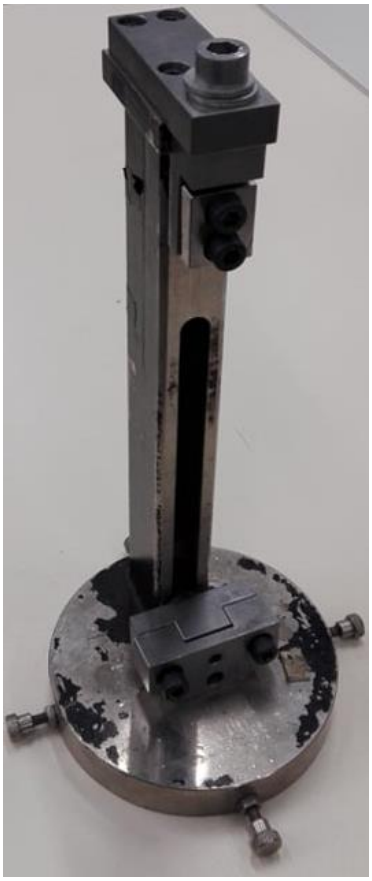

Figure 5.4 - Rosand machine´s specimen fixing structure.

Abaqus simulates the behaviour of materials based on their elastic and cohesive properties and, therefore, can accurately predict the elastic behaviour and the failure load of the adhesive joint. However, due to the complex phenomena associated with the fracture process of the joint, it can´t accurately predict the final stages of the impact test. Therefore, the impact force curve obtained via simulation can only be used to a certain extent. However, it´s possible to see that the duration on the simulation´s curve tends

closer to the duration obtained on ADFEUP´s drop weight machine. There are also some high frequency oscillations that can be noticed in the simulation´s curve, but they are absent from the experimental data. This can be associated to the particularities of the numerical model, as the damping properties of the materials are not captured by the model, but exist in the experimental tests. The result is a smoother experimental curve, but that still fits the overall trend indicated by the numerical data.

The ADFEUP´s drop weight machine´s repeatability is illustrated in Figure 5.5. Although some variability on the force pulses is observed, this is a common trait in adhesive joint´s experimental data.

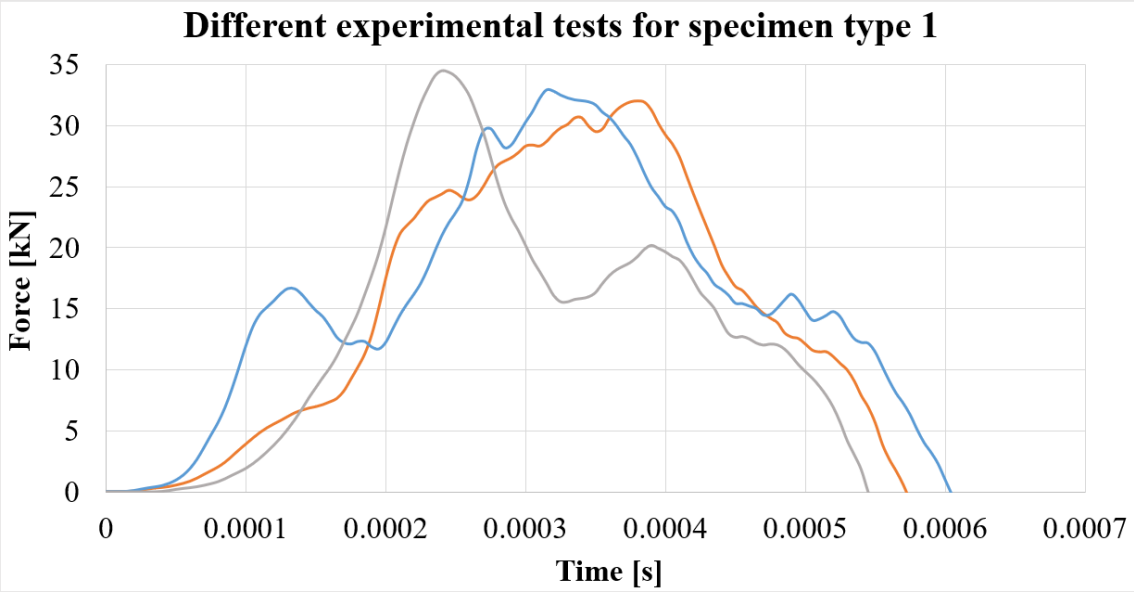

Figure 5.5 - Three different experimental tests for specimens of type 1.

Althought the results shown seem to validate the ADFEUP´s drop weight machine for adhesive joints testing, additional tests are still required in order to obtain more solid conclusions.

Chapter 6

Conclusions and Future Developments

This chapter concludes this dissertation´s report, making considerations about the achieved objectives and presenting some proposals for future developments on this drop weight machine.

6.1. Conclusions

As stated in section 1.2, the main objectives for this dissertation´s work were to implement the ARS and the new anvil-impactor assembly, to improve the electrical and pneumatic circuits, to develop the command sequence and to create a graphical interface for ADFEUP´s drop weight machine. After achieving these objectives, some tests were performed in order to validate the work done. The final result of this dissertation´s work on the drop weight machine can be seen in Figure 6.1.

The ARS has been successfully fabricated and implemented. However, due to a delayed delivery of the shock-absorbers, the mechanism has not yet been tested.

The new anvil-impactor assembly was designed, fabricated and implemented, including a piezoelectric accelerometer and a piezoelectric press force sensor in its mounting. To validate its construction, a dynamic study of the interaction between the anvil-impactor assembly and the ARS was done. The results of that study show that the assembly was well designed, although, when performing drop tests with a drop mass of 8.5 kg from the highest point, a high tensile force can be noticed (5.9 kN). This force can damage the press force sensor, which can only withstand tensile forces below 5 kN. However, since it´s possible to obtain the same amount of impact energy using different test parameters, this situation can be avoided. Despite that, the piezoelectric sensors were implemented and it was proven that, at least, the press force sensor can correctly obtain data. Once the LabAmp with 4 input channels is provided and more specimens are available, the accelerometer can be tested.

Both electrical and pneumatic circuits have been improved, including various additional components that were previously missing. It was concluded that both circuits are working as expected. Additionally, in the eventuality that these circuits ever need to be changed or reviewed, schematics have been made to ensure that the process is as simple as possible.

Similarly, the command sequence has also been improved, having many changes from the one proposed by Sousa [6]. The final result is a completely functional program that allows two different control modes for normal operation, as well as an emergency mode to minimize the risk of unexpected situations.

To easily control the implemented command sequence, a graphical interface was created and thoroughly tested, so that its correct functioning was assured.

Figure 6.1 - Final state of the ADFEUP´s drop weight machine.

Finally, some impact tests were performed in the ADFEUP´s drop weight machine. The results were posteriorly compared with the ones obtained in another machine and with numerical data collected from a simulation made on *Abaqus*, in order to validate ADFEUP´s drop weight machine functioning and, consequently, the work done in this dissertation.

To complement the information given in this dissertation´s report, an article entitled "Drop Weight Machine for Adhesive Joints Testing" was written and submitted to the "Journal of Testing and Evaluation".

Despite these objectives were successful and a functioning drop weight machine was obtained, there is still some room for more development. Some proposals for future developments are presented in the next section.

6.2. Future developments

The conception of ADFEUP´s drop weight machine is a large project that involved many contributors, being the focus of five different dissertations (including this one). Although the machine is ready to test all kinds of materials and obtain the relevant data, there are still aspects that can be improved and additional sub-systems that can be implemented so that the machine can reach its final state.

Firstly, it´s of great importance that the correct functioning of the accelerometer and the ARS is verified, in order to see if any significant changes to the machine´s design are required. This can be done once the 4 input channels LabAmp and the shock-absorbers are provided.

It´s also important that a physical barrier is implemented, so that the safety of the operators is guaranteed. This is needed not only to separate the user from the falling anvil, but also to prevent projectiles to be thrown around. To be able to it, an inductive sensor that detects whether the barrier is open or not should be implemented and then coded in the Simulink Stateflow®.

Currently, the displacement during the impact is being obtained by double integrating the acceleration´s data measured by both piezoelectric sensors. Thus, a way that doesn´t require post-process calculations to get the displacement is needed. The proposed solution is to design a new tool, coupled with a sensor that measures the linear displacement (LVDT or a linear potentiometer), to adapt to the specimen fixing structure.

In what investigation in the adhesives´ field concerns, an environmental chamber must be designed, so that adhesive joints´ properties can be tested in different surrounding conditions. To do that, one should consider the available space in the specimen fixing structure, as well as the sensors that will measure the conditions inside the chamber. Additionally, it will also be required to create a temperature and humidity controller in MATLAB Simulink.

Still regarding to adhesive´s investigation, the specimen fixing structure should have accessories that allow adhesive joints to be tested with different types of loads, since the only type possible at the moment is tensile load.

Finally, since the data acquisition start is controlled by the provided Kistler software, it´s important that this function can be integrated in the current graphical interface, so that the operation of the machine is made easier.

Bibliography

[1] J. Kuczmaszewski, *Fundamentals of metal-metal adhesive joint design*. Lublin University of Technology, 2006.

[2] L. F. da Silva, A. Öchsner, and R. D. Adams, *Handbook of adhesion technology*. Springer Science & Business Media, 2011.

[3] C. M. C. de Castro, "Desenvolvimento de um dispositivo experimental para medir a resistência ao impacto de ligações adesivas," Mater thesis, Faculty of Engineering of University of Porto, 2014.

[4] R. M. C. Barbosa, "Conceção e automatização de um dispositivo para medir a resistência ao impacto de ligações adesivas," Mater thesis, Faculty of Engineering of University of Porto, 2014.

[5] A. F. L. A. P. Ramos, "Development of a machine to measure the impact strength of adhesive joints," Mater thesis, Faculty of Engineering of University of Porto, 2016.

[6] D. R. R. de Sousa, "Development of the Automation Framework and Rebound-Capture System for a Drop-Weight Test Machine," Mater thesis, Faculty of Engineering of University of Porto, 2017.

[7] J. Machado, E. Marques, and L. F. da Silva, "Adhesives and adhesive joints under impact loadings: An overview," The Journal of Adhesion, vol. 94, no. 6, pp. 421-452, 2018.

[8] L. F. Da Silva, D. A. Dillard, B. Blackman, and R. D. Adams, *Testing adhesive joints: best practices*. John Wiley & Sons, 2012.

[9] R. D. Adams, J. J. Harris, "A critical assessment of the block impact test for measuring the impact strength of adhesive bonds," International Journal of Adhesion and Adhesives, vol. 16, no. 2, pp. 61-71, 1996.

[10] W. Chen, F. Lu, and M. J. P. Cheng, "Tension and compression tests of two polymers under quasi-static and dynamic loading," Polymer Testing J., vol. 21, no. 2, pp. 113-121, 2002.

[11] Zwick Roell. *Drop Weight Testers up to 2000 Joules*.

[12] Zwick Roell. *High-Energy Drop Weight Testers from 20,000 J*.

[13] INSTRON. *Drop Weight Testers*.

[14] IMATEK. *IM10 Drop Weight Impact Testers*.

[15] IMATEK. *DWTT Drop Weight Impact Testers*.

[16] KMS MATERIAIS TÉCNICOS. Available: http://www.kms.com.pt/index.html [Accessed Oct. 17, 2018].

[17] SKF®. *Needle roller bearings, with machined rings, with an inner ring - NKI 35/20 TN*

[18] UNIVERSALAFIR. Available: http://www.universalafir.pt/ [Accessed Oct. 17, 2018].

[19] ACE. *Industrial Shock Absorbers MC33*.

[20] ACE, "ACE Main Catalogue," ed, 2016.

[21] MIDÉ. *Accelerometers: Taking the Guesswork out of Accelerometer Selection*. Available: https://blog.mide.com/accelerometer-selection [Accessed Dec. 4, 2018].

[22] P. D. P. Nunes, "Impact strength of dissimilar joints for the automotive industry," Mater thesis, Faculty of Engineering of University of Porto, 2018.

[23] SMC. *ISO Cylinder Series C85*.

[24] Festo. *Round cylinders DSNU/ESNU*.

[25] Parker, "B Series Valves," ed.

[26] Parker, "B Series High Performance Industrial Valves," ed.

[27] Festo, "Solenoid valves MH2/MH3/MH4, fast-switching valves," ed.

[28] Festo, "Service unit combinations MSB, MS series," ed.

[29] TRANSTECNO, "Motoriduttori CC a vite senza fine - DC wormgearmotors," ed.

[30] ELECTROMEN, "EM-115 DC-MOTOR CONTROL UNIT 12-36V 25A 4-QUAD," ed.

[31] Como Drills. *918D SERIES 25mm SINGLE RATIO METAL GEARBOX*.

[32] "L298 - DUAL FULL-BRIDGE DRIVER," ed.

[33] OMRON, "Slot-type Photomicrosensor (Non-modulated) - EE-SX47/67," ed.

[34] Cherry, "MINIATURE D4 Series," ed.

[35] RS PRO. *Inductive detector 701-8253*.

[36] OMRON, "PHOTOELECTRIC SENSORS - E3FA/E3RA/E3FB/E3RB," ed.

[37] Festo, "Proximity sensors SMT/SME-8, for T-slot," ed.

[38] KISTLER, "K-Shear® Accelerometers - Dual-Purpose, Voltage Mode Accelerometers," ed.

[39] KISTLER, "Kistler LabAmp - Charge Amplifier and Data Acquisition Unit for Dynamic Measurements," ed.

[40] KISTLER, "Press Force Sensors - 0 … 100 N to 0 … 700 kN," ed.

[41] Measurment Computing, "PCIM-DDA06/16 Analog Output and Digital I/O Board User's Guide," ed.

[42] Intecno, "ME22 Micro encoder," ed.

[43] Measurment Computing, "PCI-QUAD04 Quadrature Encoder Input - User's Guide," ed.

[44] RS Pro, "240W Single Output Industrial DIN RAIL Power Supply," in *DRP-240 series*, ed.

[45] RS Pro, "96W Single Output Industrial DIN Rail Power Supply," in *MDR-100 series*, ed.

[46] RS Pro, "RS Pro 10W Single Output Industrial DIN Rail Power Supply " in *MDR-10 Series*, ed.

[47] SIEMENS, "5SM3312-0 - RES. CURRENT OP. CIRCUIT BREAKER TYPE AC WS," ed.

[48] Schneider Electric, "GB2DB21 - TeSys GB2 - thermal-magnetic circuit breaker," ed.

[49] Schneider Electric, "GB2CB09 - TeSys GB2 - thermal-magnetic circuit breaker," ed.

[50] ABB. *Detailed information for: SH201T-C10.* Available: https://new.abb.com/products/ABB2CDS231001R0104 [Accessed Jan. 5, 2019].

[51] Schneider Electric, "XALK178E - yellow station - 1 red mushroom head pushbutton - Ø40 turn to release 1NO+1NC," in *Harmony XALK*, ed.

Appendix A

Mechanical Drawings
Anti-Rebound Sub-System

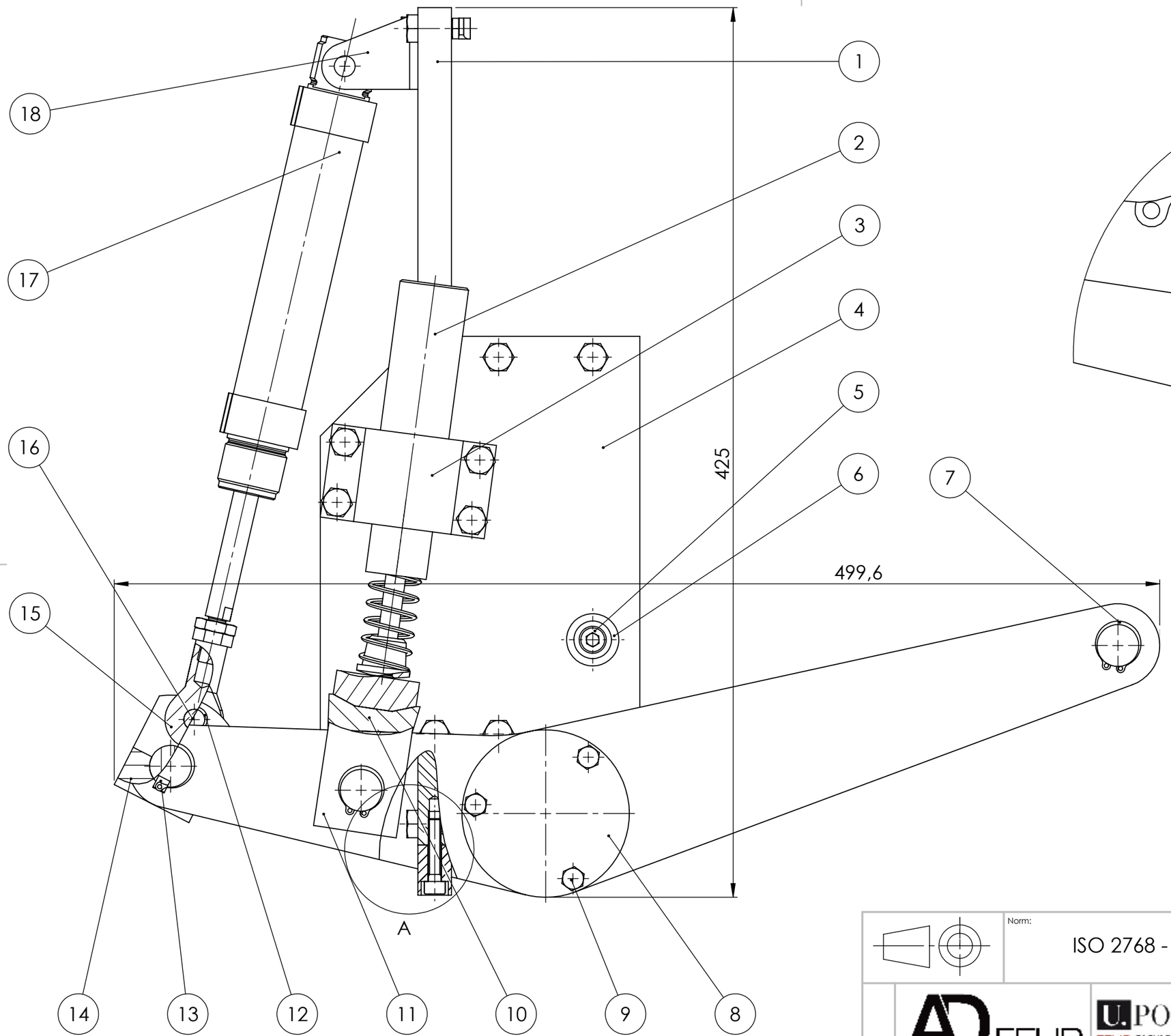

DETAIL A
SCALE 2 : 1

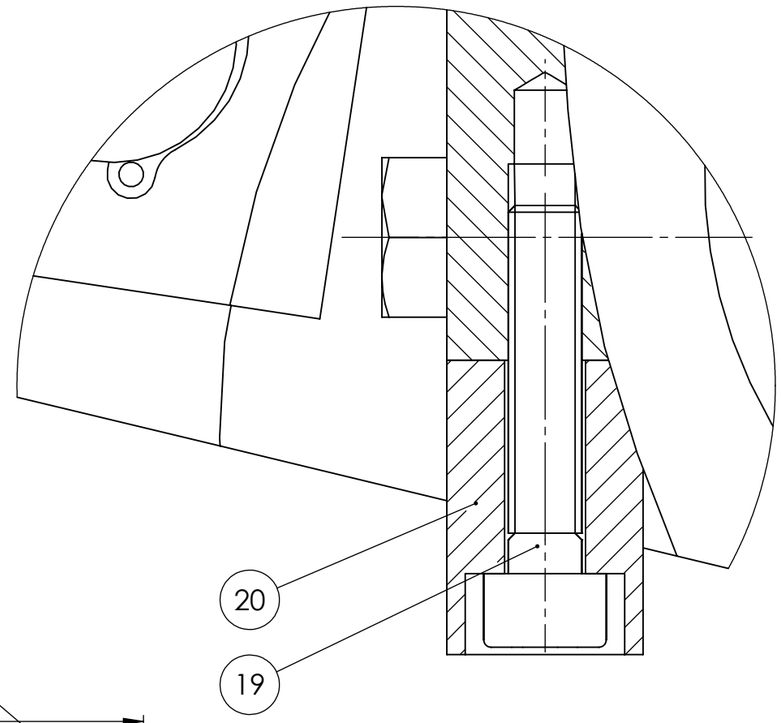

Norm: ISO 2768 - mK			Qt: 2
			SCALE: 1:2
AD FEUP	U.PORTO FEUP FACULDADE DE ENGENHARIA UNIVERSIDADE DO PORTO		TITLE: Anti-rebound sub-system
	NAME	DATE	SHEET 1 OF 3 — A3
DRAWN	Diogo do Paço Casal Antunes	23-01-2019	
CHK'D			
APPV'D			WEIGHT:

SOLIDWORKS Educational Product. For Instructional Use Only.

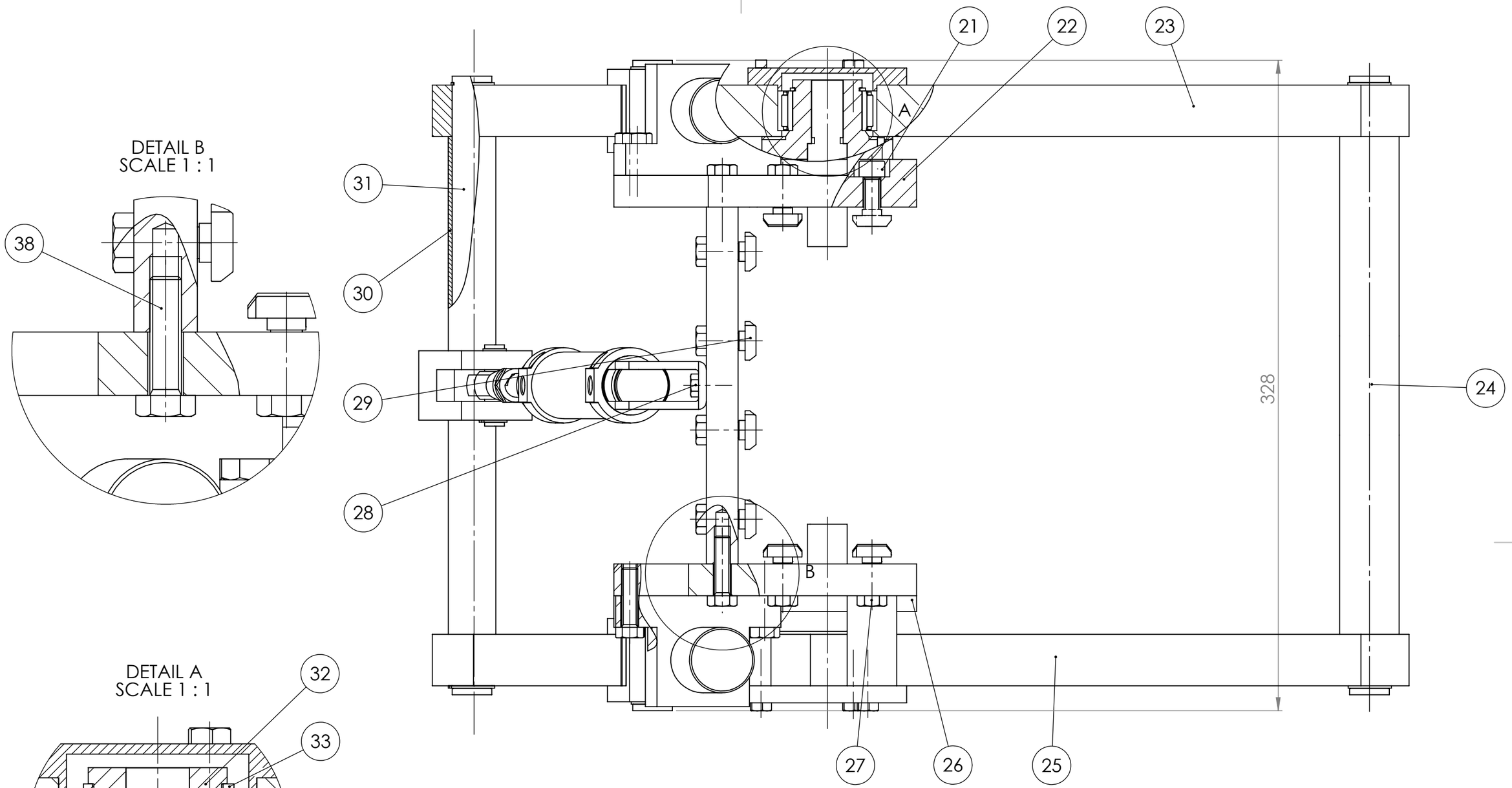

Norm: ISO 2768 - mK			Qt: 2
			SCALE: 1:2
AD FEUP	U.PORTO FEUP FACULDADE DE ENGENHARIA UNIVERSIDADE DO PORTO		TITLE: Anti-rebound sub-system
NAME	DATE	MATERIAL:	SHEET 2 OF 3 — A3
DRAWN Diogo do Paço Casal Antunes	23-01-2019		
CHK'D			
APPV'D		WEIGHT:	

SOLIDWORKS Educational Product. For Instructional Use Only.

Num.	Component	Qt.
1	Side Plate	2
2	Shock-absorber	4
3	Shock-absorber support	4
4	Front/back plate	4
5	ISO 4762 - M8x50	4
6	Stopper	4
7	DIN 471 - Φ20x1,2	16
8	Cover	4
9	ISO 4017 - M6x20	12
10	Polyurethane Part	4
11	Aligment Pad	4
12	DIN 471 - Φ10x1	4
13	DIN 6885 - 6x6x32 A	2
14	Deviator	2
15	Rod eye	2
16	Rod eye´s Axle	2
17	Pneumatic Cylinder	2
18	Cleevis Foot Mounting	2
19	ISO 4762 - M6x30	6
20	Hook	2
21	ISO 4762 - M8x25	16
22	Back Block	2
23	Back Arm	2
24	Impact Axle	2
25	Front Arm	2
26	Front Block	2
27	ISO 4017 - M8x25	28
28	ISO 4017 - M6x16	4
29	T-nut - M8	44
30	Actuator Axle´s Sleeve	4
31	Actuation Axle	2
32	ARS´s Axle part1	4
33	DIN 471 - Φ35X1,5	4
34	Needle Bearings	4
35	ARS´s Axle part 2	4
36	ISO 8734 - Φ4x6	4

Num.	Component	Qt.
37	Washers	4
38	ISO 4017 - M8x30	24

Norm: ISO 2768 - mK

AD FEUP

U.PORTO FEUP FACULDADE DE ENGENHARIA UNIVERSIDADE DO PORTO

TITLE: Anti-rebound sub-system

	NAME	DATE
DRAWN	Diogo do Paço Casal Antunes	23-01-2019
CHK'D		
APPV'D		

MATERIAL:

SHEET 3 OF 3

A4

SOLIDWORKS Educational Product. For Instructional Use Only.

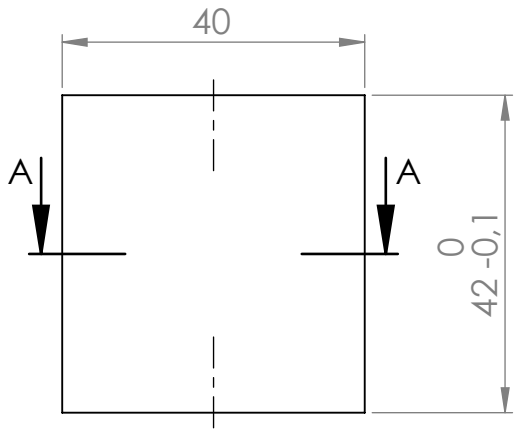

SECTION A-A
SCALE 1 : 1

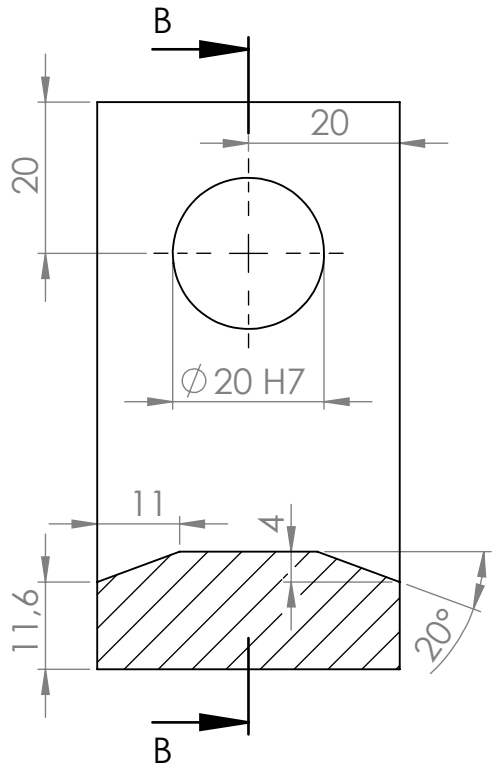

SECTION B-B
SCALE 1 : 1

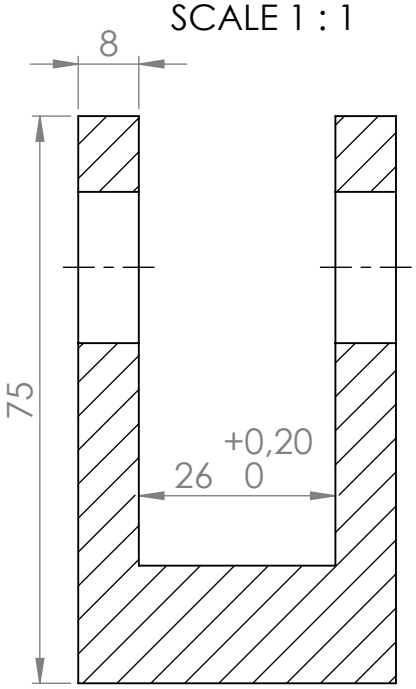

	Norm: ISO 2768 - mK	Qt: 4	
		SCALE: 1:1	
AD FEUP	U.PORTO FEUP FACULDADE DE ENGENHARIA UNIVERSIDADE DO PORTO	TITLE: Aligment pad	
NAME / DATE	MATERIAL: AW 6082 T651	DWG NO. Drawing nº1	A4
DRAWN: Diogo do Paço Casal Antunes 23-01-2019			
CHK'D			
APPV'D	WEIGHT:		SHEET 1 OF 1

SOLIDWORKS Educational Product. For Instructional Use Only.

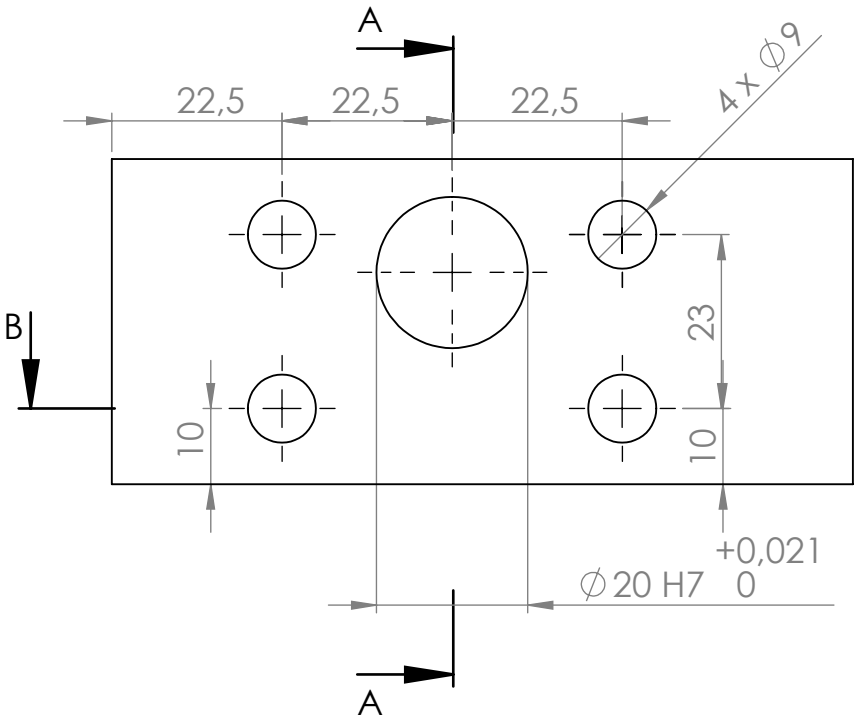

SECTION A-A
SCALE 1 : 1

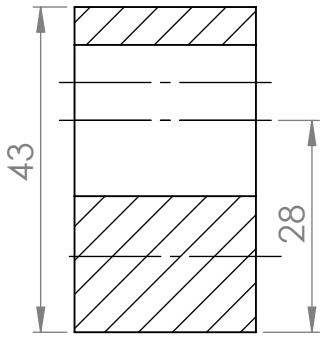

SECTION B-B
SCALE 1 : 1

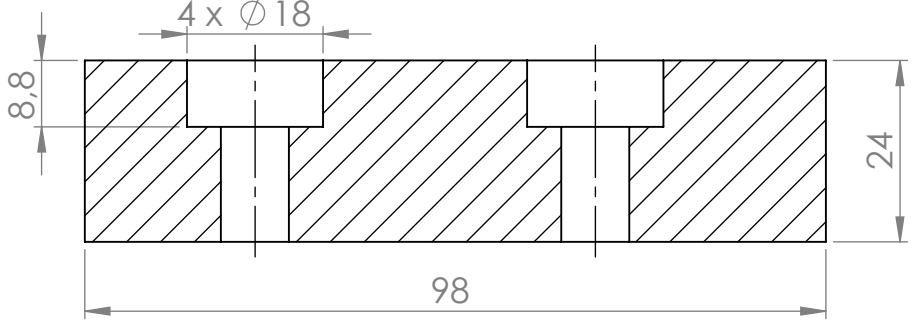

	Norm: ISO 2768 - mK	Qt: 2	
		SCALE: 1:1	
AD FEUP / U.PORTO FEUP FACULDADE DE ENGENHARIA UNIVERSIDADE DO PORTO		TITLE: Front block	
NAME / DATE	MATERIAL: AW 6082 T651	DWG NO. Drawing nº2	A4
DRAWN: Diogo do Paço Casal Antunes / 23-01-2019			
CHK'D			
APPV'D	WEIGHT:		SHEET 1 OF 1

SOLIDWORKS Educational Product. For Instructional Use Only.

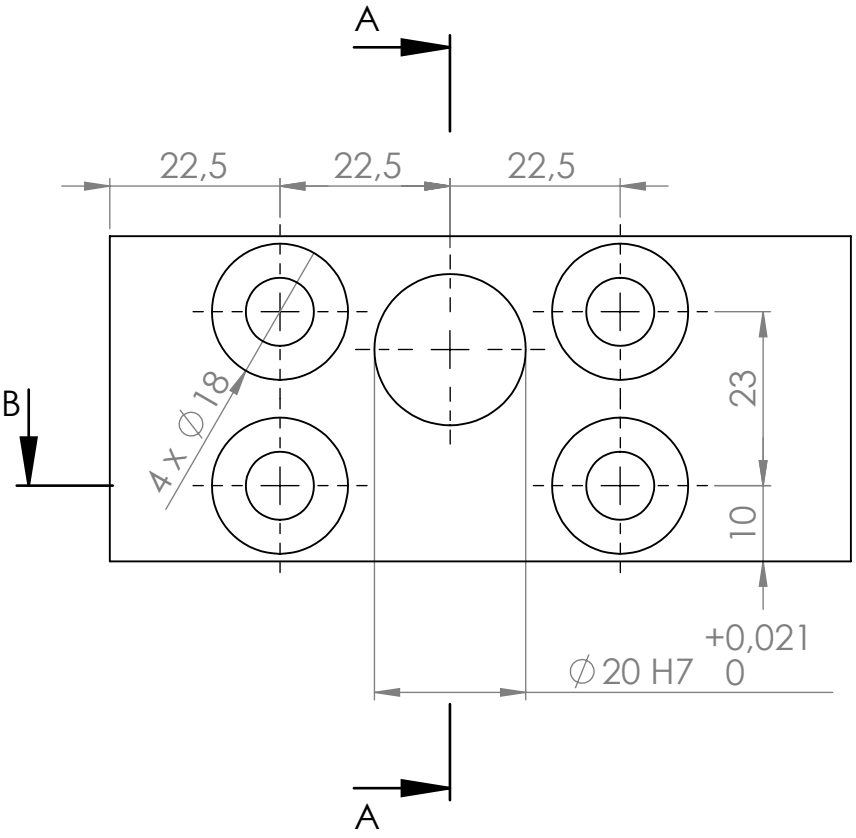

SECTION A-A
SCALE 1 : 1

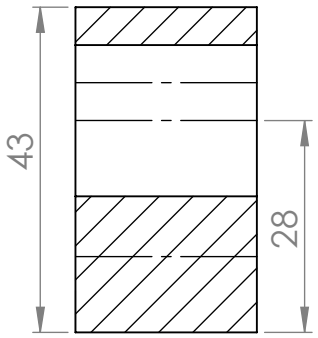

SECTION B-B
SCALE 1 : 1

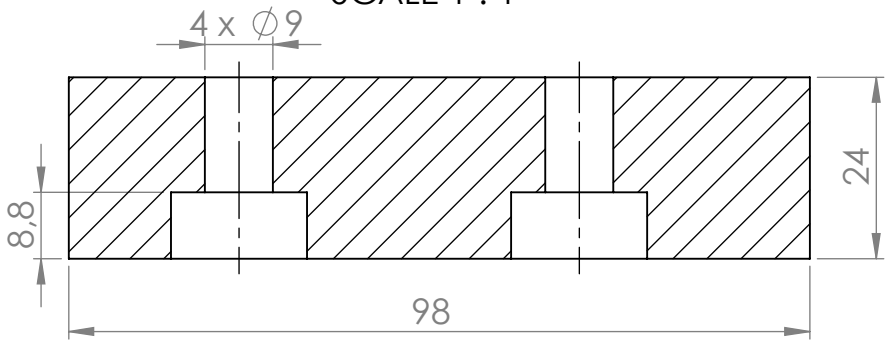

	Norm: ISO 2768 - mK		Qt: 2	
			SCALE: 1:1	
AD FEUP	U.PORTO FEUP FACULDADE DE ENGENHARIA UNIVERSIDADE DO PORTO		TITLE: Back block	
	NAME	DATE	MATERIAL: AW 6082 T651	DWG NO. Drawing nº3 A4
DRAWN	Diogo do Paço Casal Antunes	23-01-2019		
CHK'D				
APPV'D			WEIGHT:	SHEET 1 OF 1

SOLIDWORKS Educational Product. For Instructional Use Only.

DETAIL B
SCALE 1 : 1

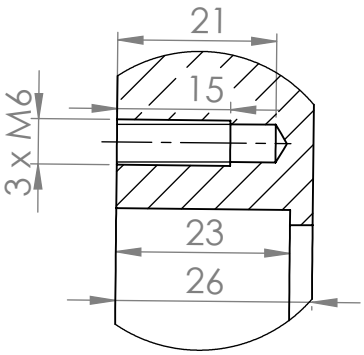

DETAIL C
SCALE 1 : 2

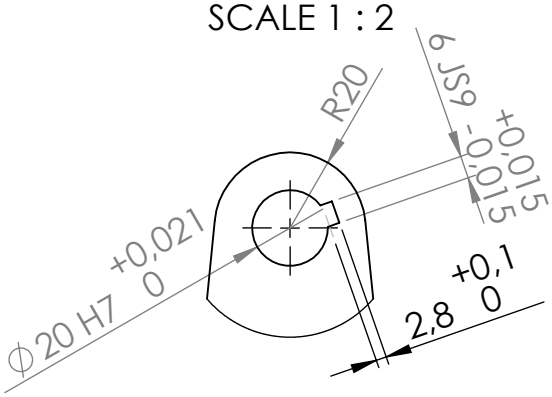

SECTION A-A
SCALE 1 : 4

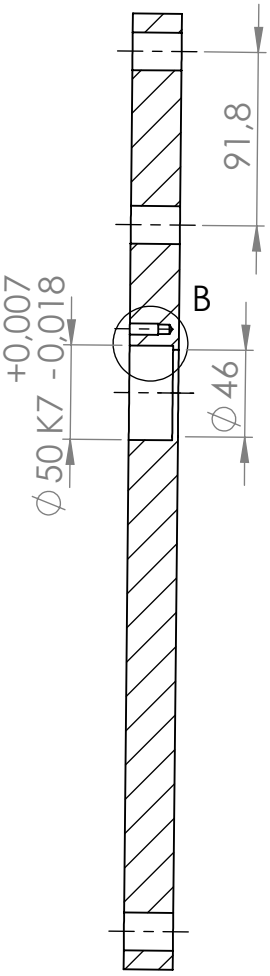

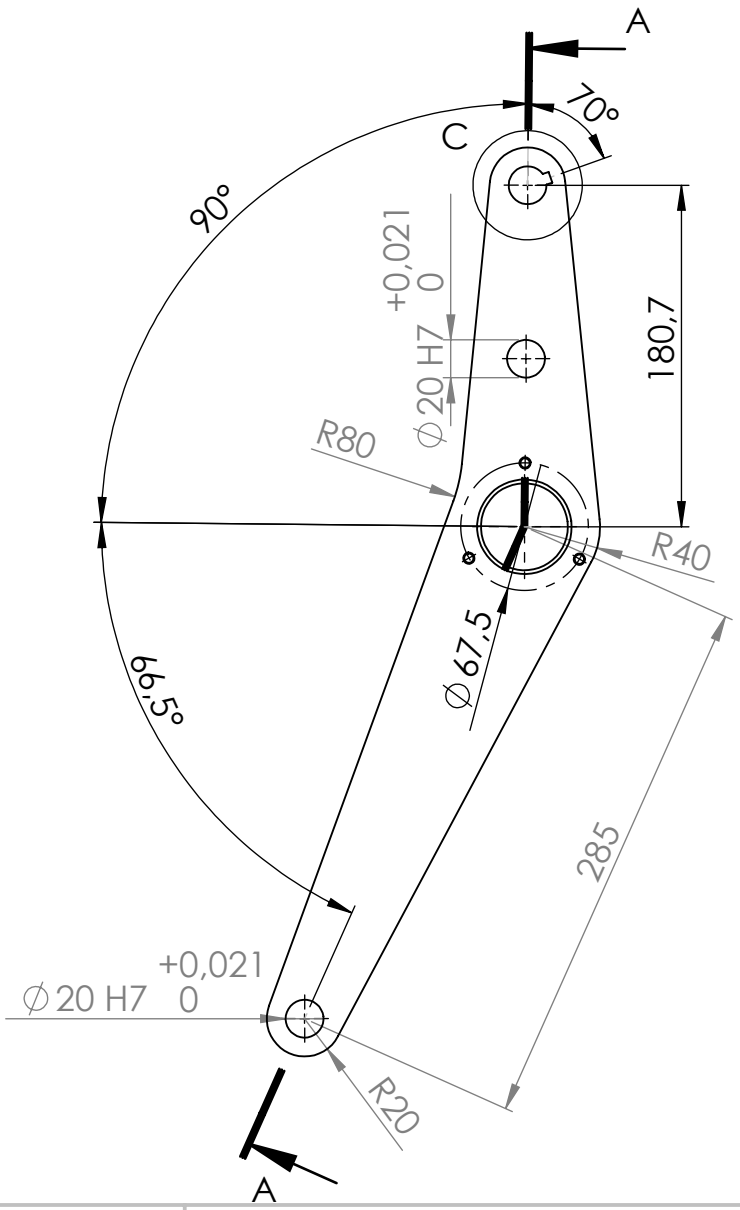

	Norm: ISO 2768 - mK	Qt: 2	
		SCALE: 1:4	
AD FEUP	U.PORTO FEUP FACULDADE DE ENGENHARIA UNIVERSIDADE DO PORTO	TITLE: Front arm	
	NAME / DATE	MATERIAL: AW 7075 T651	DWG NO. Drawing nº4 — A4
DRAWN	Diogo do Paço Casal Antunes / 23-01-2019		
CHK'D			
APPV'D		WEIGHT:	SHEET 1 OF 1

SOLIDWORKS Educational Product. For Instructional Use Only.

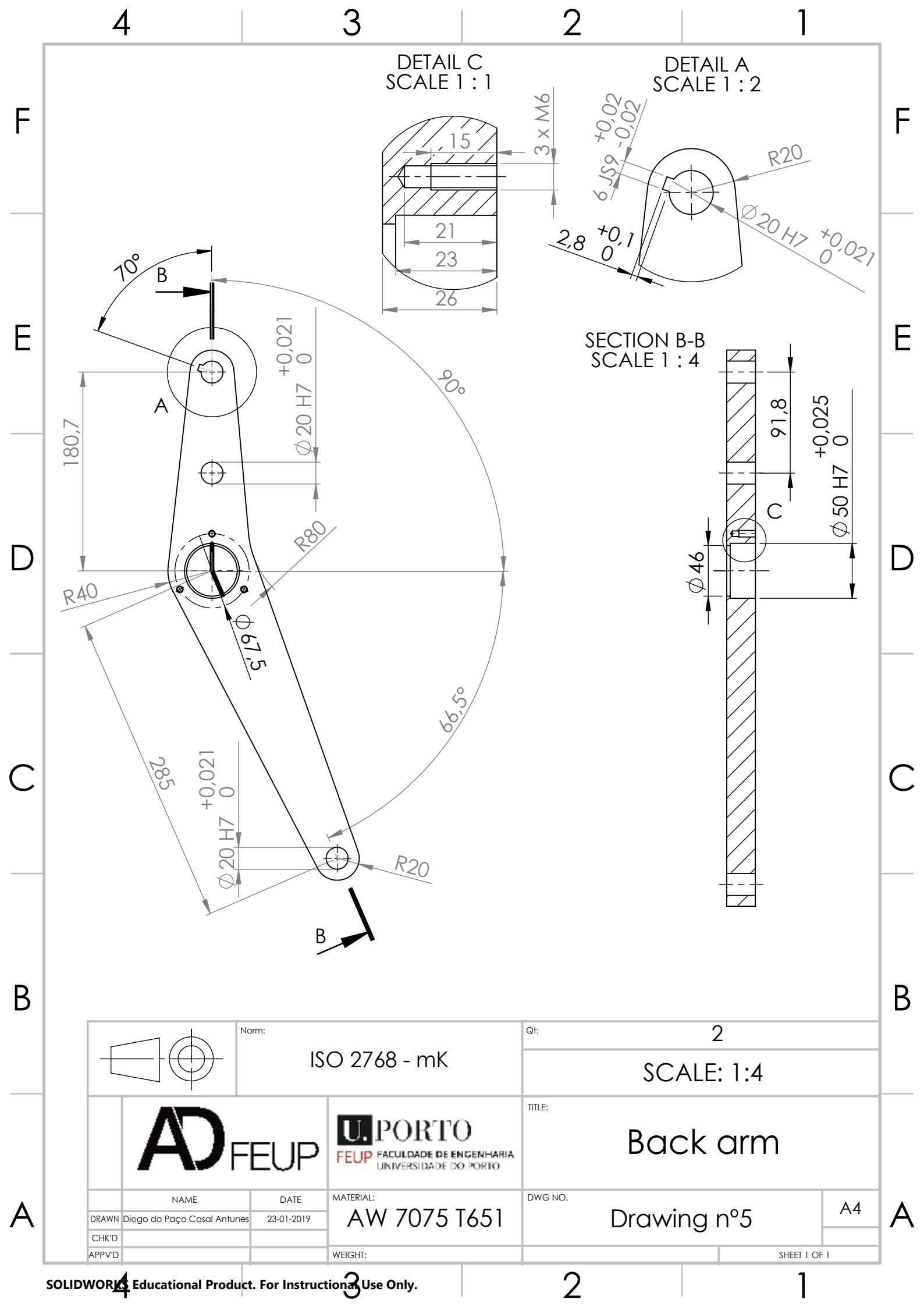

Norm: ISO 2768 - mK		Qt: 2	
		SCALE: 1:4	
AD FEUP	U.PORTO FEUP FACULDADE DE ENGENHARIA UNIVERSIDADE DO PORTO	TITLE: Back arm	
NAME	DATE	MATERIAL: AW 7075 T651	DWG NO. Drawing nº5 A4
DRAWN Diogo do Paço Casal Antunes	23-01-2019		
CHK'D			
APPV'D		WEIGHT:	SHEET 1 OF 1

SOLIDWORKS Educational Product. For Instructional Use Only.

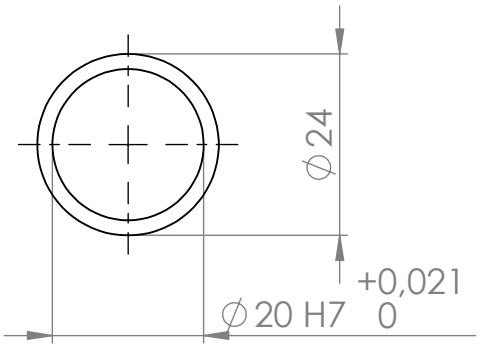

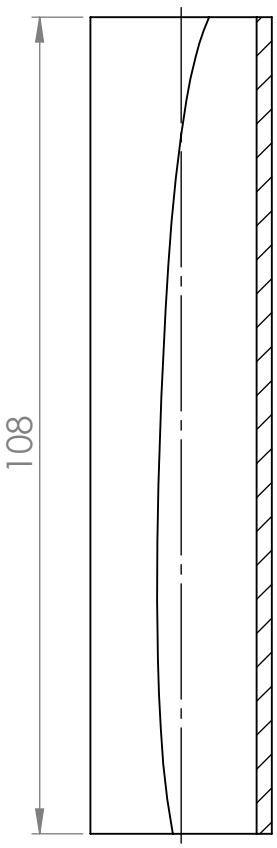

	Norm: ISO 2768 - mK		Qt: 4	
			SCALE: 1:1	
AD FEUP	U.PORTO FEUP FACULDADE DE ENGENHARIA UNIVERSIDADE DO PORTO		TITLE: Actuation axle´s sleeve	
	NAME	DATE	MATERIAL: St 52.0	DWG NO. Drawing nº6 A4
DRAWN	Diogo do Paço Casal Antunes	23-01-2019		
CHK'D				
APPV'D			WEIGHT:	SHEET 1 OF 1

SOLIDWORKS Educational Product. For Instructional Use Only.

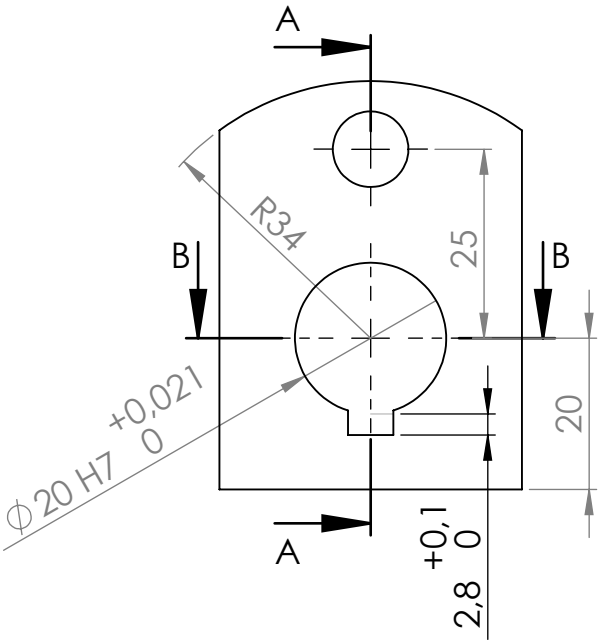

SECTION A-A

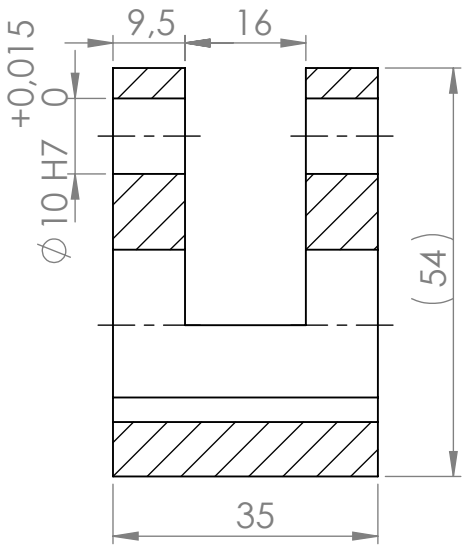

SECTION B-B

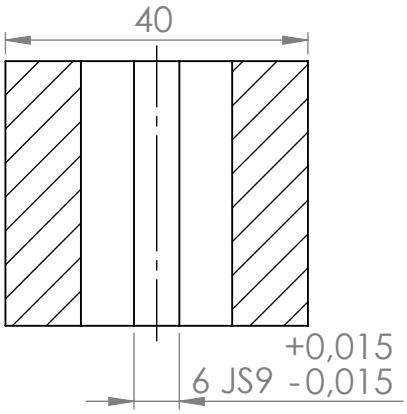

Norm: ISO 2768 - mK	Qt: 2	
	SCALE: 1:1	
AD FEUP / U.PORTO FEUP Faculdade de Engenharia Universidade do Porto	TITLE: Deviator	

	NAME	DATE	MATERIAL:	DWG NO.	
DRAWN	Diogo do Paço Casal Antunes	23-01-2019	AW 6082 T651	Drawing nº7	A4
CHK'D					
APPV'D			WEIGHT:		SHEET 1 OF 1

SOLIDWORKS Educational Product. For Instructional Use Only.

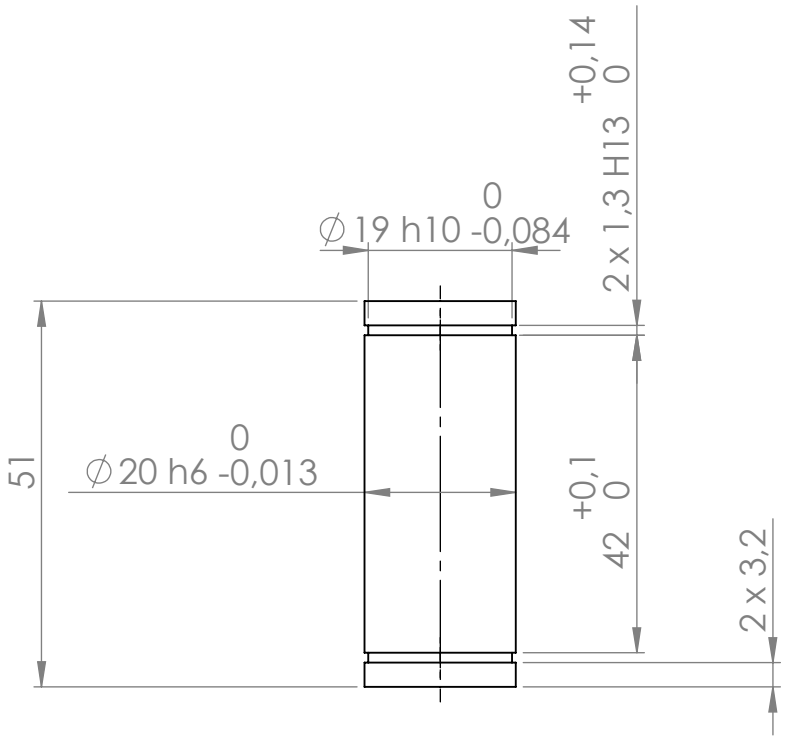

	Norm: ISO 2768 - mK	Qt: 4	
		SCALE: 1:1	
AD FEUP / U.PORTO FEUP FACULDADE DE ENGENHARIA UNIVERSIDADE DO PORTO		TITLE: Aligment pad´s axle	
NAME / DATE	MATERIAL: N540	DWG NO. Drawing nº8	A4
DRAWN: Diogo do Paço Casal Antunes / 23-01-2019			
CHK'D			
APPV'D	WEIGHT:		SHEET 1 OF 1

SOLIDWORKS Educational Product. For Instructional Use Only.

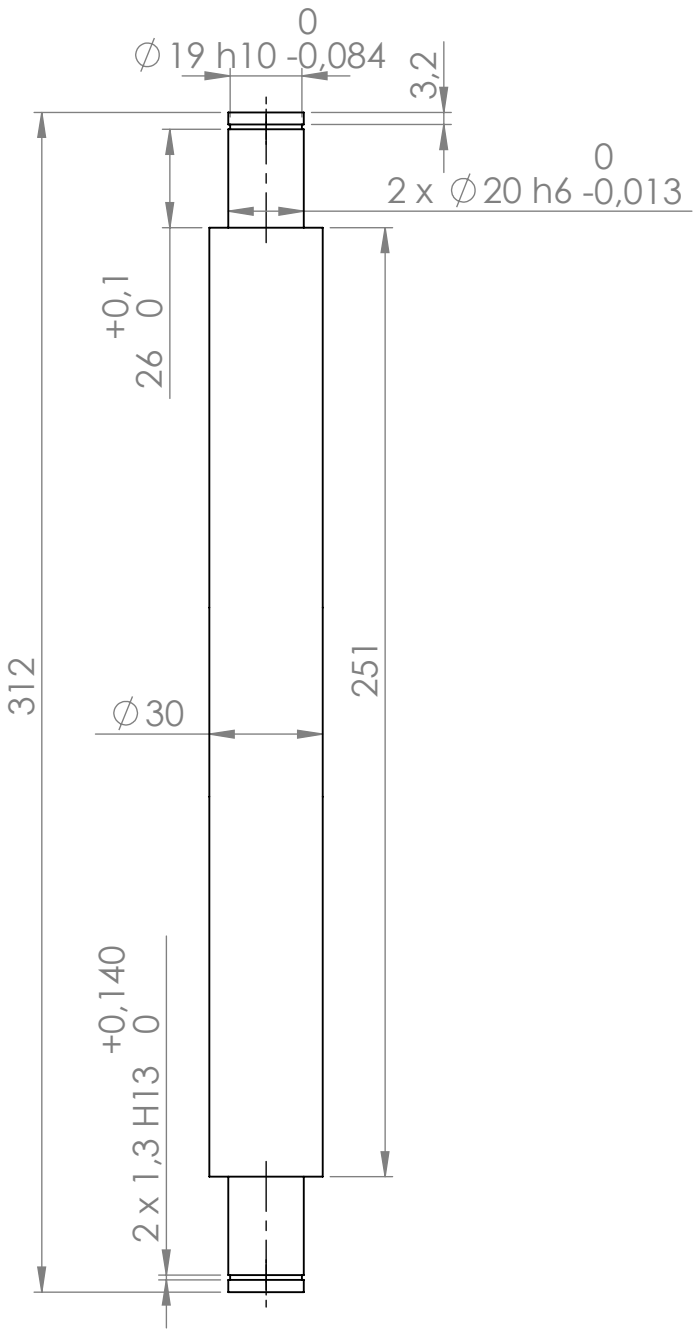

Norm: ISO 2768 - mK		Qt: 2	
		SCALE: 1:2	
AD FEUP / U.PORTO FEUP FACULDADE DE ENGENHARIA UNIVERSIDADE DO PORTO		TITLE: Impact axle	
NAME	DATE	MATERIAL: N540	DWG NO. Drawing nº9 A4
DRAWN Diogo do Paço Casal Antunes	23-01-2019		
CHK'D			
APPV'D		WEIGHT:	SHEET 1 OF 1

SOLIDWORKS Educational Product. For Instructional Use Only.

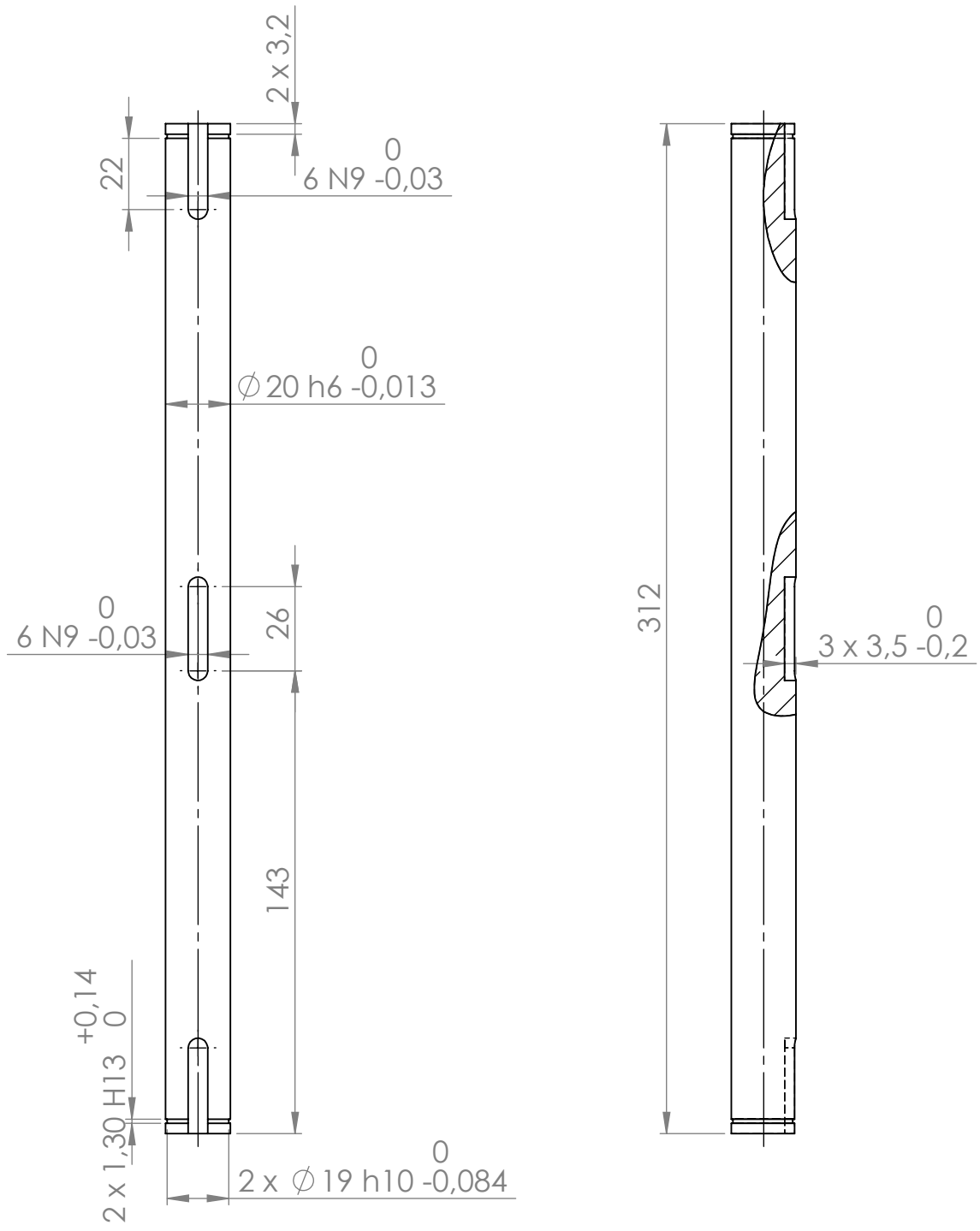

Norm: ISO 2768 - mK	Qt: 2	
	SCALE: 1:2	

AD FEUP

U.PORTO
FEUP FACULDADE DE ENGENHARIA
UNIVERSIDADE DO PORTO

TITLE:

Actuation axle

	NAME	DATE	MATERIAL:	DWG NO.	
DRAWN	Diogo do Paço Casal Antunes	23-01-2019	M310 RD	Drawing nº10	A4
CHK'D					
APPV'D			WEIGHT:		SHEET 1 OF 1

SOLIDWORKS Educational Product. For Instructional Use Only.

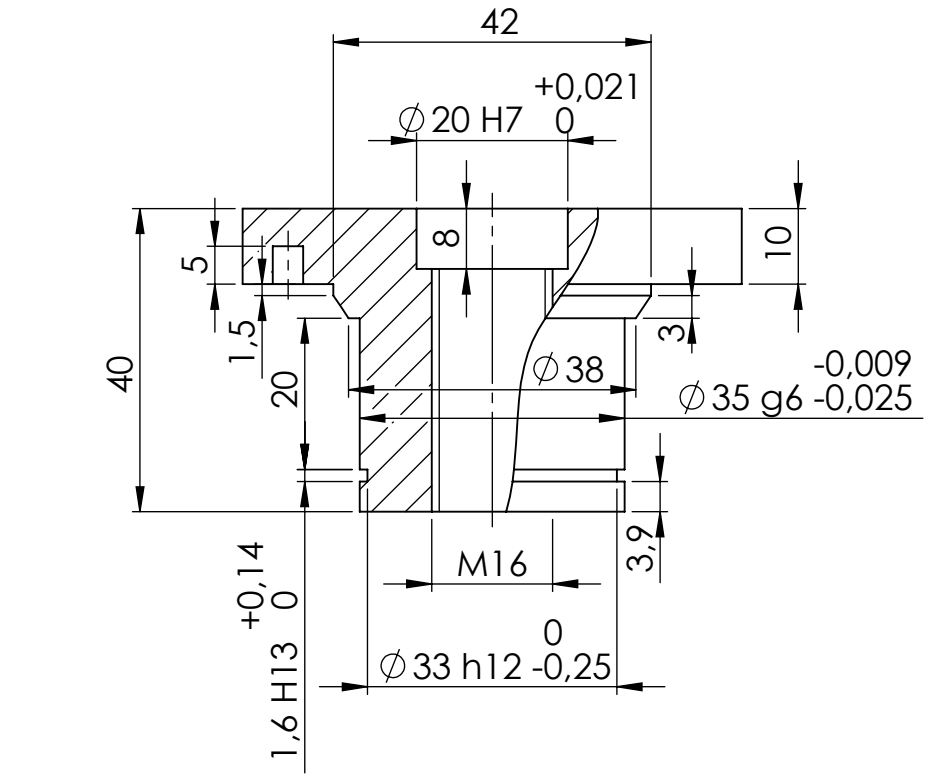

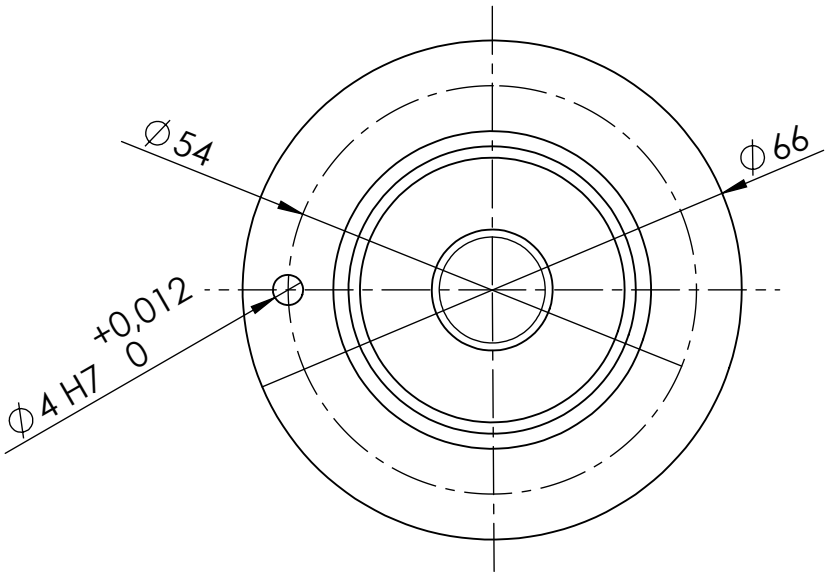

	Norm: ISO 2768 - mK		Qt: 4	
			SCALE: 1:1	
AD FEUP	U.PORTO FEUP FACULDADE DE ENGENHARIA UNIVERSIDADE DO PORTO		TITLE: ARS rotation axle	
	NAME	DATE	MATERIAL:	DWG NO.
DRAWN	Diogo do Paço Casal Antunes	23-01-2019	N540	Drawing nº11
CHK'D				A4
APPV'D			WEIGHT:	SHEET 1 OF 1

SOLIDWORKS Educational Product. For Instructional Use Only.

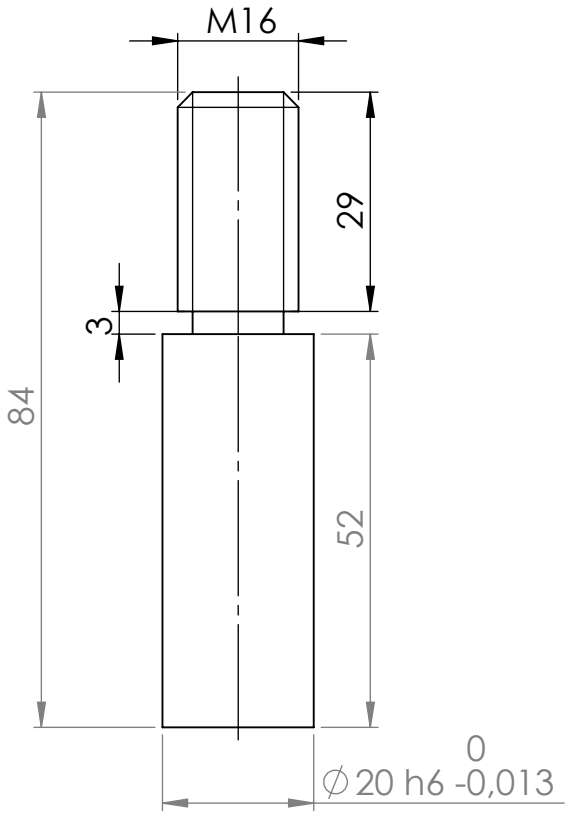

Norm: ISO 2768 - mK		Qt: 4	
		SCALE: 1:1	
AD FEUP	U.PORTO FEUP FACULDADE DE ENGENHARIA UNIVERSIDADE DO PORTO	TITLE: ARS rotation axle part 2	
	NAME / DATE	MATERIAL: N540	DWG NO. Drawing nº12 — A4
DRAWN	Diogo do Paço Casal Antunes / 23-01-2019		
CHK'D			
APP'V'D		WEIGHT:	SHEET 1 OF 1

SOLIDWORKS Educational Product. For Instructional Use Only.

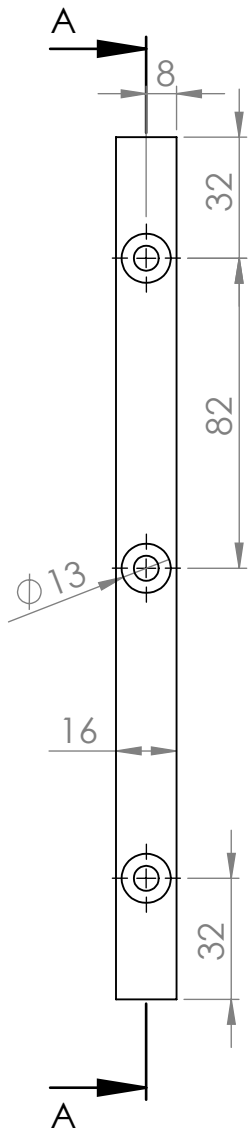

SECTION A-A
SCALE 1 : 2

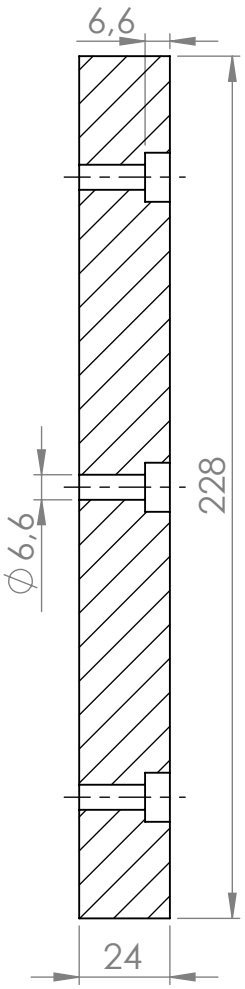

	Norm: ISO 2768 - mK			Qt: 2	
				SCALE: 1:2	
AD FEUP	U.PORTO FEUP FACULDADE DE ENGENHARIA UNIVERSIDADE DO PORTO			TITLE: Hook	
	NAME	DATE	MATERIAL:	DWG NO.	A4
DRAWN	Diogo do Paço Casal Antunes	23-01-2019	N540	Drawing nº13	
CHK'D					
APPV'D			WEIGHT:		SHEET 1 OF 1

SOLIDWORKS Educational Product. For Instructional Use Only.

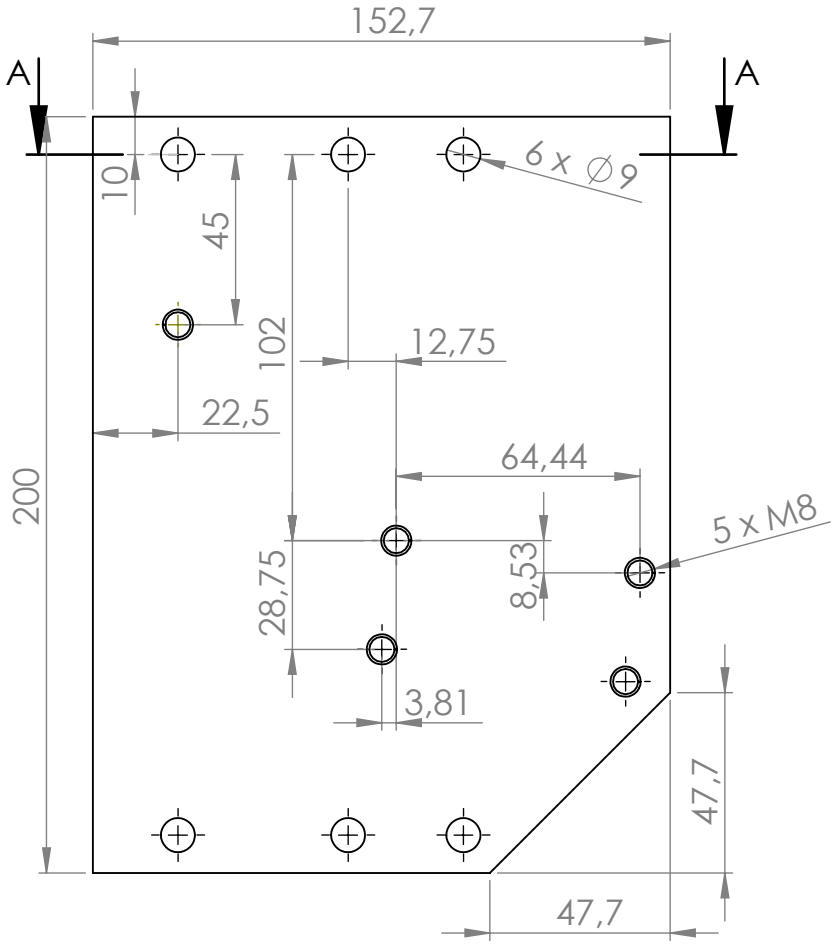

SECTION A-A
SCALE 1 : 2

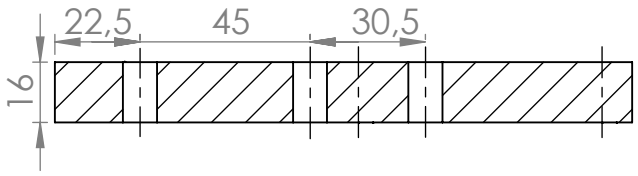

	Norm: ISO 2768 - mK		Qt: 4	
			SCALE: 1:2	
AD FEUP	U.PORTO FEUP FACULDADE DE ENGENHARIA UNIVERSIDADE DO PORTO		TITLE: Front/back plate	
	NAME	DATE	MATERIAL:	DWG NO.
DRAWN	Diogo do Paço Casal Antunes	23-01-2019	AW 6082 T651	Drawing nº14 A4
CHK'D				
APPV'D			WEIGHT:	SHEET 1 OF 1

SOLIDWORKS Educational Product. For Instructional Use Only.

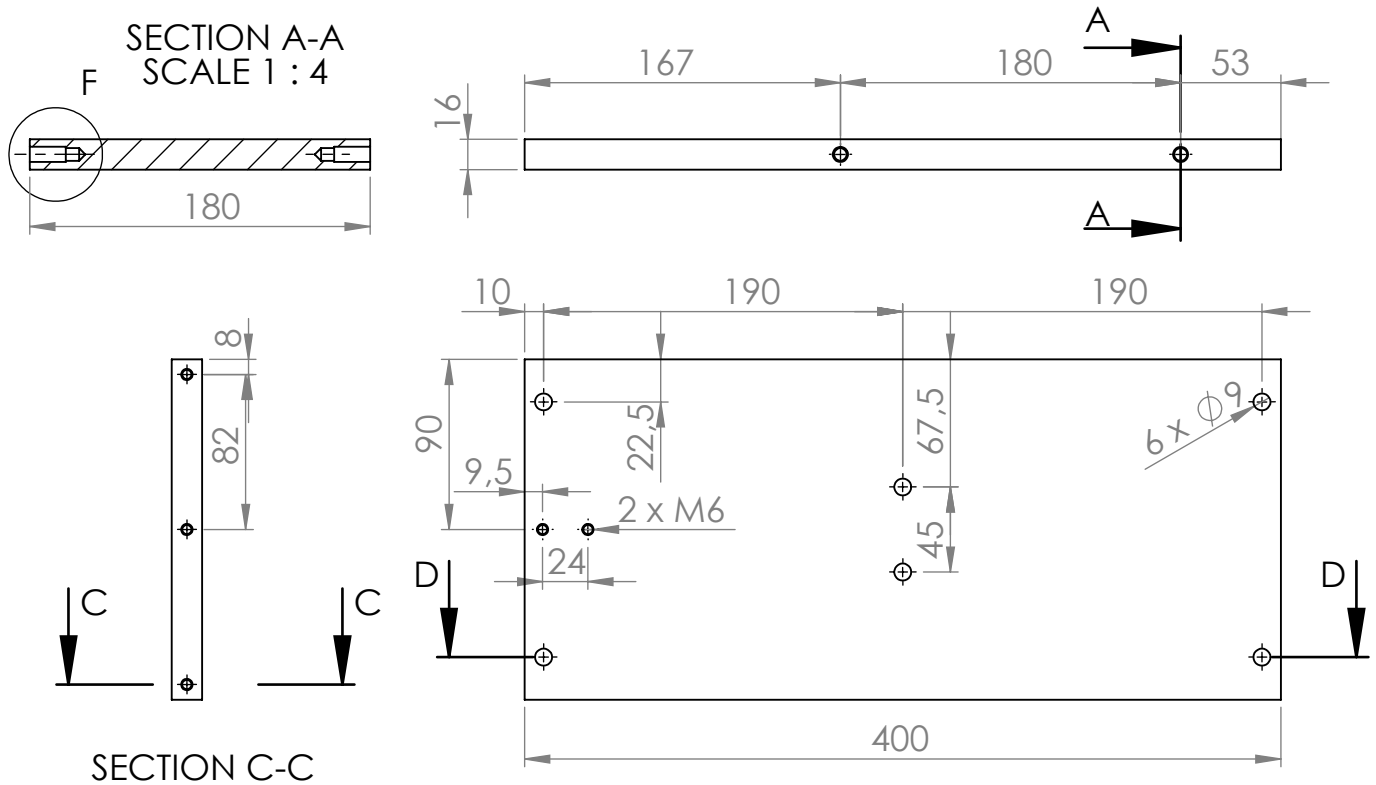

SECTION C-C
SCALE 1 : 4

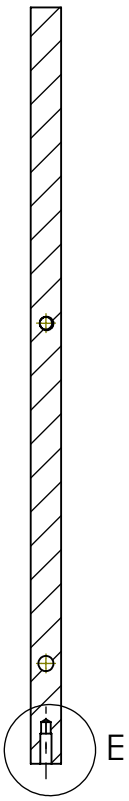

SECTION D-D
SCALE 1 : 4

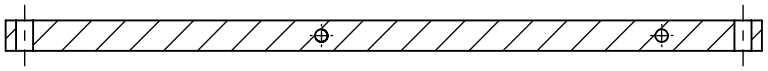

DETAIL F
SCALE 1 : 1

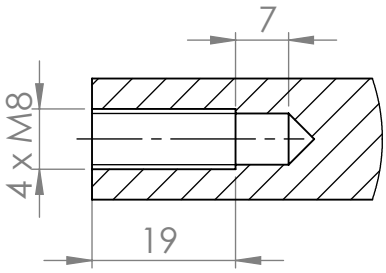

DETAIL E
SCALE 1 : 1

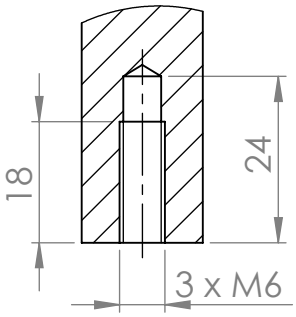

	Norm: ISO 2768 - mK	Qt: 2	
		SCALE: 1:4	
AD FEUP / U.PORTO FEUP FACULDADE DE ENGENHARIA UNIVERSIDADE DO PORTO		TITLE: Side plate	
NAME / DATE	MATERIAL: AW 6082 T651	DWG NO. Drawing nº15	A4
DRAWN: Diogo do Paço Casal Antunes / 23-01-2019			
CHK'D			
APPV'D	WEIGHT:		SHEET 1 OF 1

SOLIDWORKS Educational Product. For Instructional Use Only.

SECTION A-A
SCALE 1 : 1

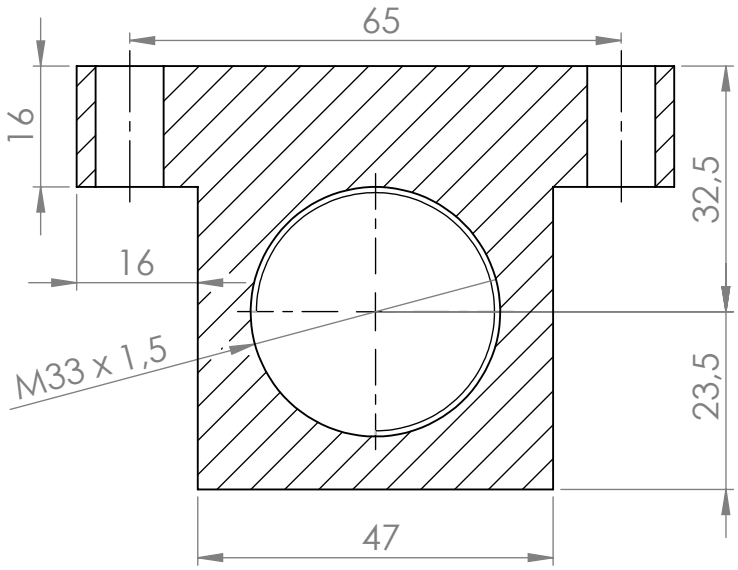

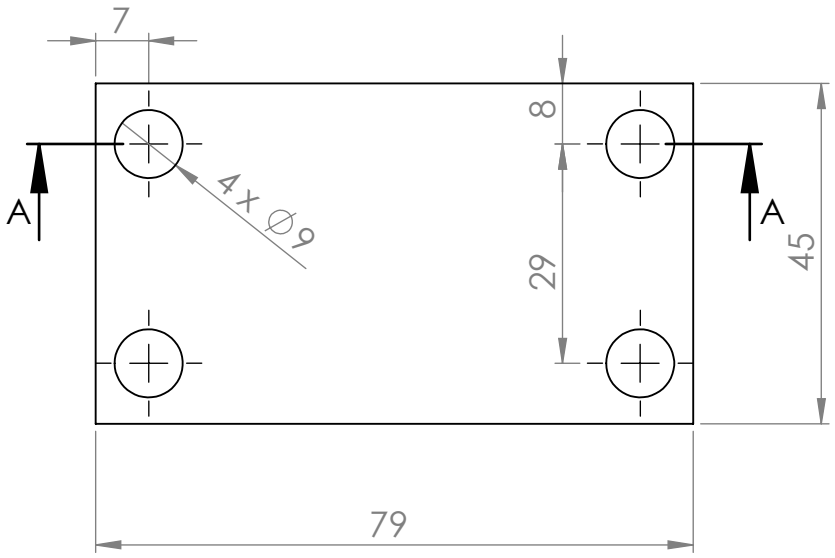

	Norm: ISO 2768 - mK	Qt: 4
		SCALE: 1:1

AD FEUP

U.PORTO
FEUP FACULDADE DE ENGENHARIA
UNIVERSIDADE DO PORTO

TITLE: Shock-absorber support

	NAME	DATE
DRAWN	Diogo do Paço Casal Antunes	23-01-2019
CHK'D		
APPV'D		

MATERIAL: AW 6082 T651

DWG NO. Drawing nº16

A4

WEIGHT:

SHEET 1 OF 1

SOLIDWORKS Educational Product. For Instructional Use Only.

SECTION A-A
SCALE 1 : 1

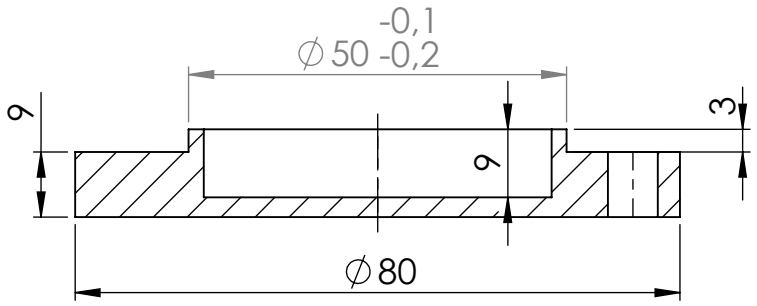

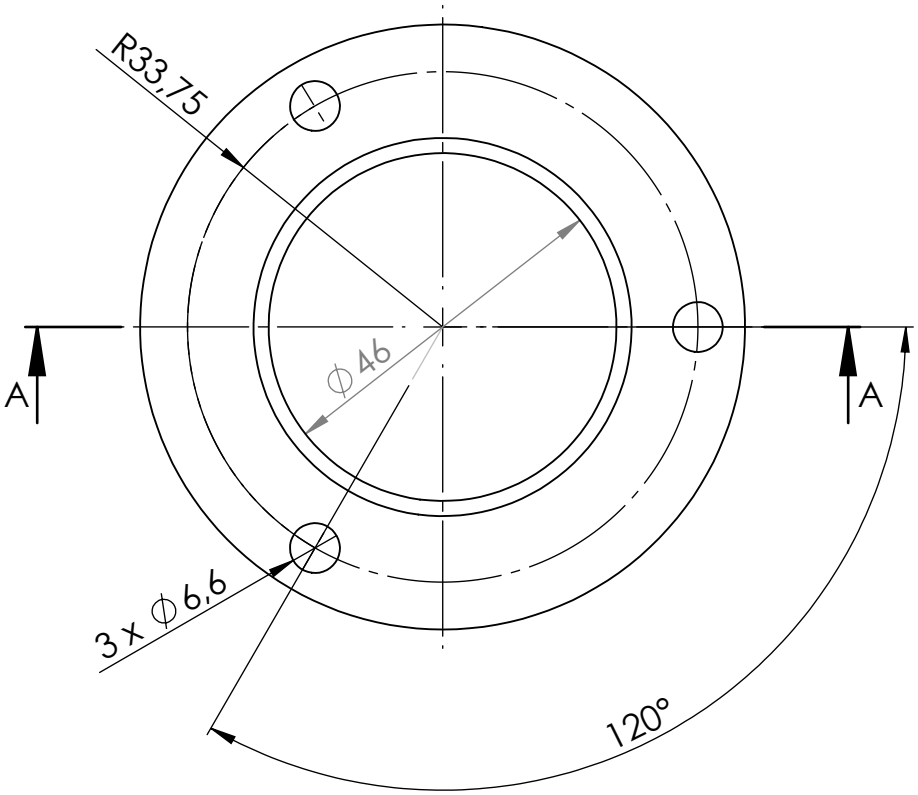

	Norm: ISO 2768 - mK	Qt: 4	
		SCALE: 1:1	
AD FEUP	U.PORTO FEUP FACULDADE DE ENGENHARIA UNIVERSIDADE DO PORTO	TITLE: Cover	
NAME / DATE	MATERIAL: AW 6082 T651	DWG NO. Drawing nº17	A4
DRAWN: Diogo do Paço Casal Antunes / 23-01-2019			
CHK'D			
APPV'D	WEIGHT:		SHEET 1 OF 1

SOLIDWORKS Educational Product. For Instructional Use Only.

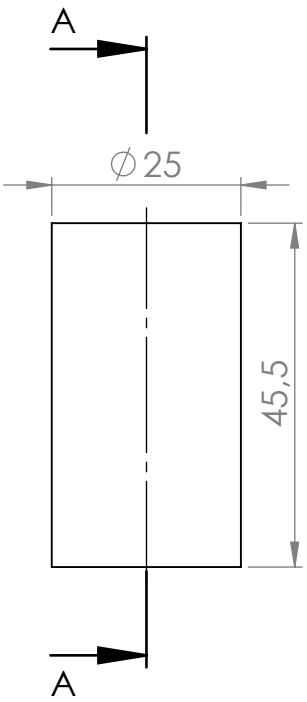

SECTION A-A
SCALE 1 : 1

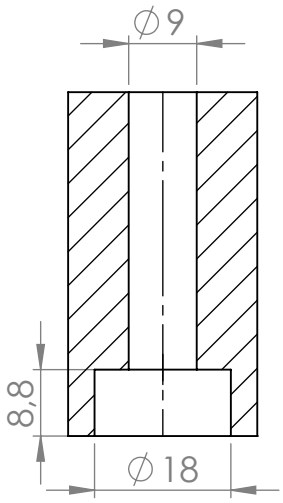

	Norm: ISO 2768 - mK		Qt: 4	
			SCALE: 1:1	
AD FEUP	U.PORTO FEUP FACULDADE DE ENGENHARIA UNIVERSIDADE DO PORTO		TITLE: Stopper	
	NAME	DATE	MATERIAL: N540	DWG NO. Drawing nº18 A4
DRAWN	Diogo do Paço Casal Antunes	23-01-2019		
CHK'D				
APPV'D			WEIGHT:	SHEET 1 OF 1

SOLIDWORKS Educational Product. For Instructional Use Only.

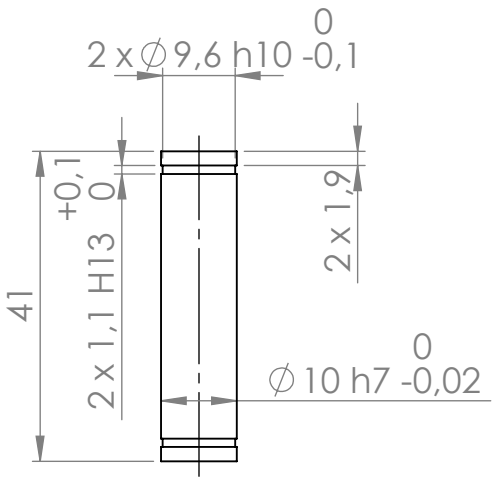

Norm: ISO 2768 - mK		Qt: 2	
		SCALE: 1:1	
AD FEUP	U.PORTO FEUP FACULDADE DE ENGENHARIA UNIVERSIDADE DO PORTO	TITLE: Rod eye´s axle	
NAME	DATE	MATERIAL: N540	DWG NO. Drawing nº21 A4
DRAWN Diogo do Paço Casal Antunes	23-01-2019		
CHK'D			
APPV'D		WEIGHT:	SHEET 1 OF 1

SOLIDWORKS Educational Product. For Instructional Use Only.

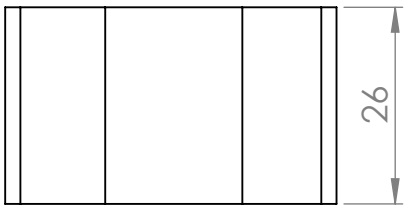

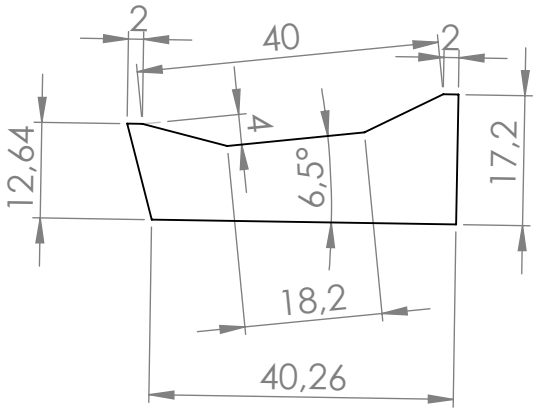

Norm: ISO 2768 - mK		Qt: 4	
		SCALE: 1:1	
AD FEUP / U.PORTO FEUP FACULDADE DE ENGENHARIA UNIVERSIDADE DO PORTO		TITLE: Polyurethane for aligment	
	NAME / DATE	MATERIAL: PUR	DWG NO. Drawing nº26 — A4
DRAWN	Diogo do Paço Casal Antunes / 23-01-2019		
CHK'D			
APPV'D		WEIGHT:	SHEET 1 OF 1

SOLIDWORKS Educational Product. For Instructional Use Only.

SECTION A-A

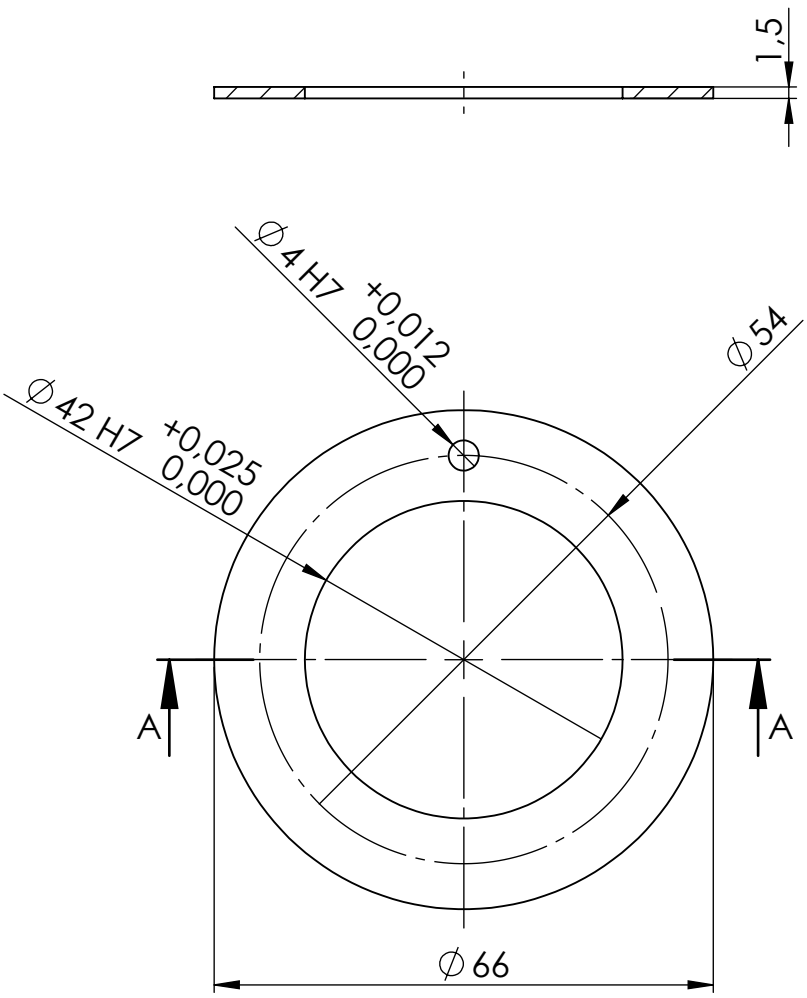

Norm: ISO 2768 - mK		Qt: 4	
SCALE: 1:1			
AD FEUP	U.PORTO FEUP FACULDADE DE ENGENHARIA UNIVERSIDADE DO PORTO	TITLE: Washer	
	NAME	DATE	MATERIAL: Bronze
DRAWN	Diogo do Paço Casal Antunes	23-01-2019	DWG NO. Drawing nº28
CHK'D			A4
APPV'D			WEIGHT: SHEET 1 OF 1

SOLIDWORKS Educational Product. For Instructional Use Only.

Appendix B

Mechanical Drawings
Anvil-Impactor Assembly

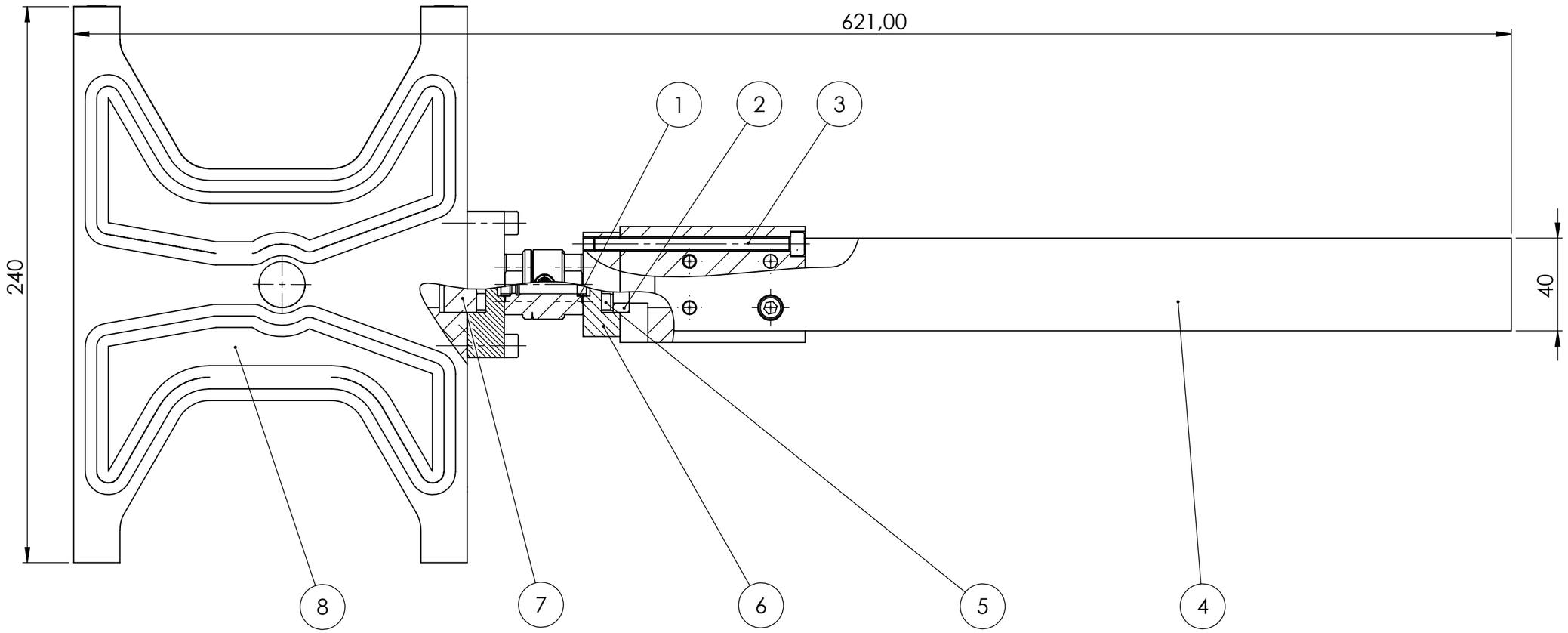

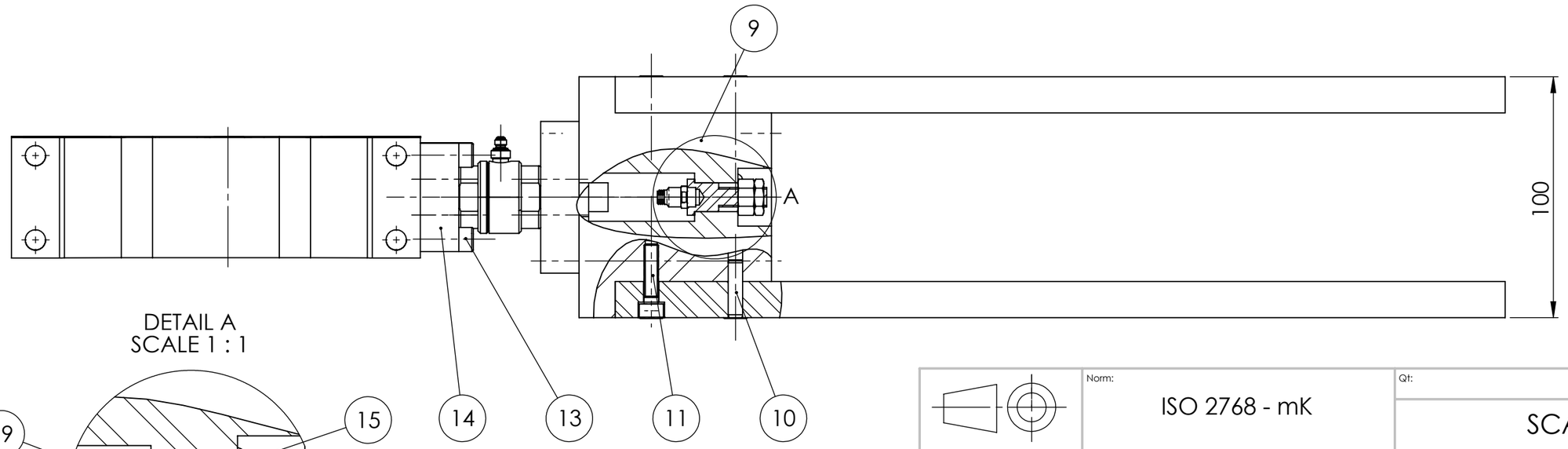

DETAIL A
SCALE 1 : 1

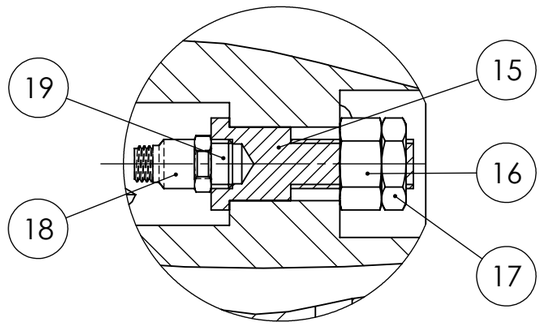

Norm: ISO 2768 - mK	Qt: 1	
	SCALE: 1:2	
AD FEUP / U.PORTO FEUP FACULDADE DE ENGENHARIA UNIVERSIDADE DO PORTO	TITLE: Anvil-impactor Assembly	
	SHEET 1 OF 2	A3

	NAME	DATE
DRAWN	Diogo do Paço Casal Antunes	23-01-2019
CHK'D		
APPV'D		
WEIGHT:		

SOLIDWORKS Educational Product. For Instructional Use Only.

Num.	Component.	Qt.
1	Sensor´s aligner ring	2
2	Lower plate aligner ring	1
3	ISO 4762 - M6x85	4
4	Impactor´s bar	2
5	ISO 4762 -M4x12	8
6	Lower plate	1
7	Upper plate aligner part	1
8	Anvil	1
9	Impactor´s base	1
10	ISO 2338 - Φ6x24	4
11	ISO 4762 - M6x30	4
12	Press force sensor	1
13	ISO 4762 - M6x25	4
14	Upper plate	1
15	Acelerometer fixing	1
16	ISO 4032 - M8x1,25	1
17	ISO 4035 - M8x1,25	1
18	Accelerometer	1
19	Mounting stud	1

Norm: ISO 2768 - mK

AD FEUP

U.PORTO FEUP FACULDADE DE ENGENHARIA UNIVERSIDADE DO PORTO

TITLE: Anvil-impactor Assembly

	NAME	DATE
DRAWN	Diogo do Paço Casal Antunes	23-01-2019
CHK'D		
APPV'D		

MATERIAL:

SHEET 2 OF 2

A4

SOLIDWORKS Educational Product. For Instructional Use Only.

SECTION B-B
SCALE 1 : 1

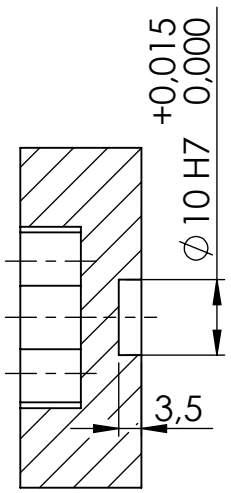

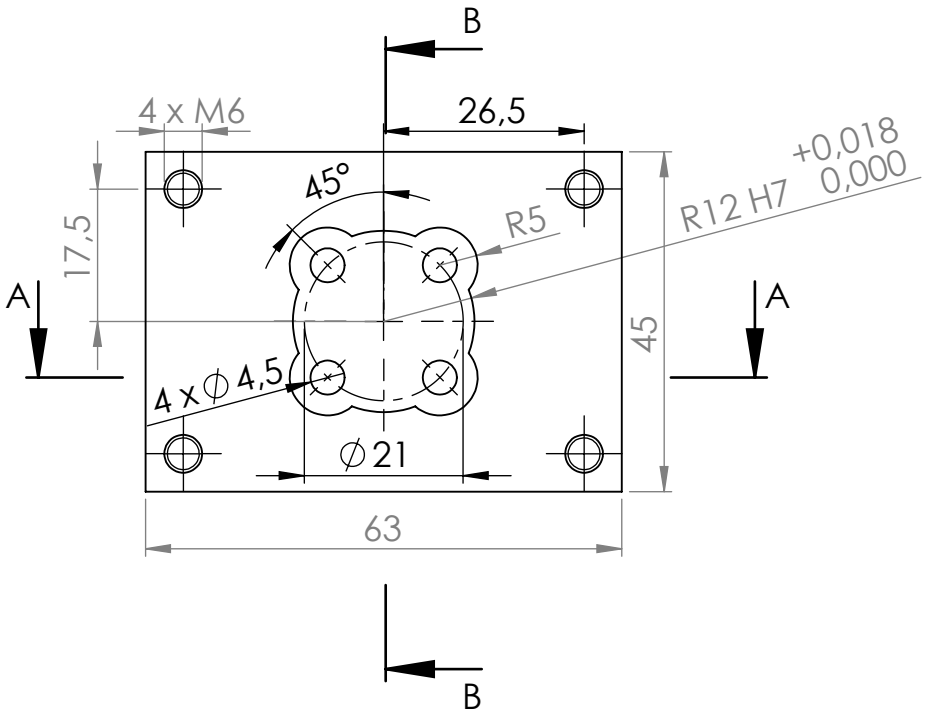

SECTION A-A
SCALE 1 : 1

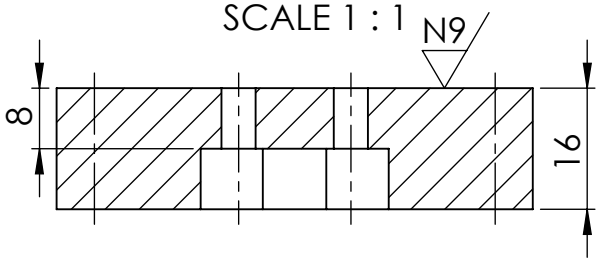

	Norm: ISO 2768 - mK	Qt: 1	
		SCALE: 1:1	
AD FEUP / U.PORTO FEUP Faculdade de Engenharia Universidade do Porto		TITLE: Impactor´s lower plate	
NAME / DRAWN: Diogo do Paço Casal Antunes / CHK'D / APPV'D	DATE: 23-01-2019	MATERIAL: N540	DWG NO. Drawing nº19 — A4
		WEIGHT:	SHEET 1 OF 1

SOLIDWORKS Educational Product. For Instructional Use Only.

SECTION B-B
SCALE 1 : 1

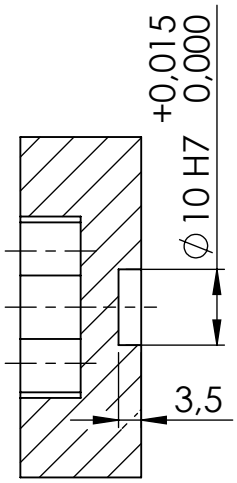

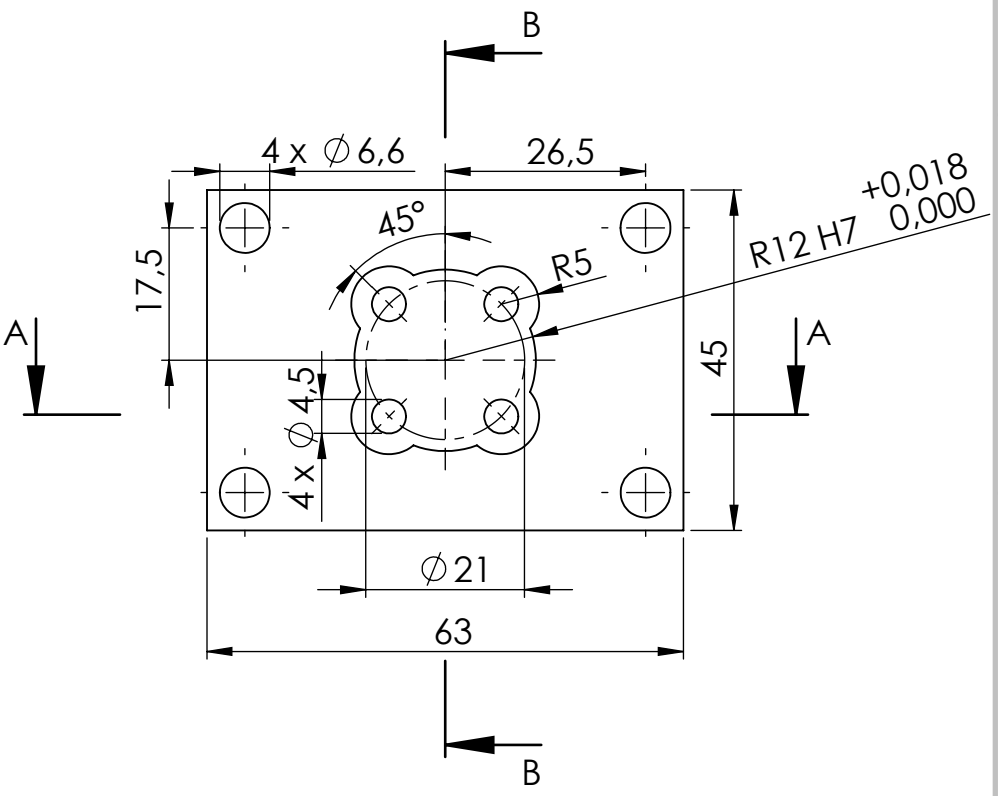

SECTION A-A
SCALE 1 : 1

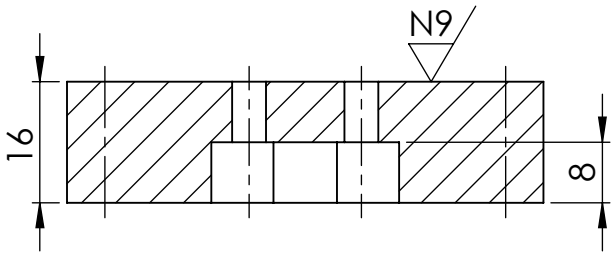

	Norm: ISO 2768 - mK	Qt: 1	
		SCALE: 1:1	
AD FEUP / U.PORTO FEUP FACULDADE DE ENGENHARIA UNIVERSIDADE DO PORTO		TITLE: Impactor´s upper plate	
NAME / DATE	MATERIAL: N540	DWG NO. Drawing nº20	A4
DRAWN: Diogo do Paço Casal Antunes / 23-01-2019			
CHK'D			
APPV'D	WEIGHT:		SHEET 1 OF 1

SOLIDWORKS Educational Product. For Instructional Use Only.

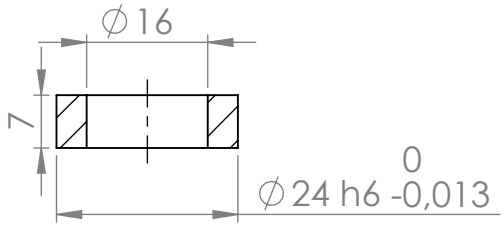

Norm: ISO 2768 - mK		Qt: 1	
SCALE: 1:1			
AD FEUP	U.PORTO FEUP FACULDADE DE ENGENHARIA UNIVERSIDADE DO PORTO	TITLE: Impactor´s lower aligment block	
	NAME	DATE	MATERIAL: N540
DRAWN	Diogo do Paço Casal Antunes	23-01-2019	DWG NO. Drawing nº22
CHK'D			A4
APPV'D			WEIGHT:
			SHEET 1 OF 1

SOLIDWORKS Educational Product. For Instructional Use Only.

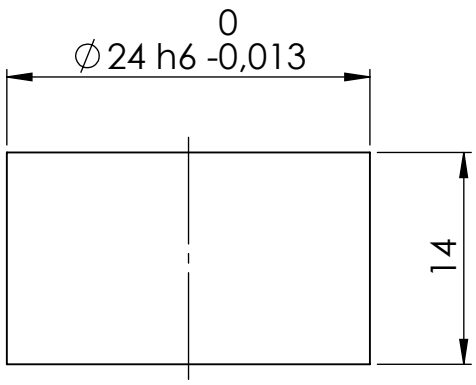

Norm: ISO 2768 - mK		Qt: 1	
SCALE: 1:1			
AD FEUP	U.PORTO FEUP FACULDADE DE ENGENHARIA UNIVERSIDADE DO PORTO	TITLE: Impactor´s lower aligment block	
NAME	DATE	MATERIAL: N540	DWG NO. Drawing nº23
DRAWN Diogo do Paço Casal Antunes	23-01-2019		A4
CHK'D			
APPV'D		WEIGHT:	SHEET 1 OF 1

SOLIDWORKS Educational Product. For Instructional Use Only.

SECTION A-A

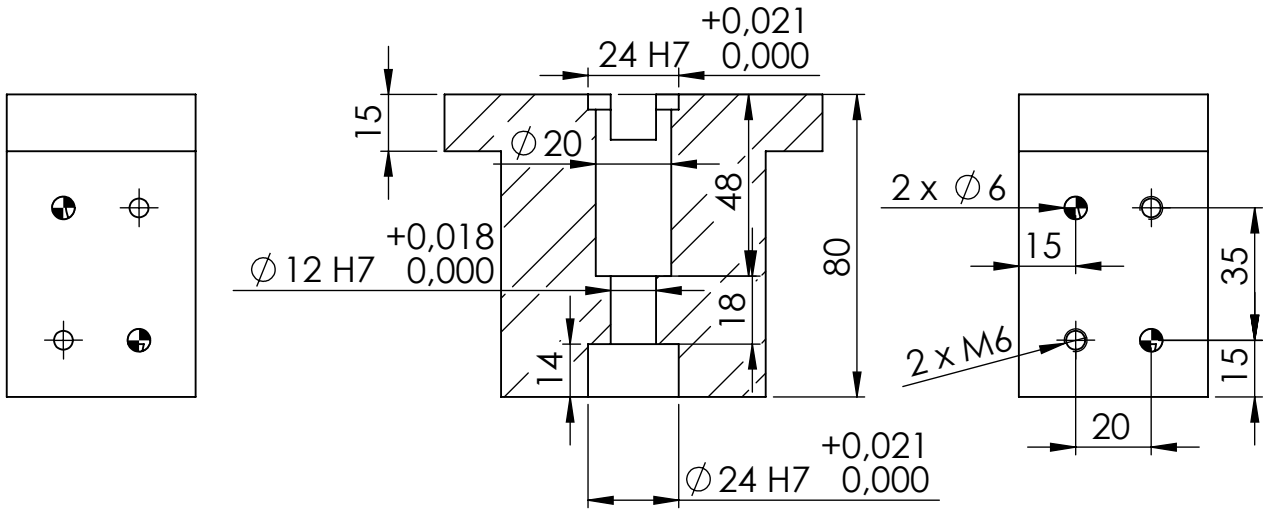

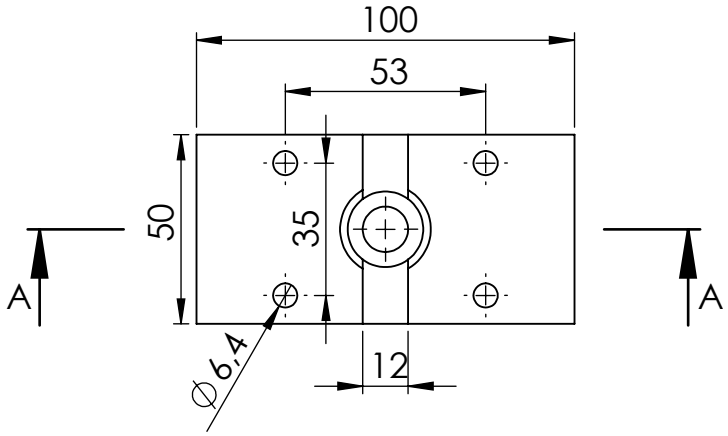

Norm: ISO 2768 - mK	Qt: 1	
	SCALE: 1:2	
AD FEUP / U.PORTO FEUP FACULDADE DE ENGENHARIA UNIVERSIDADE DO PORTO	TITLE: Impactor´s base	

	NAME	DATE	MATERIAL:	DWG NO.	
DRAWN	Diogo do Paço Casal Antunes	23-01-2019	PM 300	Drawing nº24	A4
CHK'D					
APPV'D			WEIGHT:		SHEET 1 OF 1

SOLIDWORKS Educational Product. For Instructional Use Only.

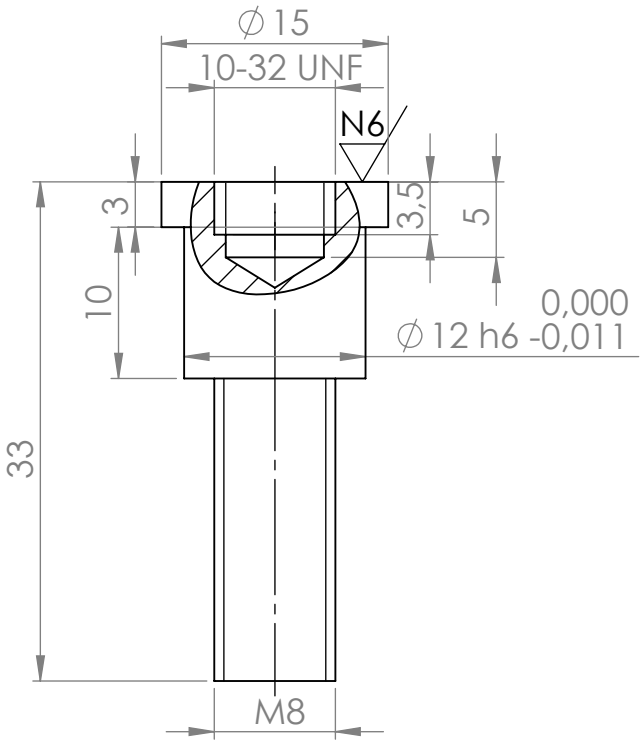

	Norm: ISO 2768 - mK	Qt: 1	
		SCALE: 2:1	
AD FEUP	U.PORTO FEUP FACULDADE DE ENGENHARIA UNIVERSIDADE DO PORTO	TITLE: Accelerometer´s fixation structure	
	NAME / DATE	MATERIAL: N540	DWG NO. Drawing nº25 — A4
DRAWN	Diogo do Paço Casal Antunes / 23-01-2019		
CHK'D			
APPV'D		WEIGHT:	SHEET 1 OF 1

SOLIDWORKS Educational Product. For Instructional Use Only.

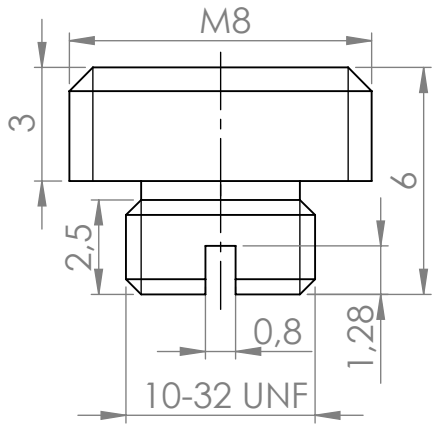

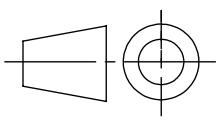

Norm: ISO 2768 - mK

Qt: 1

SCALE: 5:1

AD FEUP

U.PORTO FEUP FACULDADE DE ENGENHARIA UNIVERSIDADE DO PORTO

TITLE: Mounting Stud

	NAME	DATE
DRAWN	Diogo do Paço Casal Antunes	23-01-2019
CHK'D		
APPV'D		

MATERIAL: Screw ISO 4017 M8 - 12.9

WEIGHT:

DWG NO. Drawing nº27

A4

SHEET 1 OF 1

SOLIDWORKS Educational Product. For Instructional Use Only.

SECTION A-A

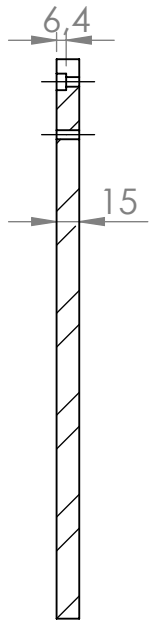

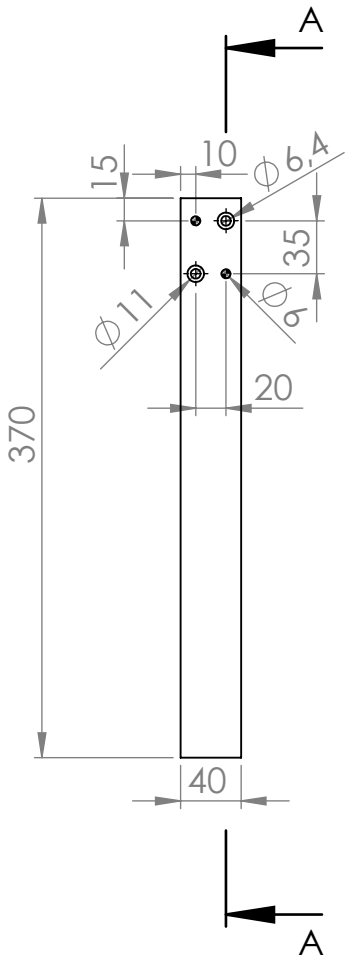

Norm: ISO 2768 - mK		Qt: 2	
		SCALE: 1:5	
AD FEUP / U.PORTO FEUP FACULDADE DE ENGENHARIA UNIVERSIDADE DO PORTO		TITLE: Impactor´s bar	
	NAME / DATE	MATERIAL: PM 300	DWG NO. Drawing nº29 — A4
DRAWN	Diogo do Paço Casal Antunes / 23-01-2019		
CHK'D			
APPV'D		WEIGHT:	SHEET 1 OF 1

SOLIDWORKS Educational Product. For Instructional Use Only.

Appendix C

Matlab Simulink
Dynamic Behaviour Model

Dynamic model

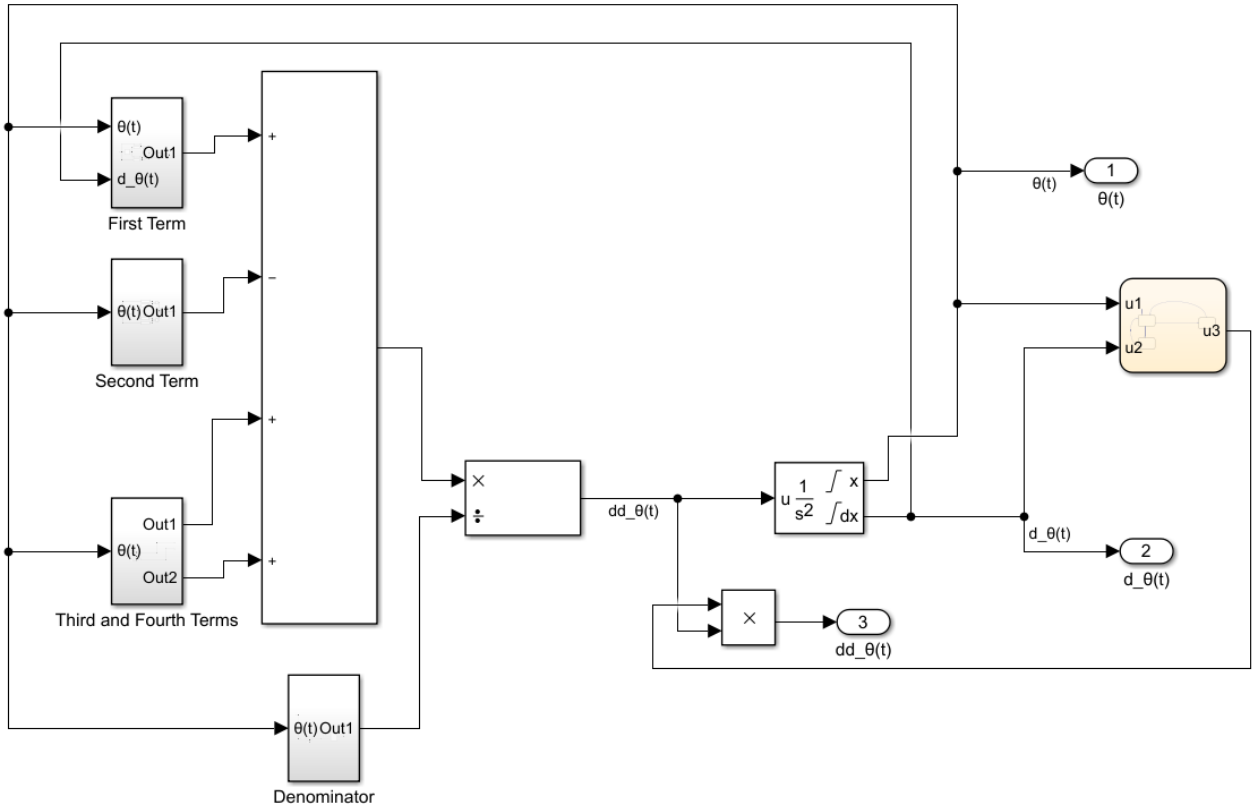

First Term

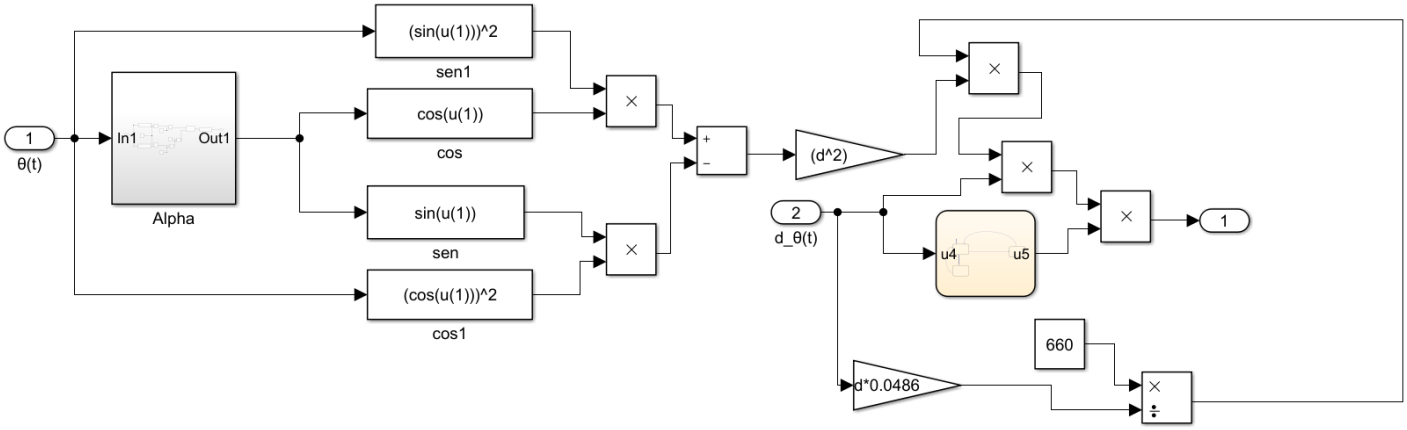

Second Term

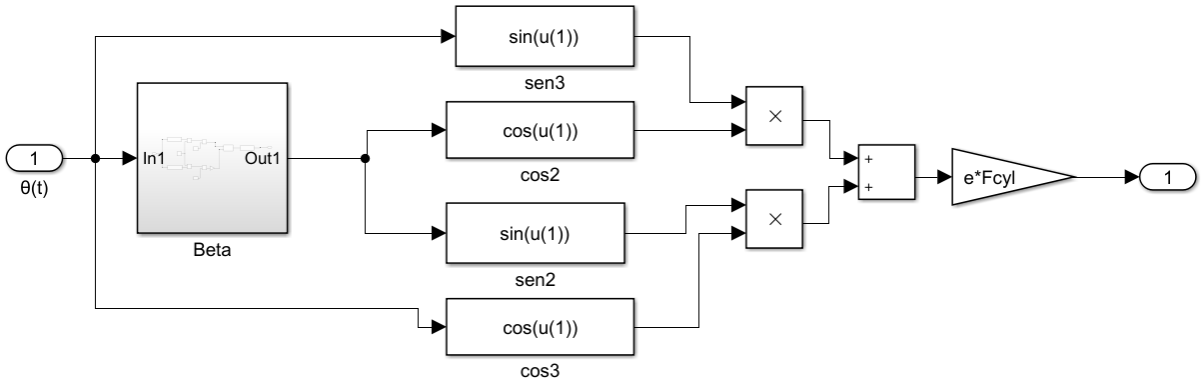

Third and Fourth Term

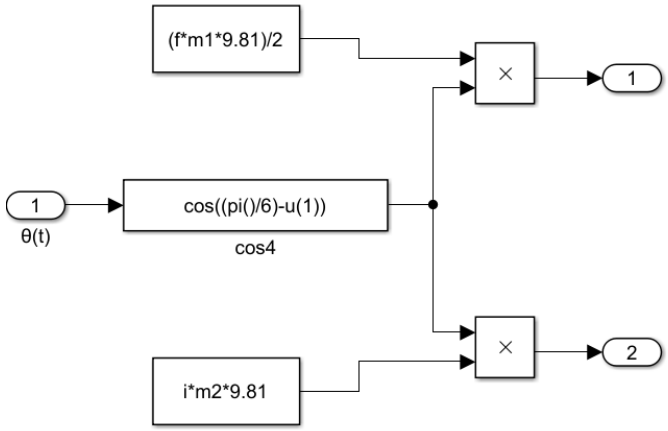

Denominator

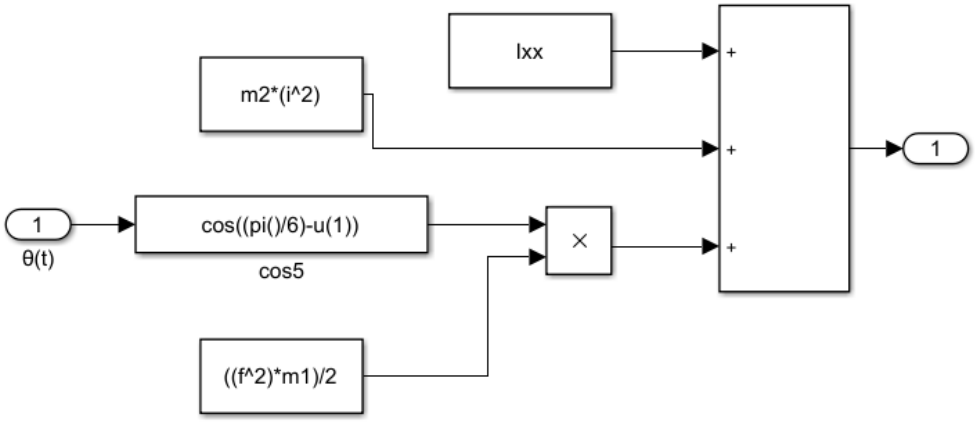

Angular position throughout time, Θ(t), when drop mass is 56 kg

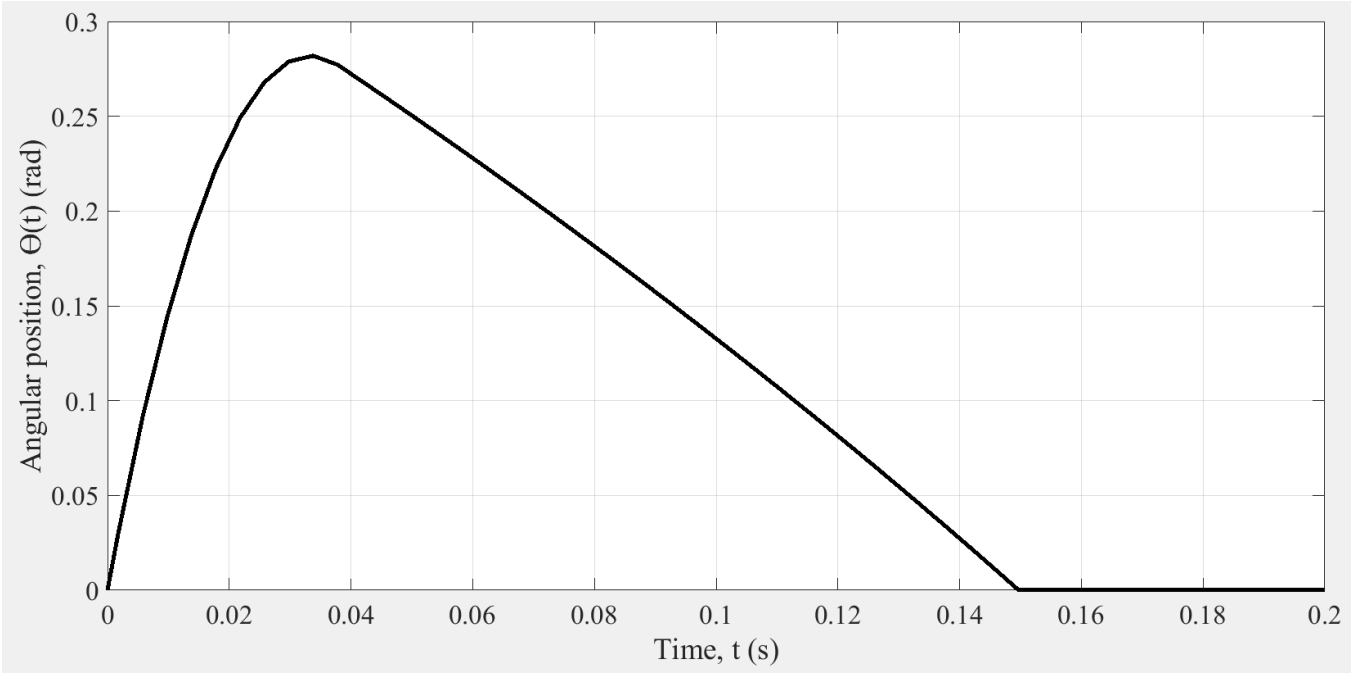

Angular velocity throughout time, $\dot{\theta}(t)$, when drop mass is 56 kg

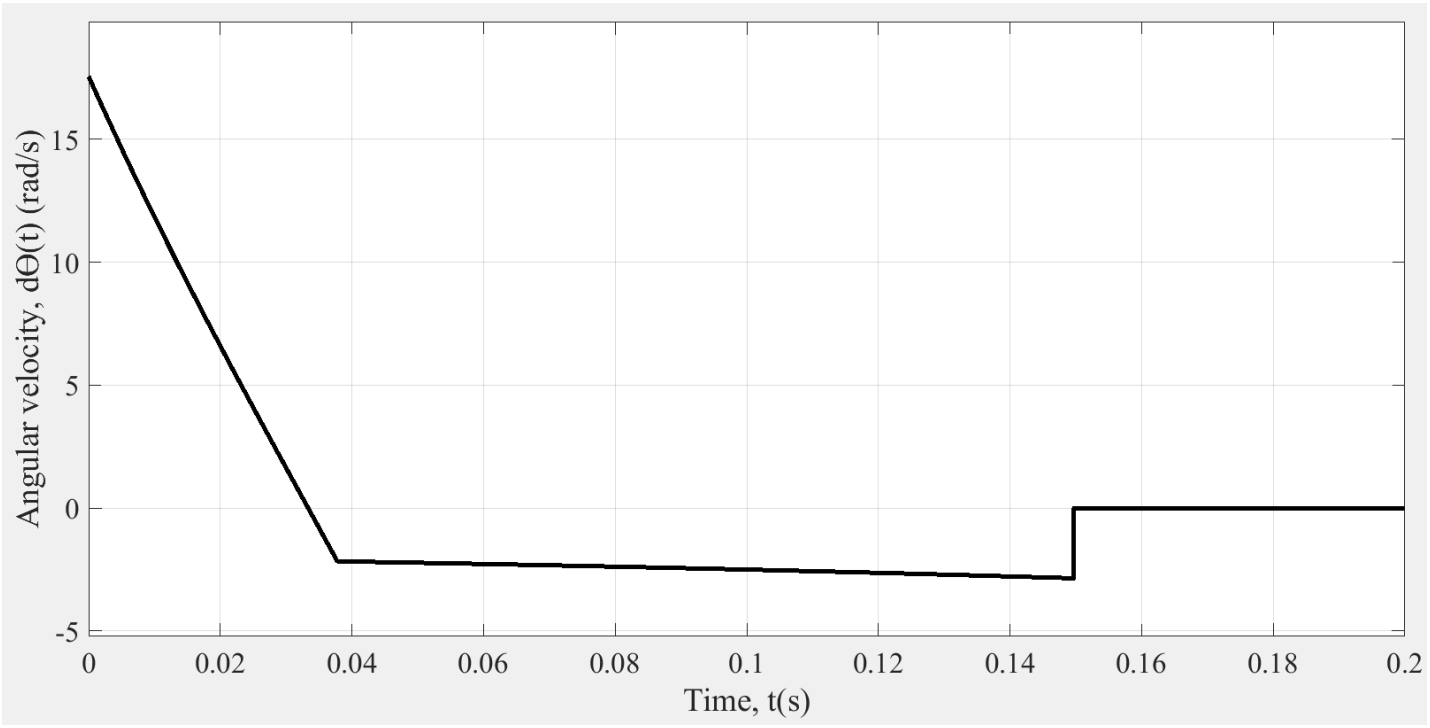

Angular acceleration throughout time, $\ddot{\theta}(t)$, when drop mass is 56 kg

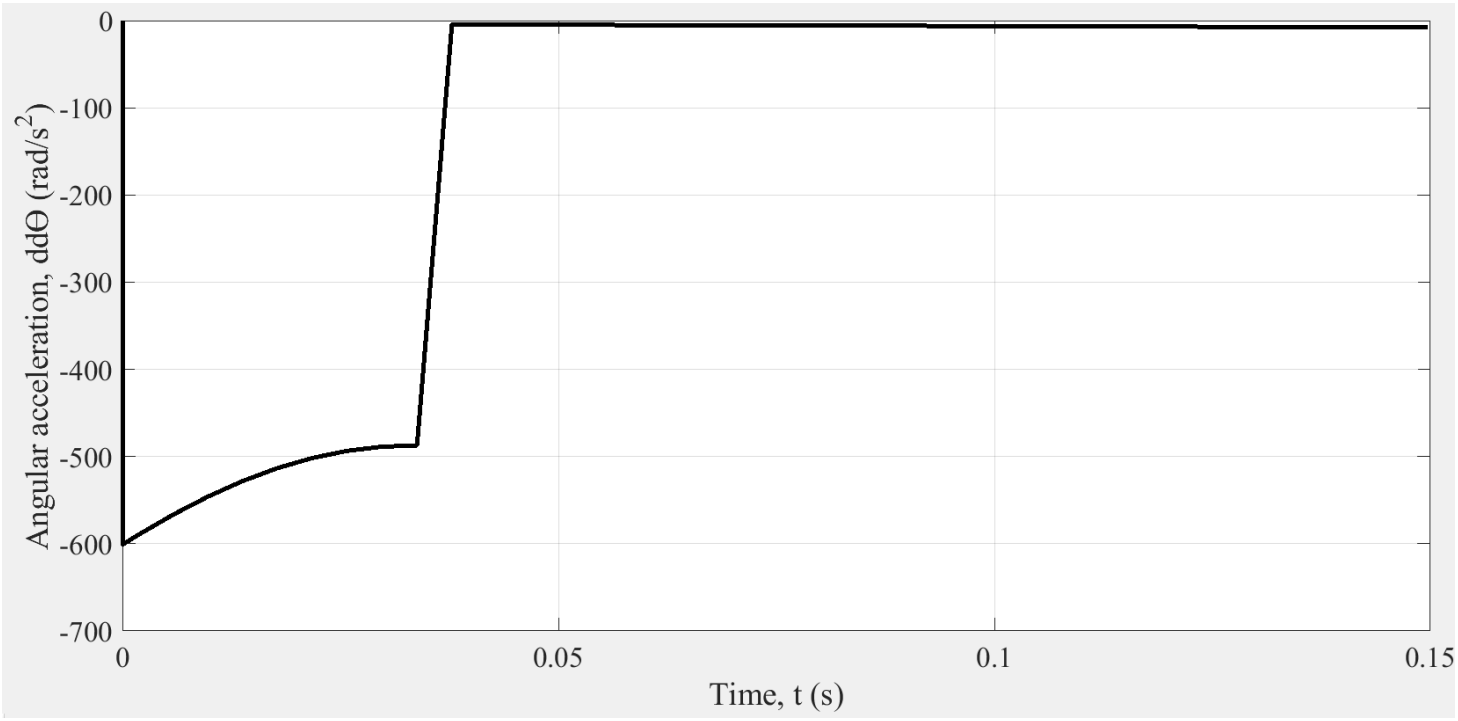

Angular position throughout time, Θ(t), when drop mass is 8.5 kg

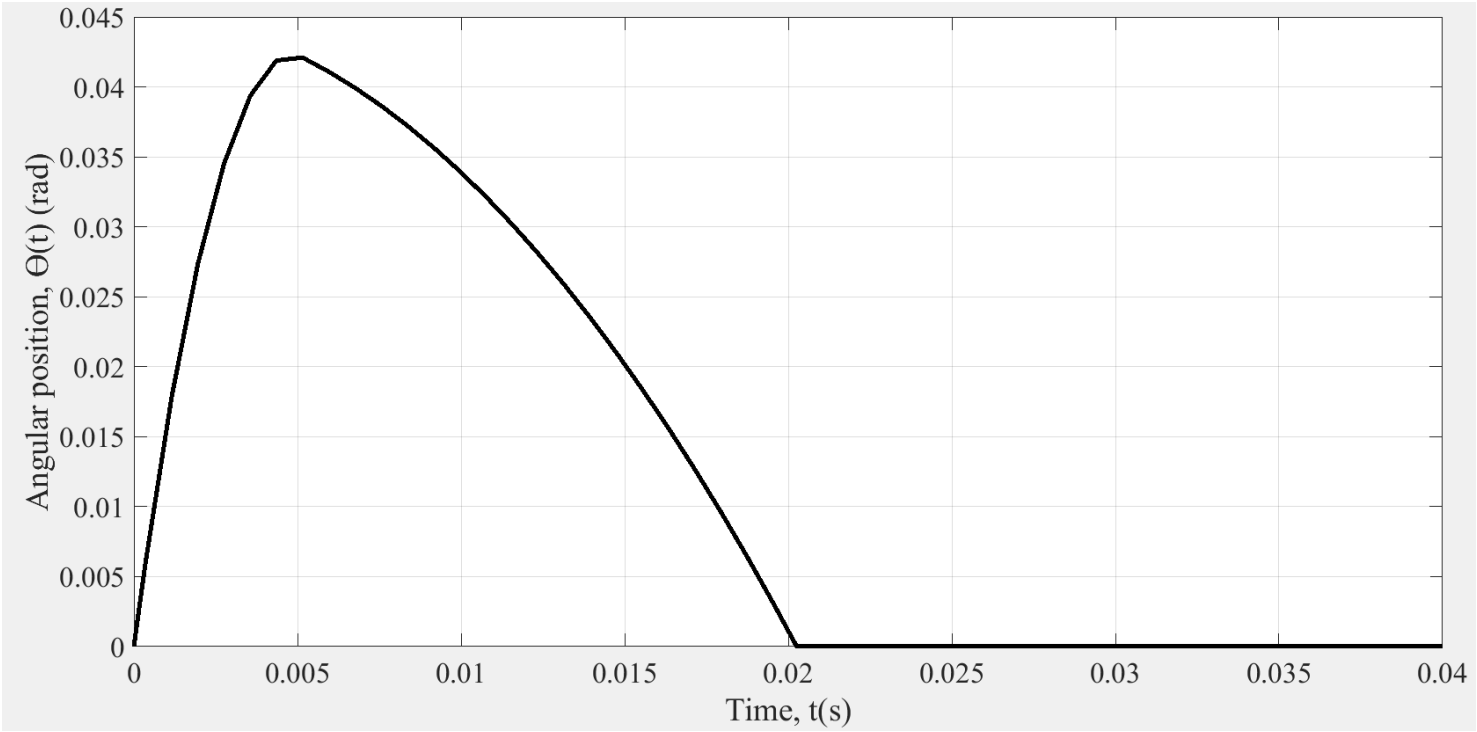

Angular velocity throughout time, $\dot{\Theta}(t)$, when drop mass is 8.5 kg

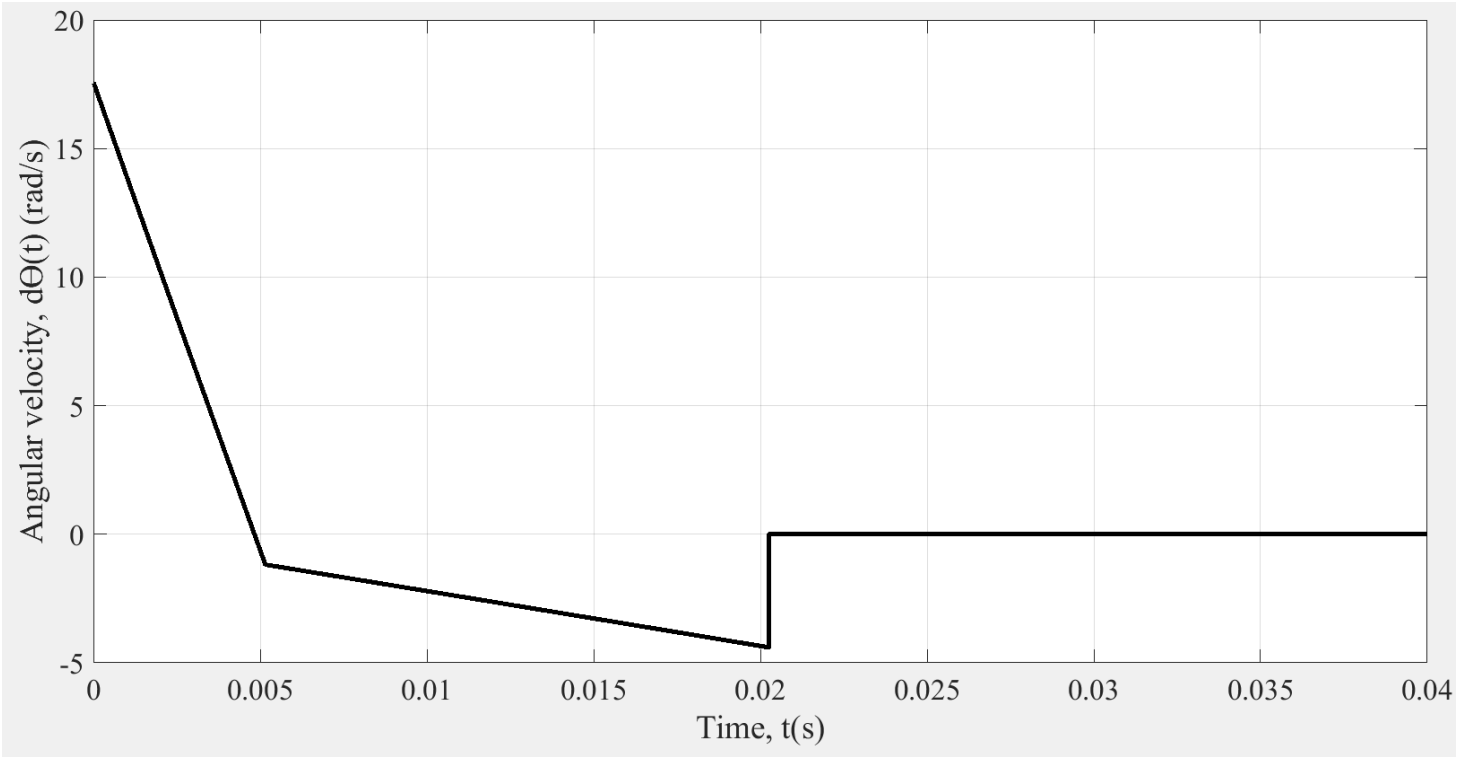

Angular acceleration throughout time, $\ddot{\theta}(t)$, when drop mass is 8.5 kg

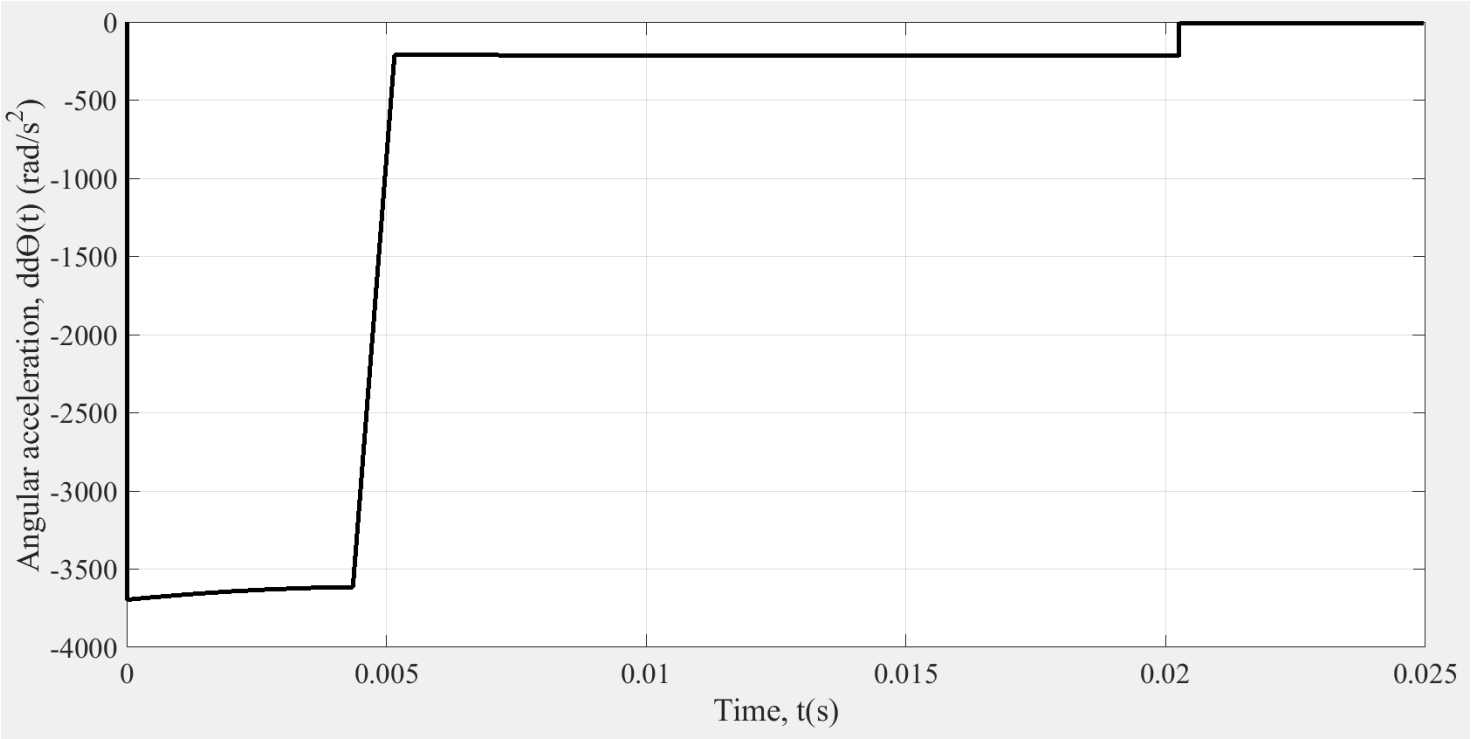

Appendix D

Electrical circuit

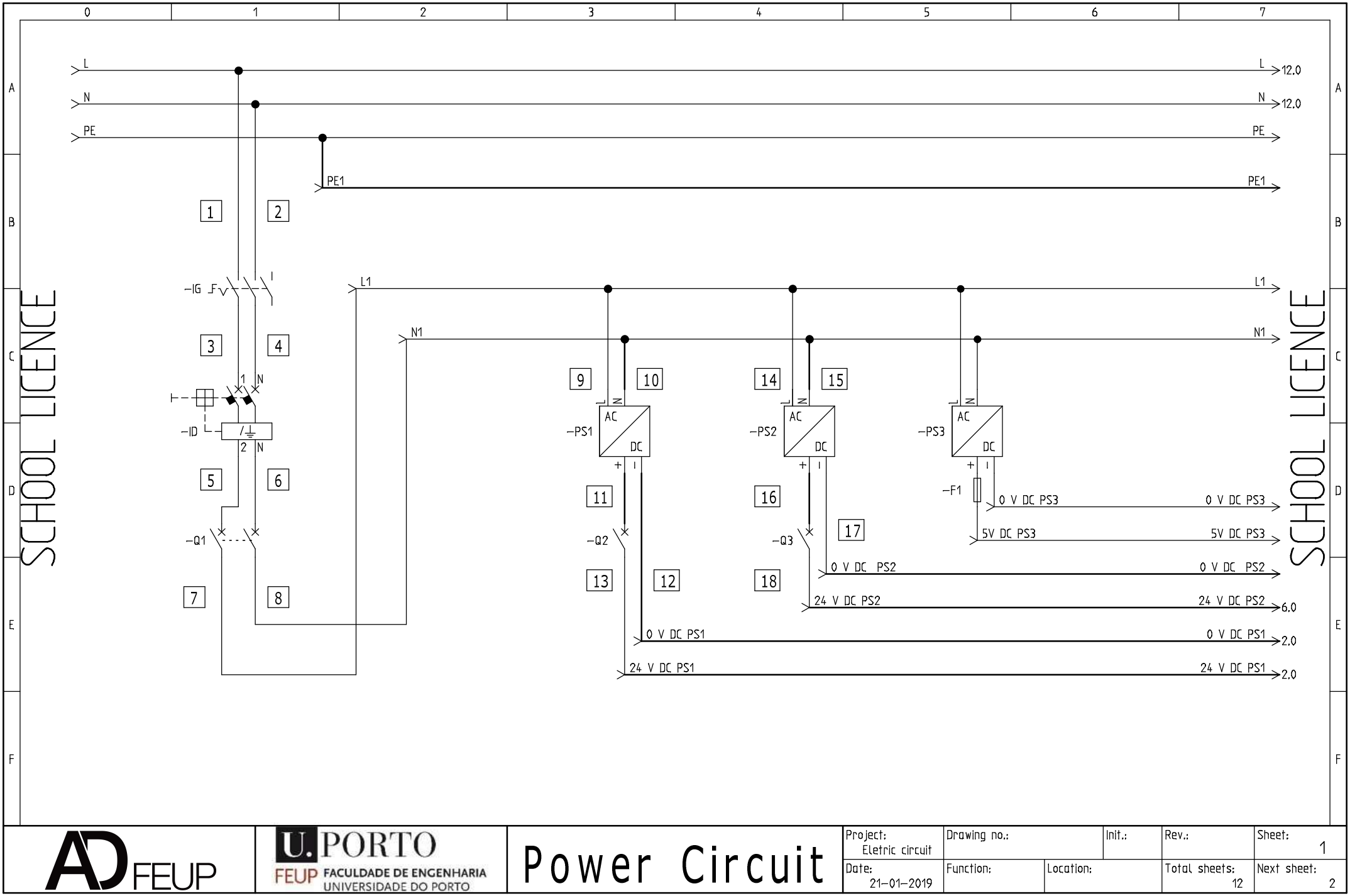

FEUP

U.PORTO
FEUP FACULDADE DE ENGENHARIA
UNIVERSIDADE DO PORTO

Power Circuit

Project: Eletric circuit	Drawing no.:	Init.:	Rev.:	Sheet: 1
Date: 21-01-2019	Function:	Location:	Total sheets: 12	Next sheet: 2

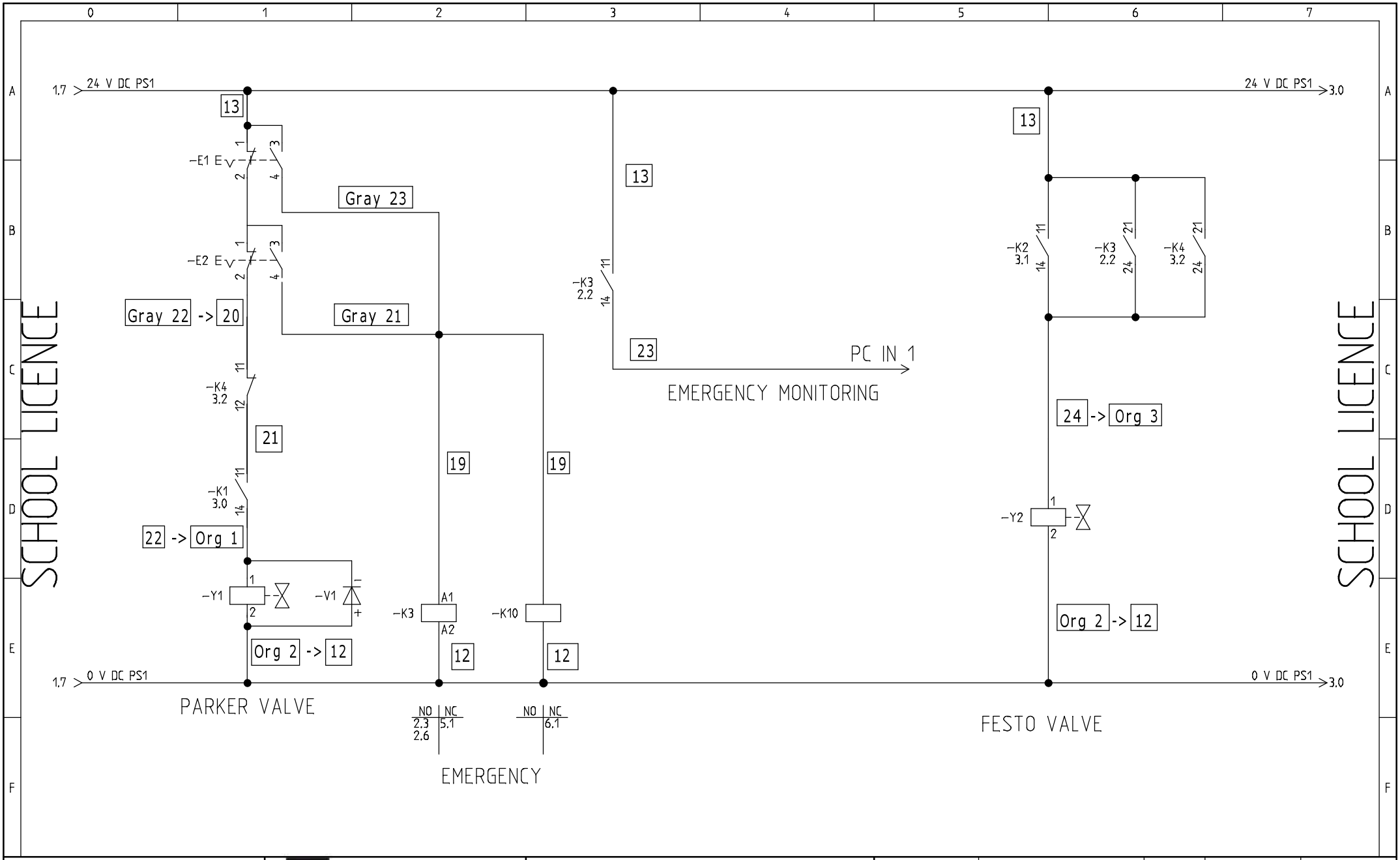

AD FEUP

U.PORTO
FEUP FACULDADE DE ENGENHARIA
UNIVERSIDADE DO PORTO

Solenoid & Emergency Actuation

Project: Eletric circuit	Drawing no.:	Init.:	Rev.:	Sheet: 2
Date: 21-01-2019	Function:	Location:	Total sheets: 12	Next sheet: 3

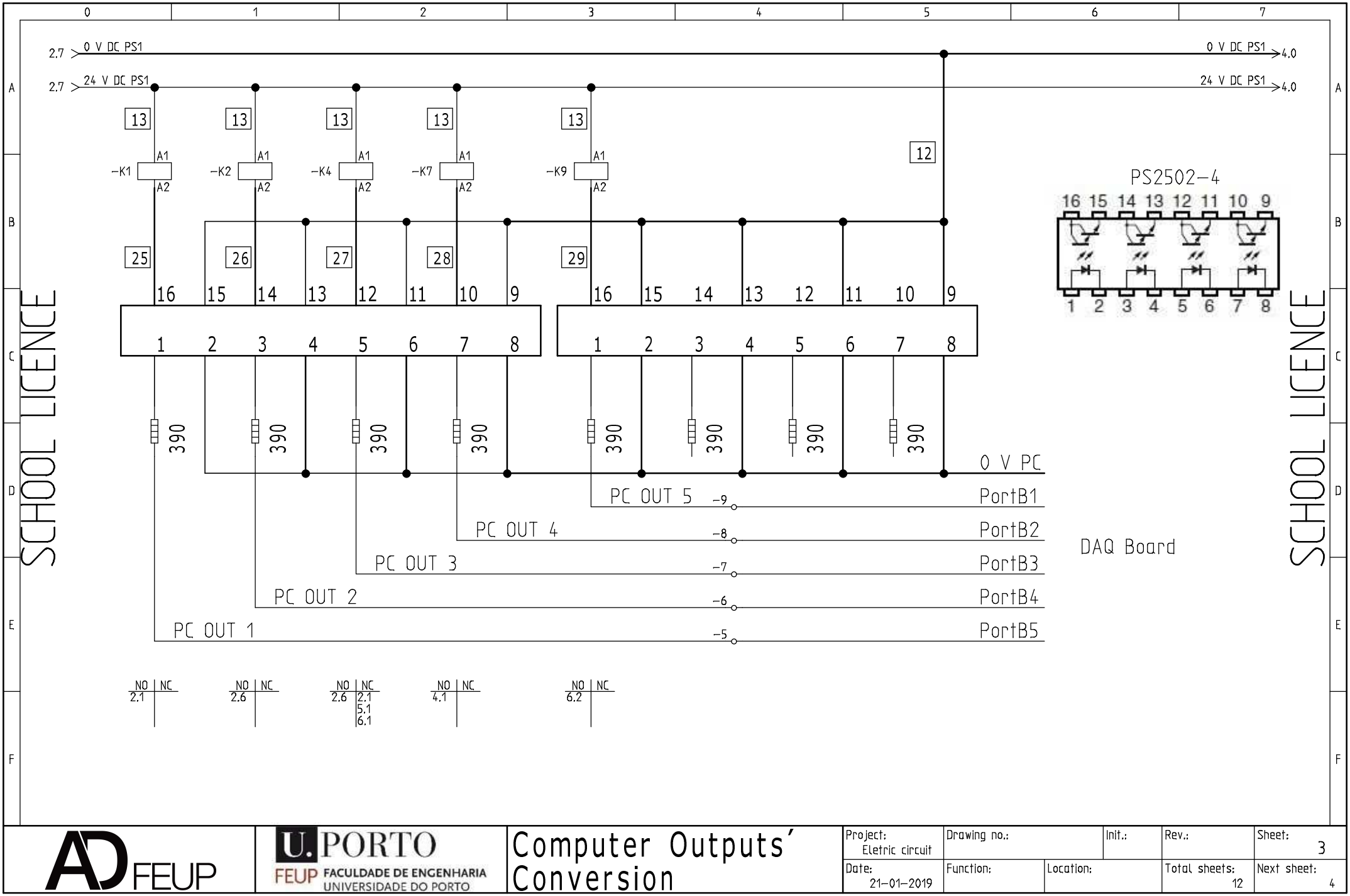

AD FEUP	U.PORTO FEUP FACULDADE DE ENGENHARIA UNIVERSIDADE DO PORTO	Computer Outputs' Conversion	Project: Eletric circuit	Drawing no.:	Init.:	Rev.: / Sheet: 3
			Date: 21-01-2019	Function: / Location:		Total sheets: 12 / Next sheet: 4

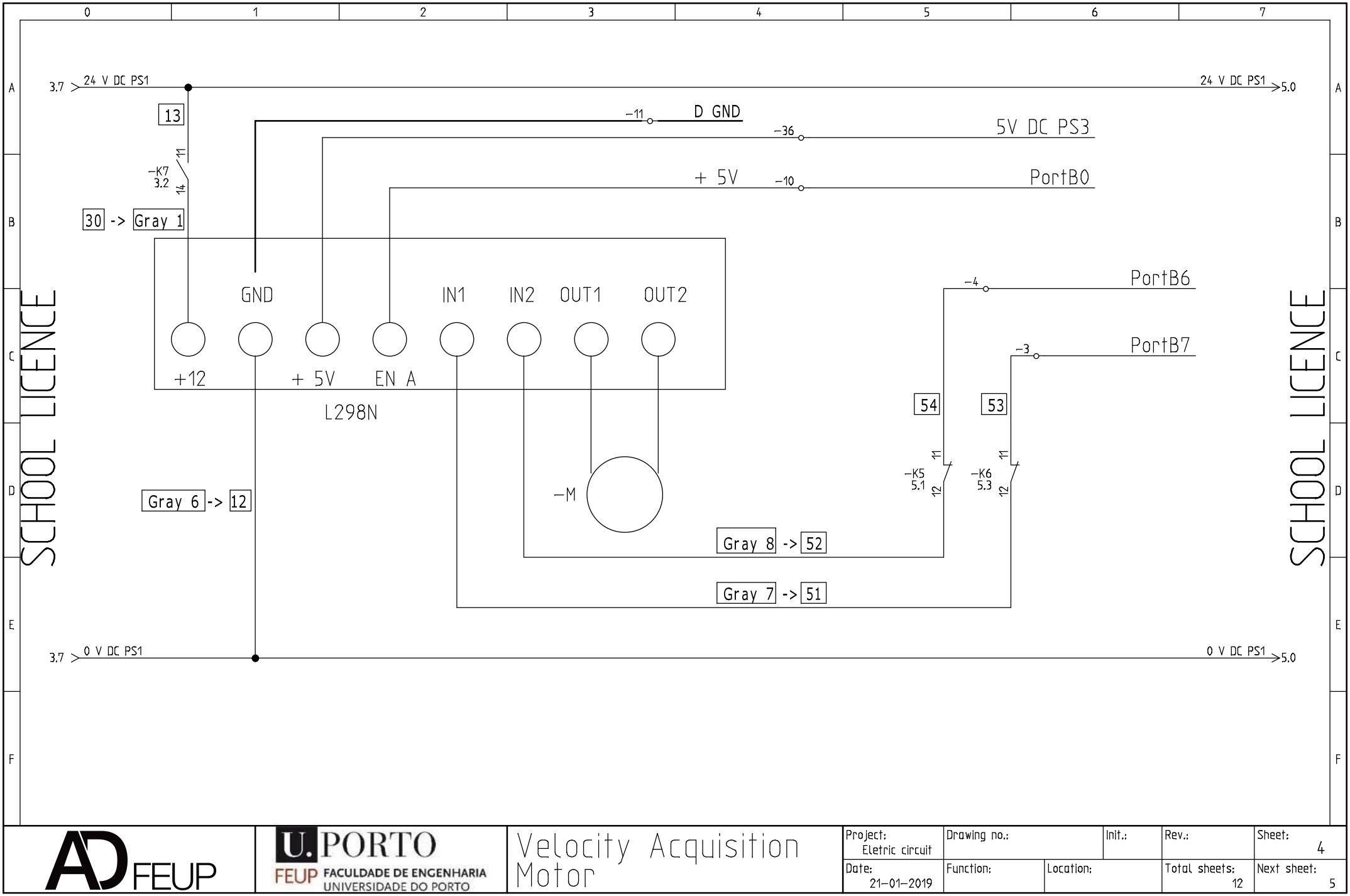

AD FEUP	U.PORTO FEUP FACULDADE DE ENGENHARIA UNIVERSIDADE DO PORTO	Velocity Acquisition Motor	Project: Eletric circuit	Drawing no.:	Init.:	Rev.: / Sheet: 4
			Date: 21-01-2019	Function: / Location:		Total sheets: 12 / Next sheet: 5

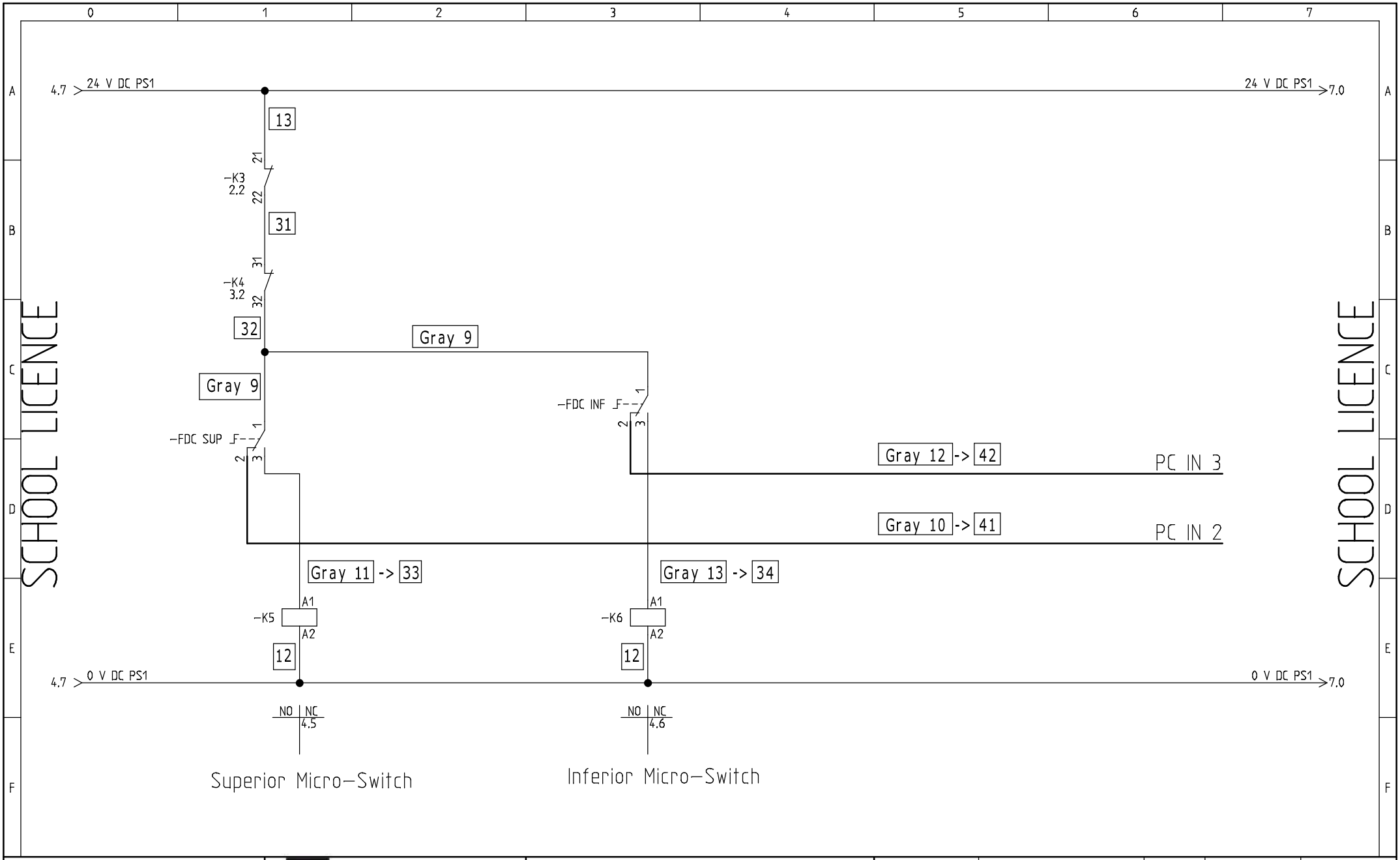

AD FEUP	U.PORTO FEUP FACULDADE DE ENGENHARIA UNIVERSIDADE DO PORTO	Micro-Switches	Project: Eletric circuit	Drawing no.:	Init.:	Rev.:	Sheet: 5
			Date: 21-01-2019	Function:	Location:	Total sheets: 12	Next sheet: 6

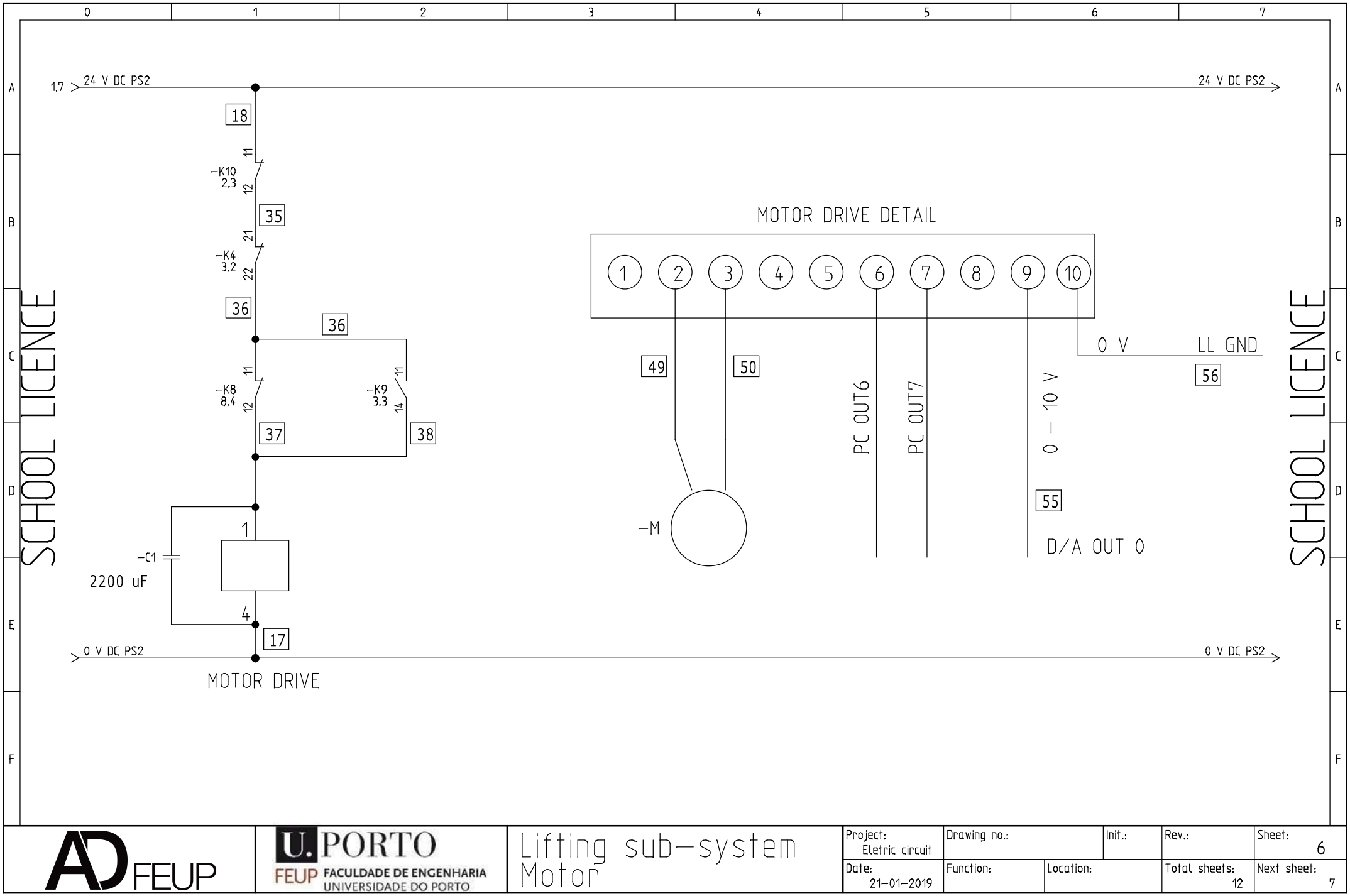
0
1
2
3
4
5
6
7
A
B
C
D
E
F
1.7
24 V DC PS2
24 V DC PS2
18
11
-K10
2.3
12
35
21
-K4
3.2
22
36
36
11
-K8
8.4
12
37
11
-K9
3.3
14
38
1
-C1
2200 uF
4
17
0 V DC PS2
0 V DC PS2
MOTOR DRIVE
SCHOOL LICENCE
SCHOOL LICENCE
MOTOR DRIVE DETAIL
1
2
3
4
5
6
7
8
9
10
49
50
PC OUT6
PC OUT7
0 – 10 V
0 V
LL GND
56
55
D/A OUT 0
-M
AD FEUP
U.PORTO
FEUP FACULDADE DE ENGENHARIA
UNIVERSIDADE DO PORTO
Lifting sub-system
Motor
Project: Eletric circuit
Drawing no.:
Init.:
Rev.:
Sheet: 6
Date: 21-01-2019
Function:
Location:
Total sheets: 12
Next sheet: 7

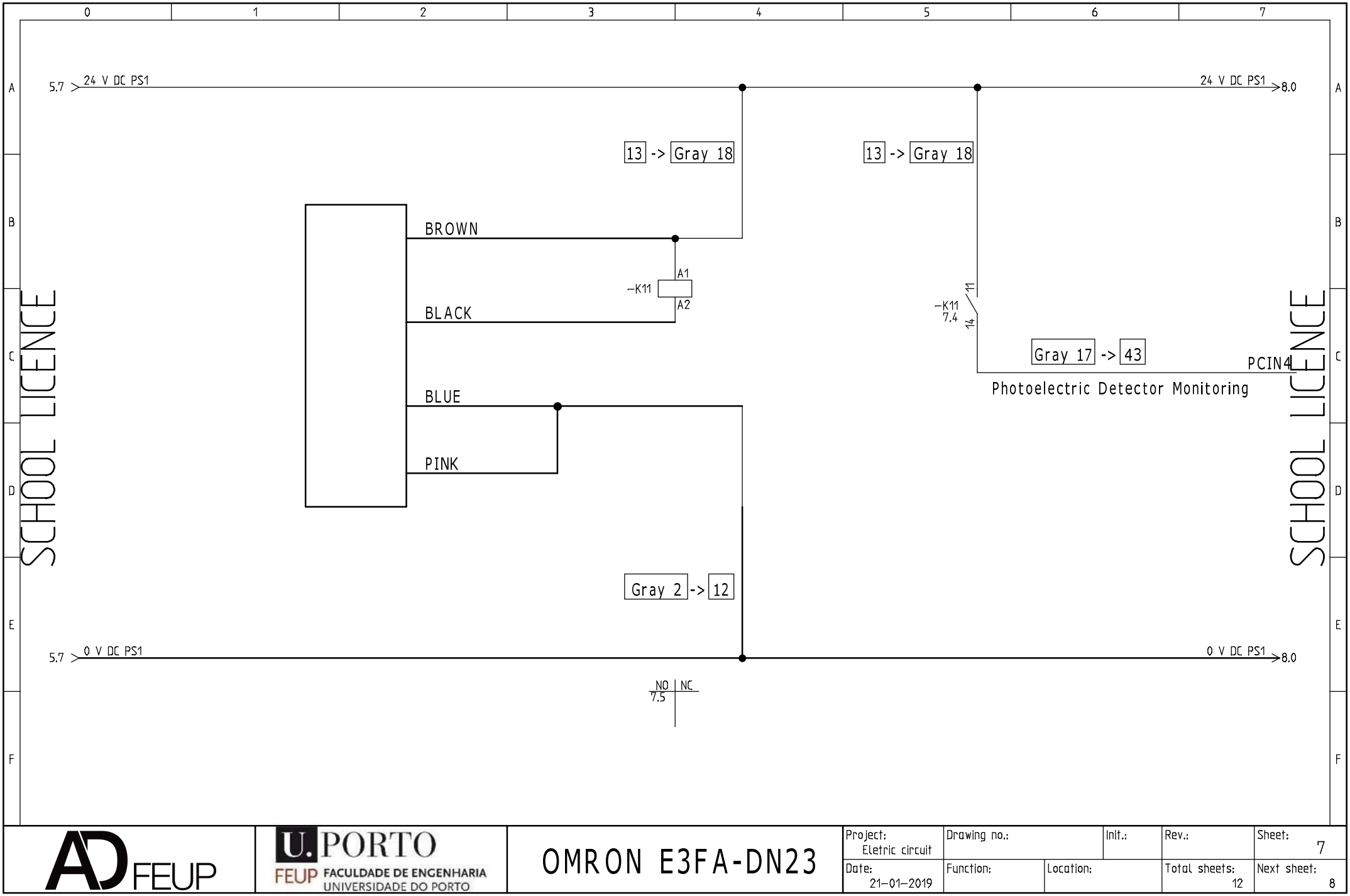

AD FEUP	U.PORTO FEUP FACULDADE DE ENGENHARIA UNIVERSIDADE DO PORTO	OMRON E3FA-DN23	Project: Eletric circuit	Drawing no.:	Init.:	Rev.:	Sheet: 7
			Date: 21-01-2019	Function:	Location:	Total sheets: 12	Next sheet: 8

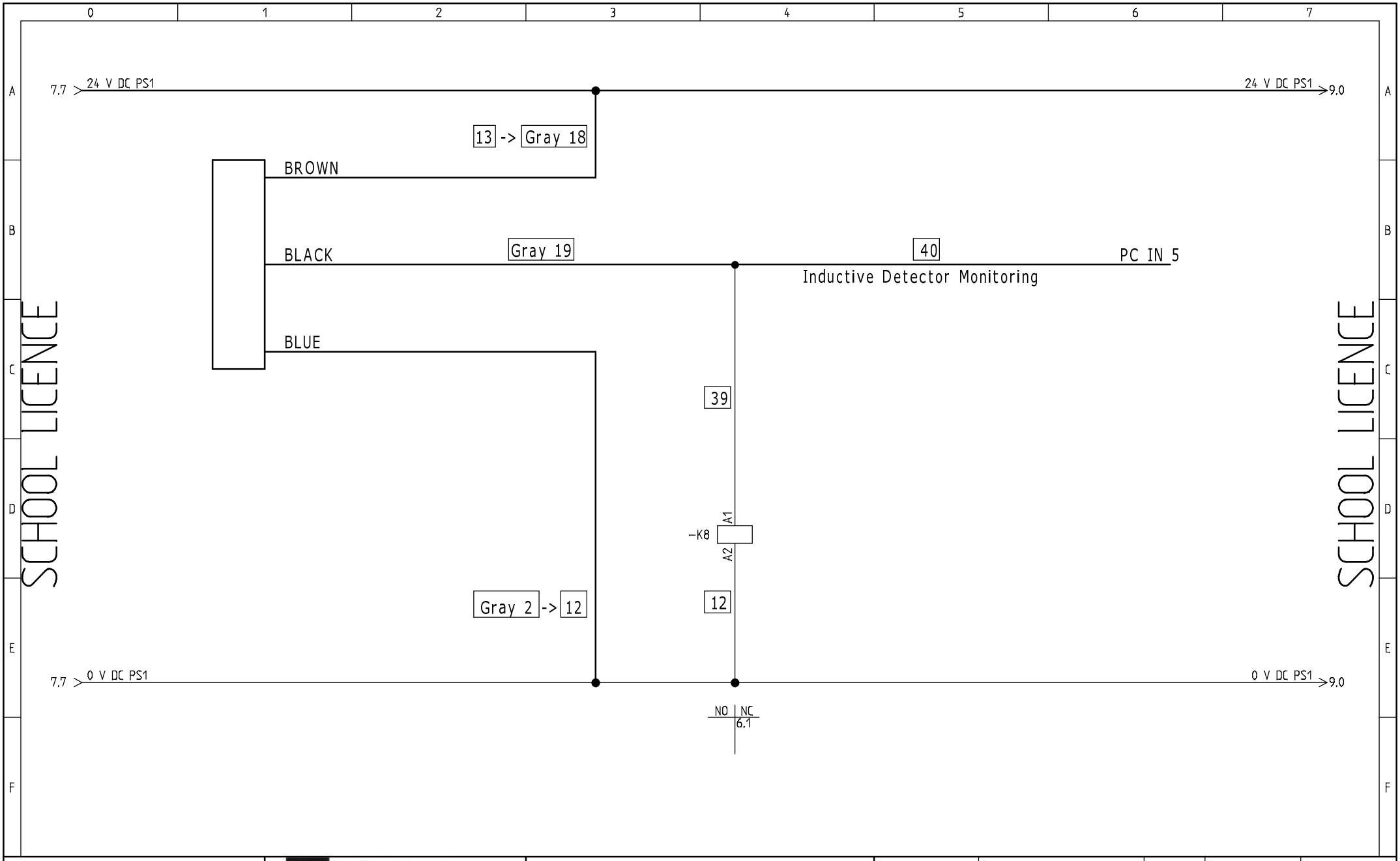

AD FEUP	U.PORTO FEUP FACULDADE DE ENGENHARIA UNIVERSIDADE DO PORTO	IME12-04PS ZW K F38	Project: Eletric circuit	Drawing no.:	Init.:	Rev.:	Sheet: 8
			Date: 21-01-2019	Function:	Location:	Total sheets: 12	Next sheet: 9

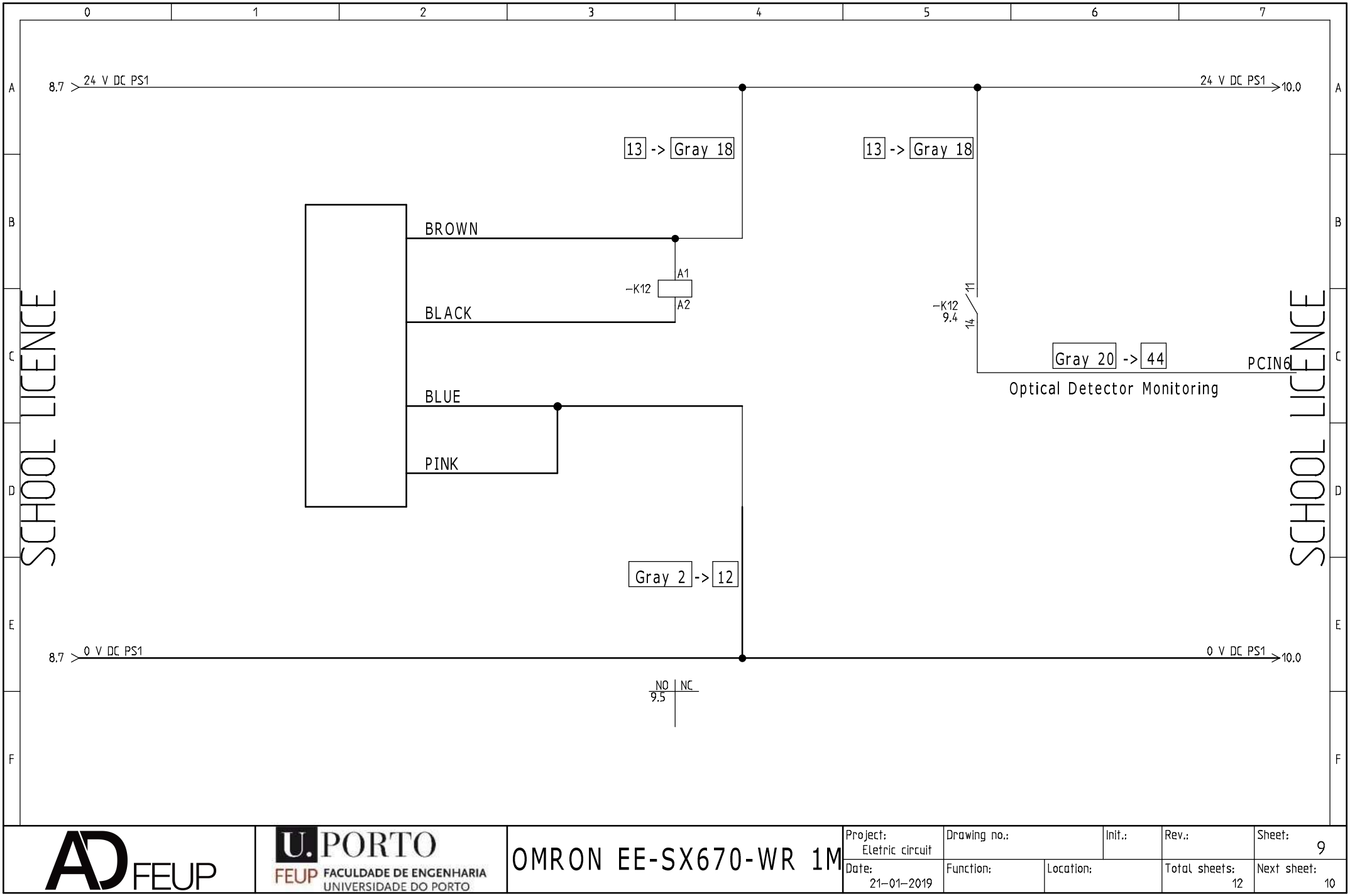

AD FEUP	U.PORTO FEUP FACULDADE DE ENGENHARIA UNIVERSIDADE DO PORTO	OMRON EE-SX670-WR 1M	Project: Eletric circuit	Drawing no.:	Init.:	Rev.:	Sheet: 9
			Date: 21-01-2019	Function:	Location:	Total sheets: 12	Next sheet: 10

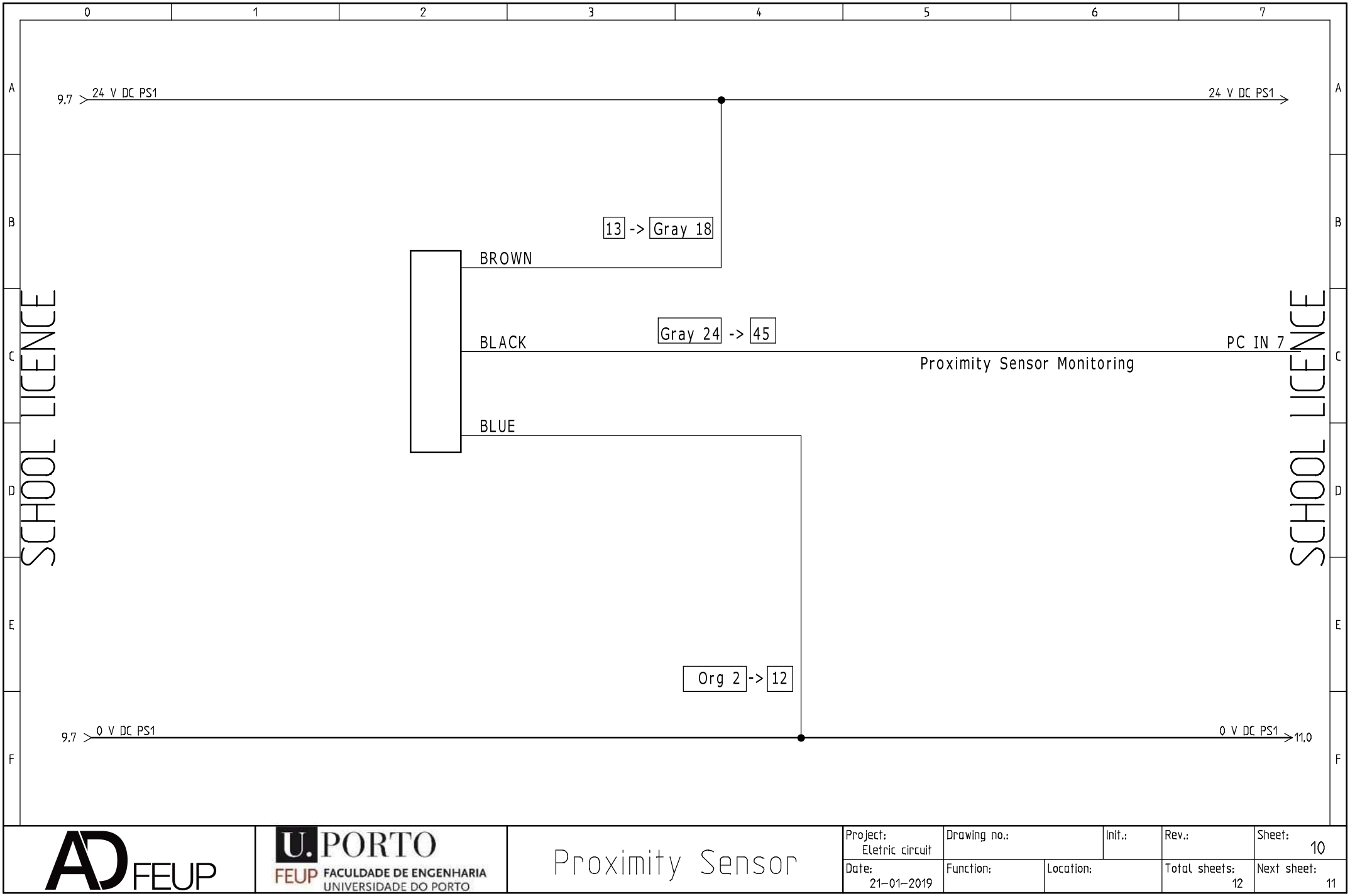

AD FEUP

U.PORTO
FEUP FACULDADE DE ENGENHARIA
UNIVERSIDADE DO PORTO

Proximity Sensor

Project: Eletric circuit	Drawing no.:	Init.:	Rev.:	Sheet: 10
Date: 21-01-2019	Function:	Location:	Total sheets: 12	Next sheet: 11

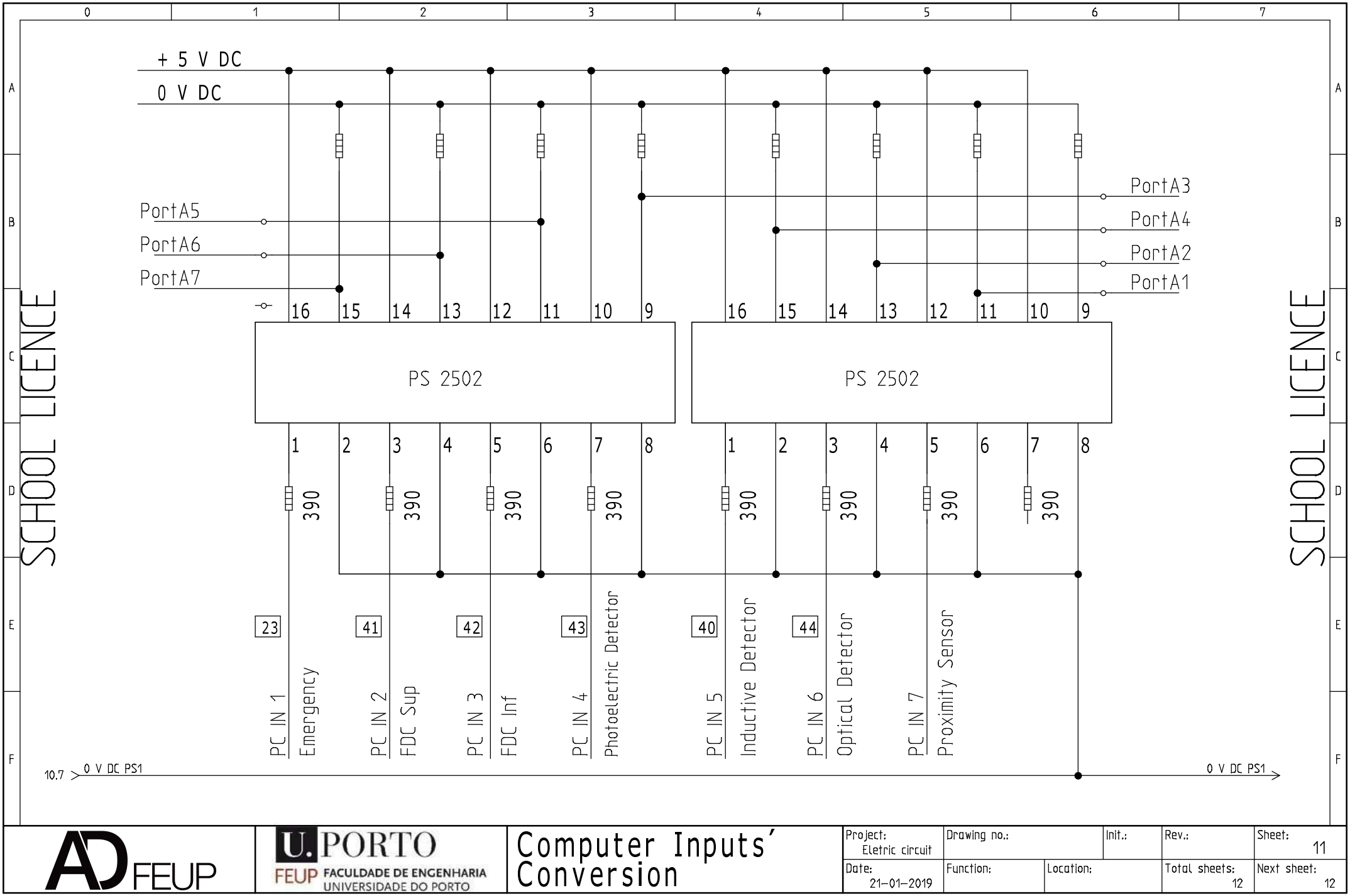

AD FEUP	U.PORTO FEUP FACULDADE DE ENGENHARIA UNIVERSIDADE DO PORTO	Computer Inputs' Conversion	Project: Eletric circuit	Drawing no.:	Init.:	Rev.: / Sheet: 11
			Date: 21-01-2019	Function: / Location:		Total sheets: 12 / Next sheet: 12

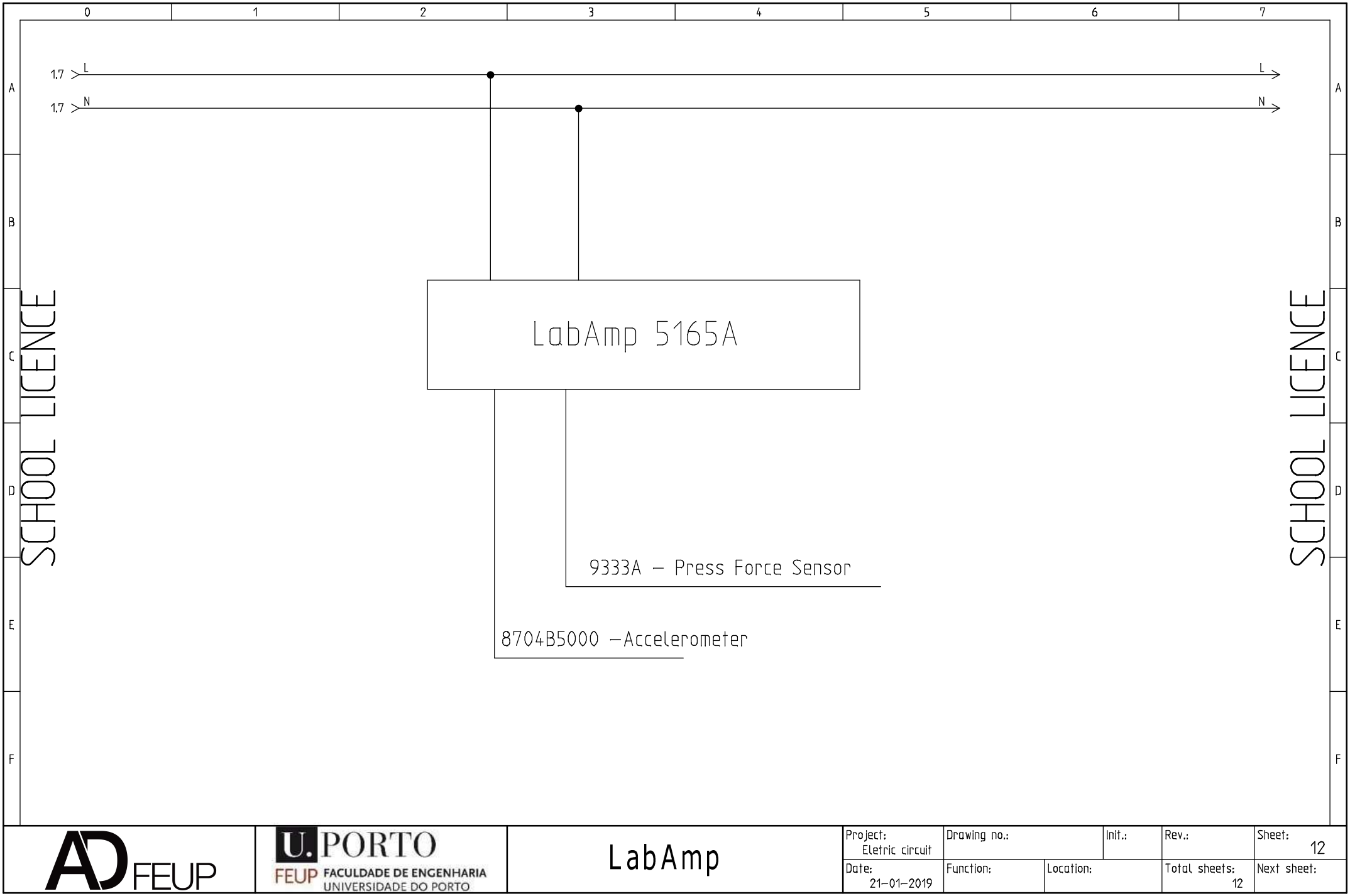

AD FEUP

U.PORTO
FEUP FACULDADE DE ENGENHARIA
UNIVERSIDADE DO PORTO

LabAmp

Project: Eletric circuit	Drawing no.:	Init.:	Rev.:	Sheet: 12
Date: 21–01–2019	Function:	Location:	Total sheets: 12	Next sheet:

Appendix E

Software Variables

Variable´s Name	Initial Value	Type	Function
EncoderPos	-	Input	Informs encoder current position (in counts)
manualVel	-	Input	Sets carriage velocity
CalcHeight	-	Input	Calculated/inserted drop height
AtPos	-	Input	Informs if carriage is at position
Emergency	-	Input	Declares an emergency
emergencyDone	-	Input	Declares emergency situation handled
motorUp_Em	-	Input	Orders to move carriage upwards (when in emergency mode)
motorDown_Em	-	Input	Orders to moves carriage downwards (when in emergency mode)
manualRelease_Em	-	Input	Orders to release anvil (when in emergency mode)
manualVELAQ_Down_Em	-	Input	Orders to move velocity acquisition´s moving platform down (when in emergency mode)
manualVELAQ_Up_Em	-	Input	Orders to move velocity acquisition´s moving platform up (when in emergency mode)
Rcs_activation_Em	-	Input	Orders the anti-rebound sub-system activation (when in emergency mode)
Rcs_deactivation_Em	-		Orders the anti-rebound sub-system deactivation (when in emergency mode)
beginManual	-	Input	Starts manual mode
manualDone	-	Input	Ends manual mode
manualRelease	-	Input	Orders to release anvil (when in manual mode)
beginTest	-	Input	Starts test mode
cancelTest	-	Input	Cancels test mode
Test_done	-	Input	Informs the test is finished
testLift	-	Input	Orders to lift carriage to the CalcHeight
testRelease	-	Input	Orders to release anvil (when in test mode)
motorDown	-	Input	Orders to move carriage downwards (whether in test or manual mode)
motorUp	-	Input	Orders to move carriage upwards (whether in test or manual mode)

ManualVELAQ_Up	-	Input	Orders to move velocity acquisition´s moving platform up (when in manual mode)
ManualVELAQ_Down	-	Input	Orders to move velocity acquisition´s moving platform down (when in manual mode)
Rcs_activation_man	-	Input	Orders the anti-rebound sub-system activation (when in manual mode)
Rcs_deactivation_man	-	Input	Orders the anti-rebound sub-system deactivating (when in manual mode)
sensorInd	-	Input	Signals that carriage is in its upper limit
sensorAnvil	-	Input	Signals that anvil is right under the carriage
sensorZero	-	Input	Signals that the optical detector´s beam is being interrupted
currTime	-	Input	Informs the current time
cylinder_sensor	-	Input	Informs position of the anti-rebound sub-system´s cylinders
FDC_Inf	-	Input	Informs that velocity acquisition sub-system´s moving platform is at its lowest point
FDC_Sup	-	Input	Informs that velocity acquisition sub-system´s moving platform is at its highest point
VELAQ_DOWN	0	Output	Order´s the velocity acquisition sub-system´s moving platform to descend
VELAQ_UP	0	Output	Order´s the velocity acquisition sub-system´s moving platform to ascend
VELAQ_Enable	1	Output	Enables the L298N board
VELAQ_Power	1	Output	Enables the powering of the velocity acquisition sub-system´s motor
PosControl	0	Output	Starts the position control of the carriage
Ref	0	Output	Sets the height for the position of the anvil
motorVel	0	Output	Defines velocity of the lifting sub-system´s motor

AnvilRelease	0	Output	Orders to release the anvil
Forward	0	Output	Orders carriage to move upwards
Reverse	0	Output	Orders carriage to move downwards
InductiveOverride	0	Output	Overrides the inductive detector signal
realVel	-1	Output	Informs real impact velocity
Valve2	0	Output	Activates solenoid that controls anti-rebound sub-system´s valve
emergency_output	0	Output	Signals that emergency situation was declared to the interface
a	0	Output	Informs the interface that the point of impact was defined and the anvil is ready to be lifted
vel_ready	0	Output	Informs the interface that realVel can be collected
AnvilAttached	0	Local	Informs if anvil is attached to the carriage or not
t0	0	Local	Instant that the first comb passes through the optical detector
t1	0	Local	Instant that the second comb passes through the optical detector
AnvilHeight	0.18	Const.	Lifting height when testing if anvil is attached
VELAQ_Dist	0.014	Const.	Distance between the combs